1993-06

Normal modes of oscillation of the VULCAN PHALANX close-in weapon system

MacNeil, Donald P.

Monterey, California. Naval Postgraduate School

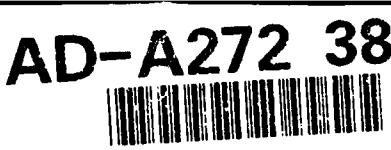

NAVAL POSTGRADUATE SCHOOL
Monterey, California

THESIS

NORMAL MODES OF OSCILLATION
OF THE VULCAN PHALANX
CLOSE-IN WEAPON
SYSTEM

by

Donald P. MacNeil

June 1993

Thesis Advisors: William B. Colson
Joshua H. Gordis

Approved for public release; distribution is unlimited

REPORT DOCUMENTATION PAGE

Form Approved
OMB No. 0704-0188

1. AGENCY USE ONLY (Leave blank)	2. REPORT DATE	3. REPORT TYPE AND DATES COVERED
	June 1993	Master's Thesis

4. TITLE AND SUBTITLE
NORMAL MODES OF OSCILLATION OF THE VULCAN PHALANX CLOSE-IN WEAPON SYSTEM

5. FUNDING NUMBERS

6. AUTHOR(S)
Donald P. MacNeil

7. PERFORMING ORGANIZATION NAME(S) AND ADDRESS(ES)
Naval Postgraduate School
Monterey, CA. 93943-5000

8. PERFORMING ORGANIZATION REPORT NUMBER

9. SPONSORING / MONITORING AGENCY NAME(S) AND ADDRESS(ES)
Naval Postgraduate School
Monterey, CA. 93943-5000

10. SPONSORING / MONITORING AGENCY REPORT NUMBER

11. SUPPLEMENTARY NOTES
The views expressed in this thesis are those of the author and do not reflect the official policy of the Department of Defense or the U.S. Government.

12a. DISTRIBUTION / AVAILABILITY STATEMENT
Approved for public release; distribution unlimited.

12b. DISTRIBUTION CODE

13. ABSTRACT (Maximum 200 words) A study of the PHALANX CLOSE-IN WEAPON SYSTEM's (CIWS) Mk149 round and the M61A1 Gatling gun focused on modeling the various design factors that influence projectile trajectory and accuracy.

The PHALANX currently experiences random and variable dispersion values which can diminish the PHALANX' ability to destroy incoming targets. The focus of the analysis was on determining and understanding the dynamical modes of oscillation and forced response dynamics.

A model of the PHALANX' M61A1 Gatling gun was developed in great detail and its normal modes of vibration and natural frequencies were computed. Because dynamic response is comprised of modal responses, it is critical that the modes of the gun are understood. Various excitation forces were applied, simulating a range of firing bursts, and displacements of the firing barrel were recorded in all translational directions.

Animation of the normal modes of vibration indicate that PHALANX' six-barrel system plays a significant role in the lower order normal modes, and possibly the most significant contribution to dispersion. Also, results of the dynamic response reveal barrel tip displacements, that are consistent with well documented dispersion values.

The FEM provides a timely method to evaluate proposed design modifications and subsequent analysis. This model will be valuable as part of the Optimized Barrel Design project currently underway.

14. SUBJECT TERMS
Finite Element Method and Theory, Mechanical Vibration, Phalanx CIWS, Normal Modes, Dispersion, Forced response, Frequency Response, Transient Response.

15. NUMBER OF PAGES
177

16. PRICE CODE

17. SECURITY CLASSIFICATION OF REPORT	18. SECURITY CLASSIFICATION OF THIS PAGE	19. SECURITY CLASSIFICATION OF ABSTRACT	20. LIMITATION OF ABSTRACT
UNCLASSIFIED	UNCLASSIFIED	UNCLASSIFIED	UL

NSN 7540-01-280-5500

Standard Form 298 (Rev 2-89)
Prescribed by ANSI Std 239-18

Approved for public release: distribution is unlimited.

NORMAL MODES OF OSCILLATION OF THE VULCAN PHALANX CLOSE-IN WEAPON SYSTEM

by

D. P. MacNeil

Lieutenant, United States Navy

B. S., United States Naval Academy, 1986

Submitted in partial fulfillment of the

requirements for the degree of

MASTER OF SCIENCE IN PHYSICS

from the

NAVAL POSTGRADUATE SCHOOL

June 1993

Author: [redacted]

Donald P. MacNeil

Approved by: [redacted]

William B. Colson, Thesis Advisor

[redacted]

Joshua Gordis, Thesis Advisor

[redacted]

Karlheinz E. Woehler, Chairman,

Department of Physics

ABSTRACT

A study of the PHALANX CLOSE-IN WEAPON SYSTEM's (CIWS) Mk149 round and the M61A1 Gatling gun focused on modeling the various design factors that influence projectile trajectory and accuracy.

The PHALANX currently experiences random and variable dispersion values which can diminish the PHALANX' ability to destroy incoming targets. The focus of the analysis was on determining and understanding the dynamical modes of oscillation and forced response dynamics.

A model of the PHALANX' M61A1 Gatling gun was developed in great detail and its normal modes of vibration and natural frequencies were computed. Because dynamic response is comprised of modal responses, it is critical that the modes of the gun are understood. Various excitation forces were applied, simulating a range of firing bursts, and displacements of the firing barrel were recorded in all translational directions.

Animation of the normal modes of vibration indicate that PHALANX' six-barrel system plays a significant role in the lower order normal modes, and possibly the most significant contribution to dispersion. Also, results of the dynamic response reveal barrel tip displacements, that are consistent with well documented dispersion values.

The FEM provides a timely method to evaluate proposed design modifications and subsequent analysis. This model will be valuable as part of the Optimized Barrel Design project currently underway.

Table of Contents

ACKNOWLEDGEMENT

The author is grateful for support of this work by the Naval Postgraduate School, and the Naval Surface Warfare Center, Dahlgren VA. The author would also like to thank Dr. W. B. Colson and Dr. Joshua Gordis for their guidance, patience, and continual support. A special thanks to my partner, LT J. C. Peterschmidt, for his support and efforts during the project. The completion of this research was due to the support and guidance of many. I would personally like to thank LCDR Paul White, Michael Hatch, Scott Martin, Dick Sirolla, and Yuji Wilson for their support, insight, and guidance throughout the project. Finally, the author would like to thank his supportive fiancee Barbara, for her patience and assistance while completing this thesis.

I. INTRODUCTION

Ship air defense against supersonic anti-ship missiles (ASMs) is based on a defense in depth concept. The outer defense is provided by shipboard long and medium range missiles, followed by 5"/54 caliber guns, short range SEA SPARROW missiles, and ultimately the VULCAN PHALANX close in weapon system (CIWS). As the last line of defense, PHALANX will automatically engage and destroy ASMs that penetrate a ship's primary defense envelope at a range where ballistic missile fragments will not damage the ship. It also provides ASM defense for ships operating in other than defense-in-depth scenarios.

CIWS is a quick reaction, closed-loop spotting fire control weapon system designed to defend against "leaks" in a ship's outer air defense. It is designed to destroy targets at a range far enough from the ship to prevent the subsequent missile fragments from continuing on and inflicting significant collateral damage to the ship. It must also mesh well with the other defensive weapon systems to provide sufficient overlap, but not to engage while the longer range systems can still be effective. PHALANX was developed by the former GENERAL DYNAMICS Co., Pomona Division, starting in the mid 1960's, and entered service in the early 1970's. Today, typically two PHALANX mounts can be found on nearly every U.S. Navy ship including the auxiliary and support vessels. PHALANX can also be found on warships of many foreign navies including Japan's newest AEGIS destroyer. It has become the benchmark of ship self-defense weapons. The weapon system is shown in Figure 1.1 and the MK 149 20 mm round is shown in Figure 1.2. (Ref. 1)

The heart of the PHALANX is the versatile M61A1 Gatling gun, providing a high rate of fire (selectable 4500 or 3000 shots per minute SPM) with a specifically designed high kinetic energy round, in order to provide the necessary

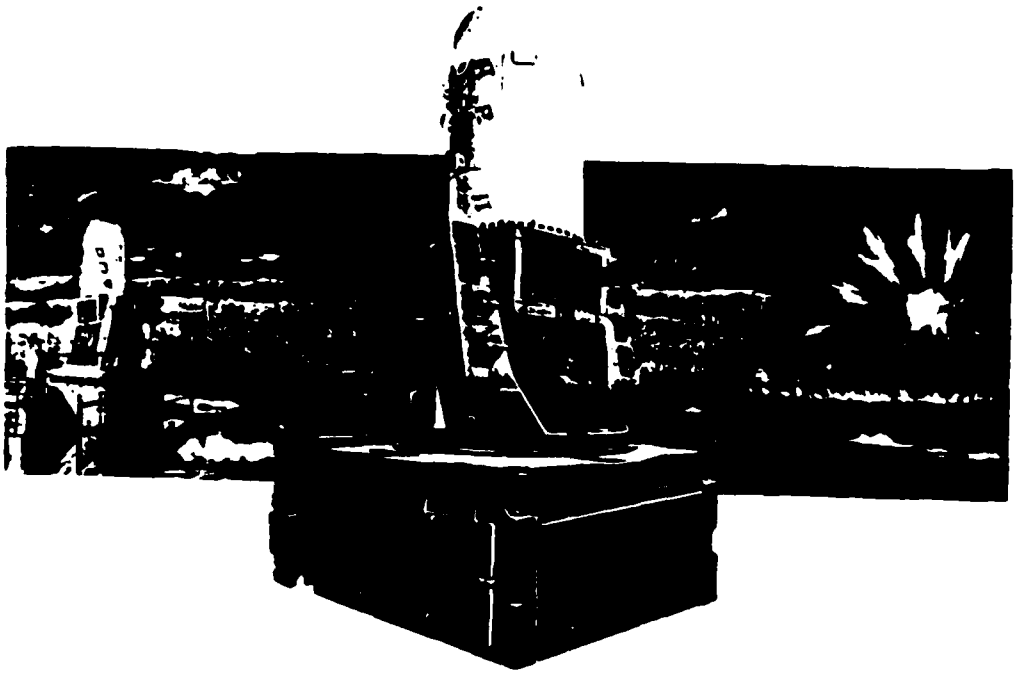

Figure 1.1. The PHALANX Close-in Weapon System.

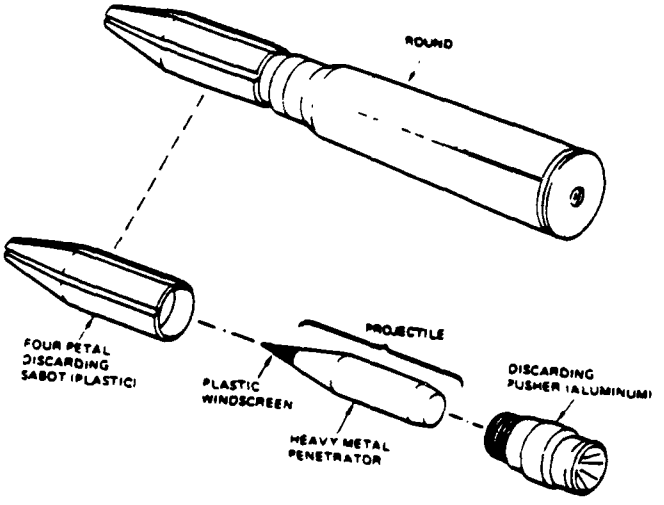

Figure 1.2. MK 149 PHALANX round.

lethality. The high kinetic energy round weighs approximately 0.70 kg and has a muzzle velocity of 1200 m/s which allows for flat trajectories, simplifying the fire control problem. (Ref. 2)

The fire control uses closed-loop spotting in that the system's radar tracks both outgoing rounds and the incoming target. The relatively flat trajectory reduces the complexity of tracking the outgoing rounds. The basic fire control algorithm uses information from spotting of the outgoing rounds and the incoming target, in order to correct the difference between the two, and ultimately achieve missile destruction. It is important to distinguish that the closed loop spotting data is of the outgoing round before it reaches the target area. This saves valuable time. A typical open loop fire control, assesses corrections to outgoing rounds only after observing that the outgoing round has hit or missed. The closed loop spotting system and the high firing rate are the cornerstone of PHALANX' quick reaction. (Ref. 3)

The Phalanx (CIWS) consists of a pair of radar antennae for search and track sharing a common transmitter. They are mounted on top of the housing for the M61A1 20 MM Gatling gun with a 1500 round magazine drum below. The entire assembly moves as a unit, engaging diving as well as sea skimming missiles. There is also an anti-surface mode to defend against small patrol craft at close range. The system is designed to track and engage incoming air targets automatically. However, the surface mode currently requires human intervention via optical sensors to point the gun at small surface targets.(Ref. 4)

A. DISPERSION

All gun / ammunition systems have a dispersion figure. In fact, the large number of bullets delivered by PHALANX coupled with their dispersion create a "wall of bullets" that many propose is the crux of PHALANX' effectiveness. It is proposed that the overall dispersion of PHALANX should not exceed 1 milliradian. (Ref. 5)

If a number of rounds are fired from a weapon against a target, there will be a dispersion in both the vertical and lateral directions. For smaller caliber ammunition, like the 20 mm MK 149 round, the lateral and vertical displacements tend to be equal. The resulting symmetric distribution can closely resemble a Gaussian distribution. Figure 3 illustrates the concept of radial dispersion showing the cone angle through which a given percentage of rounds pass.

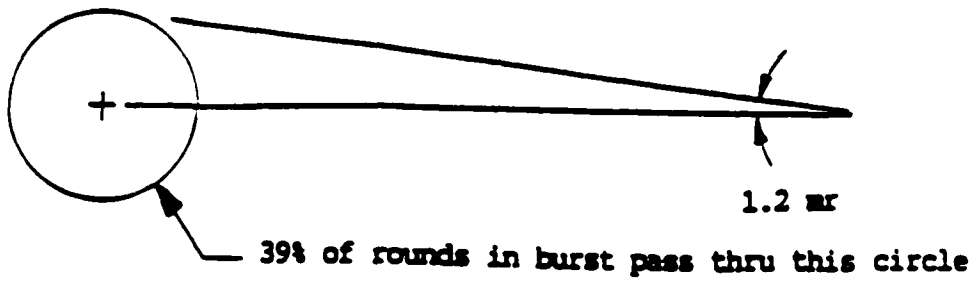

Figure 1.3. Radial dispersion.

Typically, dispersion is measured in terms of the standard deviation of a Gaussian distribution. The dispersion value is quoted for 1 σ , about 39%. The Gaussian distribution is an appropriate approximation for the actual distribution, since dispersion is caused by many small random errors.

However, Figure 1.4 indicates that the dispersion pattern of the PHALANX can be something other than Gaussian. Figure 1.4 is a comparison of one example of dispersion data, taken by HUGHES MISSILE at 3000 SPM, to a Gaussian distribution. (Ref. 6)

When a gun is manufactured, it will be tested for accuracy and dispersion against a test specification. The resulting dispersion value varies and tends to increase by about 50 percent when a gun is fired in bursts as compared to single shot. Also, as a gun wears during its life, the dispersion will increase by up to 20 percent before refurbishment is considered necessary (Ref. 7). For the PHALANX the quoted dispersion value is 1.4 mradian at one standard deviation (Ref. 8).

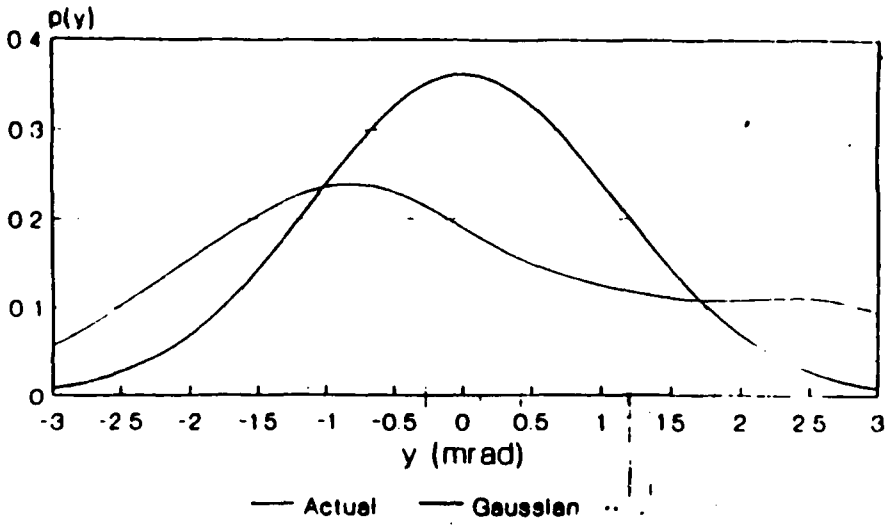

Figure 1.4. Comparison of dispersion data to a Gaussian distribution.

As mentioned earlier, the advances in technology have improved the measurement of dispersion. Figure 1.5 shows the typical arrangement for a dispersion firing. The OEHLER AAS is an acoustic measuring device that has four microphones at the corners of a frame. As the rounds pass through this frame, the time difference between the acoustic signal arriving at the four individual microphones determines the position the round. In addition, there is a batten board placed behind the OEHLER system to provided a "hardcopy" of the dispersion pattern. (Ref. 9)

B. PROBLEM DEFINITION

Currently, the M61A1 Gatling gun mounted in PHALANX exhibits inconsistent dispersion performance. This dispersion was not measured accurately until the advent of an Accurate Automated Spotting System developed by the OEHLER Company. PHALANX dispersion measurements conducted at HUGHES MISSILE show that the six-barrel system gives a dispersion pattern greater than that of a single barrel fired separately. Bursts of 100, 150, 250, and 375 shots with firing rates of 3000 and 4500 SPM are used during dispersion firings. Dispersion

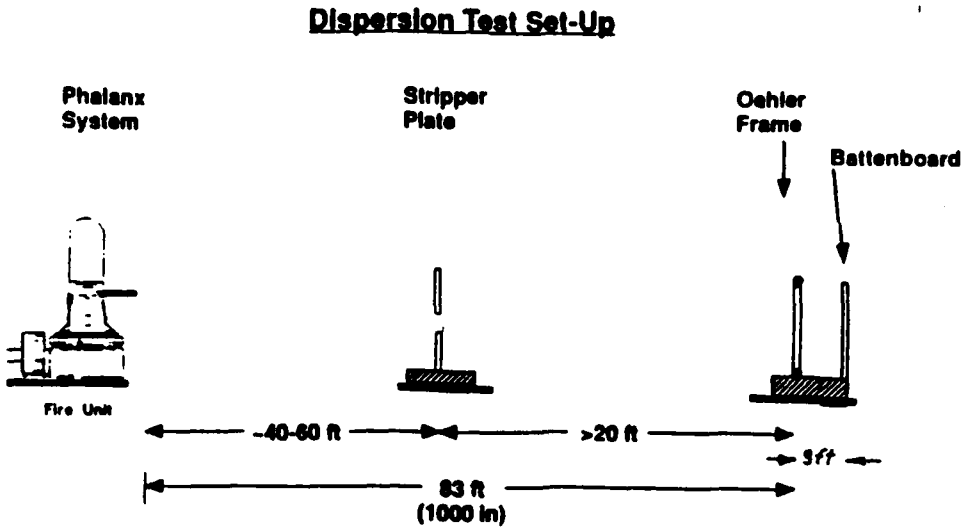

Figure 1.5. Dispersion firing test set up.

firings show individual barrels having their own Mean Point of Impact (MPI), with the six MPI's forming a polygon. Figure 1.6 illustrates a specific example. The individual MPI's are identified by circles with the respective barrel number in the center. The shaded image in the center represents the target's aspect at 1000 feet with a 200 foot off range. Dispersion in both elevation and azimuth are indicated, and both are measured in mradians. The six-barrel group, over a number of short bursts, can produce mean dispersion up to 2 mradians, with typical values ranging between 1 and 2 mradians. The dispersion from a single barrel is only about 1 mradian.

This dispersion leaves a deficiency in a ship's defensive posture. This random and variable dispersion can diminish the gun's ability to hit missiles at its maximum range, since a 2 mrad dispersion results in a 4 meter spread at 2000 meters. Dispersion values documented over the course of several years shows dispersion values from 0.9 mradians to as high as 2 mradians. The dynamic oscillation of the six-barrel system are considered important to understanding the dispersion problem. A 3 mm deflection at the barrel tip results in an angular

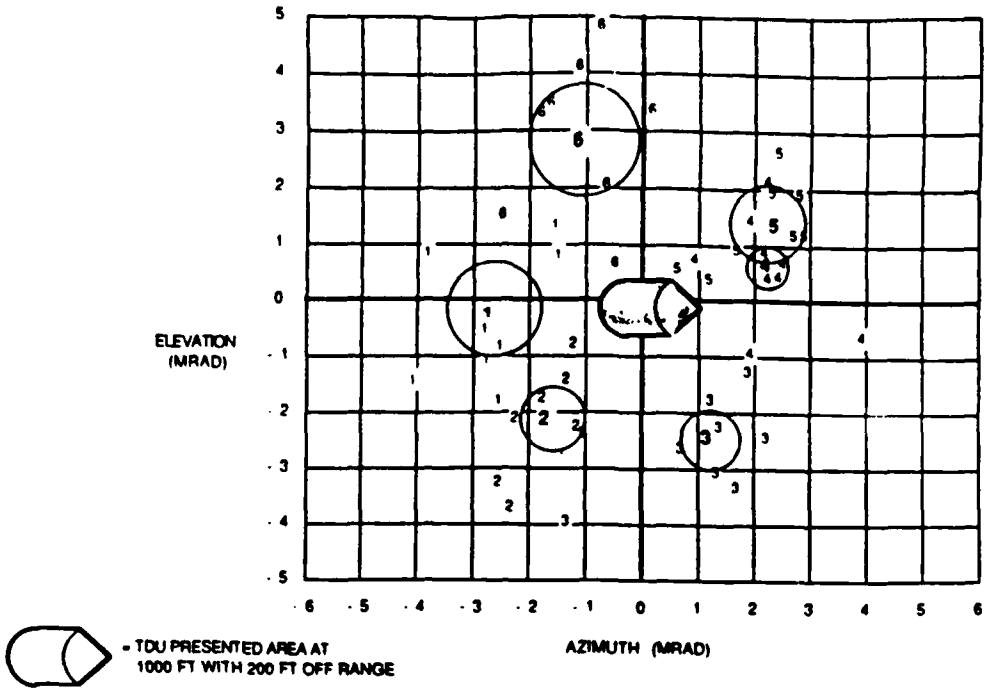

Figure 1.6. Dispersion Pattern.

dispersion of approximately 2 mradians. Hughes Missile has designed and implemented three different muzzle restraints, in order to restrict motion of the end of the six-barrel group. The restraint has been successful in eliminating the largest dispersion values, however significant dispersion values still occur.(Ref. 10)

Due to the complexity of the PHALANX weapon system, there are several sources contributing to the overall dispersion of the system. First of all, there are gun / barrel alignment and vibration problems, yaw of the rounds exiting the barrel upon firing and errors in the control systems. All of these sources taken individually are random and difficult to quantify. Attempting to understand the effects of their combined input is a tremendous task. The goal of this analysis is to understand the role of mechanical oscillations of the six-barrel system in the dispersion of the PHALANX system. In developing the gun model, all parts were considered to be perfect with zero tolerances. Also, there is no consideration for ammunition or control system errors.

C. SCOPE OF THE RESEARCH

In order to fully understand the physics behind the dispersion of the PHALANX M61A1 Gatling gun, a finite element model of the entire gun and its associated mountings was developed. The finite element model provides the capability to solve for and animate the natural modes of oscillation. The model can analyze PHALANX design modifications and can be used for in-depth forced response analysis. The development of the model and the design decisions, supporting theory, and calculations are the scope of this thesis. A brief discussion on dispersion, how it is measured, and a discussion for the motivation to pursue this research follows in the introduction.

D. MOTIVATION

Motivation for the research was provided by Prof. W. B. Colson's PH4911 computer simulation class at the Naval Postgraduate School. One of the assigned projects was an air drag modeling problem, describing bullet trajectories and fragments from a missile destroyed by the VULCAN PHALANX.

The C program, describing fragment trajectories, accepts input data on range, coefficient of drag, characteristic terminal velocity, missile fragment cross-sectional area, air density, and missile initial velocity as input. A listing of the program is shown in Appendix A. The output from the program graphically displays three views of the ballistic missile fragment's trajectories, and reports the number of fragments that hit the ship and miss the ship. The program assumes exponential and Gaussian distributions for various parameters. The missile was designed to break up into 20 fragments of various sizes, shapes, and masses. The fragments had various initial velocities distributed as Gaussian with a standard deviation of 10 m/s in each direction. The terminal velocity is given by

$$V_t = \sqrt{\frac{2mg}{c_d \rho A}} \quad , \qquad (1)$$

where m is the fragment mass, g is the gravitational acceleration, c_d is the coefficient of drag, ρ is the density of air, and A is the cross-sectional area of the missile fragment. By distributing the terminal velocities, the randomness of the size, shape and masses of each fragment was assured.

Figure 1.7 shows three views of the fragments' trajectories. The side view has the ship at the extreme right hand side with the missile fragments inbound from the left hand side. The top view is from a vantage directly above the horizontal plane of the ship and missile, while the end view is looking outward from the ship toward the inbound missile fragments, similar to what a radar would "see".

For this particular run, the characteristic terminal velocity is $V_t = 99\text{m/s}$, the missile's initial supersonic velocity is $v_o = 1100\text{m/s}$, and the range of missile breakup is $R = 600$ m away from the ship. A typical fragment has drag coefficient $C_d = 1$, cross-sectional area $A = 0.01\text{m}^2$, mass $m = 5$ kg, with the acceleration of gravity $g = 9.8\text{m/s}^2$, and air density of $\rho = 1\text{kg/m}^3$.

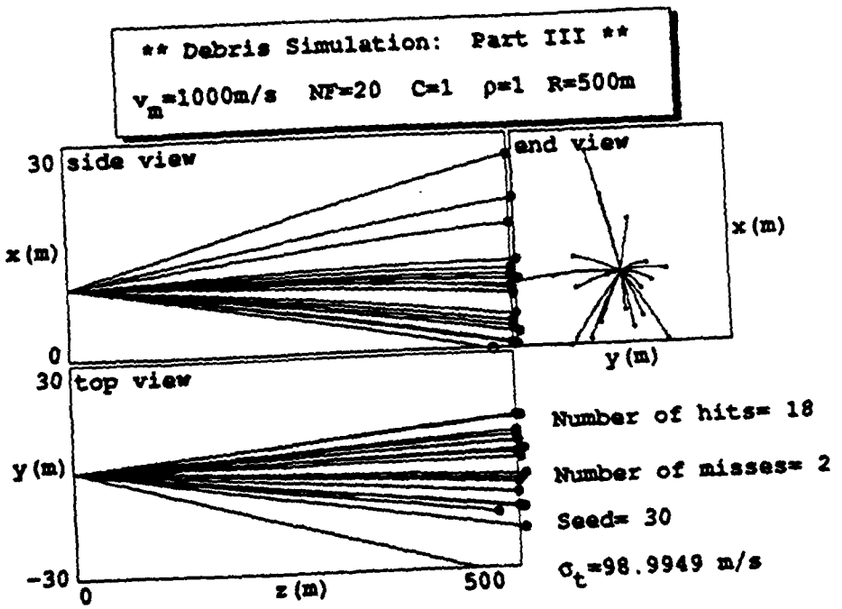

Figure 1.7. Ballistic missile fragment trajectories.

TABLE 1 summarizes the number of fragments that hit the ship as a function of range.

TABLE 1. MISSILE FRAGMENT SUMMARY

Range	Hits	Average. No. Hits
1500	1	
1500	1	
1500	2	1.3
1200	3	
1200	5	
1200	3	3.6
900	3	
900	3	
900	8	4.6
600	14	
600	8	
600	12	11

The trend of the number of hits in TABLE 1 is convincing; anti-ship missiles must be destroyed at PHALANX' maximum range, in order to prevent significant collateral damage. Therefore, the sources of PHALANX' dispersion must be understood and corrected.

II. BACKGROUND

A. FINITE ELEMENT THEORY

In order to investigate the mechanical dynamics behind the dispersion of PHALANX, it was decided that a Finite Element Analysis (FEA) would be used. The high rotation rates and excessive temperatures associated with an operating PHALANX preclude the use of conventional hardware testing. A finite element computer code called I-DEAS (Integrated Design Engineering Analysis) was select to develop the PHALANX model. I-DEAS is a complete structural analysis software package. The package contains modules that allow the drafting, solid modeling, finite element modeling, dynamic testing, and ultimately manufacturing of a component. This thesis used the finite element and system dynamic analysis modules of I-DEAS. Because of the integration of these modules, the development and subsequent analysis is readily accomplished.

Basically the finite element method (FEM) is a numerical method for obtaining approximate solutions to partial differential equations which predict displacements and the effects of stress on a structure. The process of modeling calls for the discretization of a continuous structure into a mesh of small elements. Each element has a simple geometric shape and information to formulate the governing equations in the form of a mass and stiffness matrices. The elements represent a type of structural behavior, i.e. beam, shell, or plate. The unknown generalized coordinates for each element are their associated nodal displacements. An equation of motion can be defined for each respective element. A specific solution to each element is defined in terms of the individual nodal displacements. Scaling the general solution of this equation to include all elements of the structure results in a set of equations that can be solved for all unknown nodal

displacements. Subdividing the physical structure and combining the separate equations for each element provides a solution to the whole physical system.

The art of finite element modeling (FEM) is to choose the correct type and number of elements to have the model solution converge on the correct values without using an excessively large number of elements or nodes. The experienced FEM engineer uses sound engineering judgement in developing a model.

The finite element (FE) engineer must ensure the proper element type and density are chosen to accurately model the true structure's behavior.

Nodes are defined in space with three coordinate values at locations determined by the FE engineer. They are the interconnecting points of elements and define the "boundaries" of individual elements. Nodes are discretized according to six physical degrees of freedom (DOF). Each node may have up to six DOF (translations in x, y, z, and their respective rotations). The DOF's of a node are determined by the type of the element. The total number of physical DOFs is simply determined by the summation of each node's DOFs. The DOF of a model are important for the following reasons: 1) the number of physical DOFs determines the maximum number of modes of vibration, and 2) It determines the number of equations of motion that the finite element method must formulate. There is one equation for each DOF. A FE engineer attempts to operate within a DOF budget, but ensuring that the behavior of the structure is modeled properly. He must keep the size of the problem within realistic limits for the FEM's algorithm. For displacement based finite element formulation, the error introduced into the formulation monotonically decreases with an increasing number of elements.

Boundary conditions and forces are also applied to nodes, and the formulation of the finite elements are based on nodal displacement values. In the gun model, nodal displacements are restricted to be linear and elastic. This classifies the overall analysis to be linear.

The linear restriction is justified. Preliminary calculations show that dispersion values of 1-2 mrad requires barrel tip displacement to be approximately 3 mm. A force versus deflection curve is shown in Figure 2.1. It shows that within the region of interest, 0 to 3 mm deflection, the force has linear behavior. The curve in Figure 2.1 was developed by loading the six-barrel system, at the barrel tips, and measuring the deflection along the length of the barrel cluster. The load was applied using a hydraulic ram under the muzzle tip of the six-barrel system. Data was taken for both the loading and unloading of the six-barrel system, demonstrating a hysteresis effect. Figure 2.1 shows two curves, a solid line and a dashed line. this was done to demonstrate the reproducibility of the results. Only the "upper" portion of the hysteresis loop is linear. This represents the loaded condition.

The overall behavior of the curve, through 300 pounds-force and about 8 mm deflection, is non-linear. But in the lower section of the curve, 0 - 50 pounds-force and 3 mm deflection, the curve is approximately linear. Since a displacement of 0.3 inches at the barrel tip results in about 2 mradians of dispersion. Therefore, the linear elastic assumption is taken to be valid.

A finite element is formulated from an assumed form of the internal strain equation for each element. The user defines physical and material properties of each element. The physical properties describe the elements thickness in the case of thin shell elements, or the beam cross-section for beam elements. The material properties are found in a metals handbook for a specific material type. In addition, the material is categorized as isotropic, orthotropic, or anisotropic. All elements in the gun model were isotropic.

There is an individual equation of motion for each physical DOF for each node. The gun model has 22,500 physical DOF. Therefore, the FEM involves the solution of 22,500 equations. In order to simplify the manipulation of these equations, the algorithm writes them in matrix form. With the relative nodal

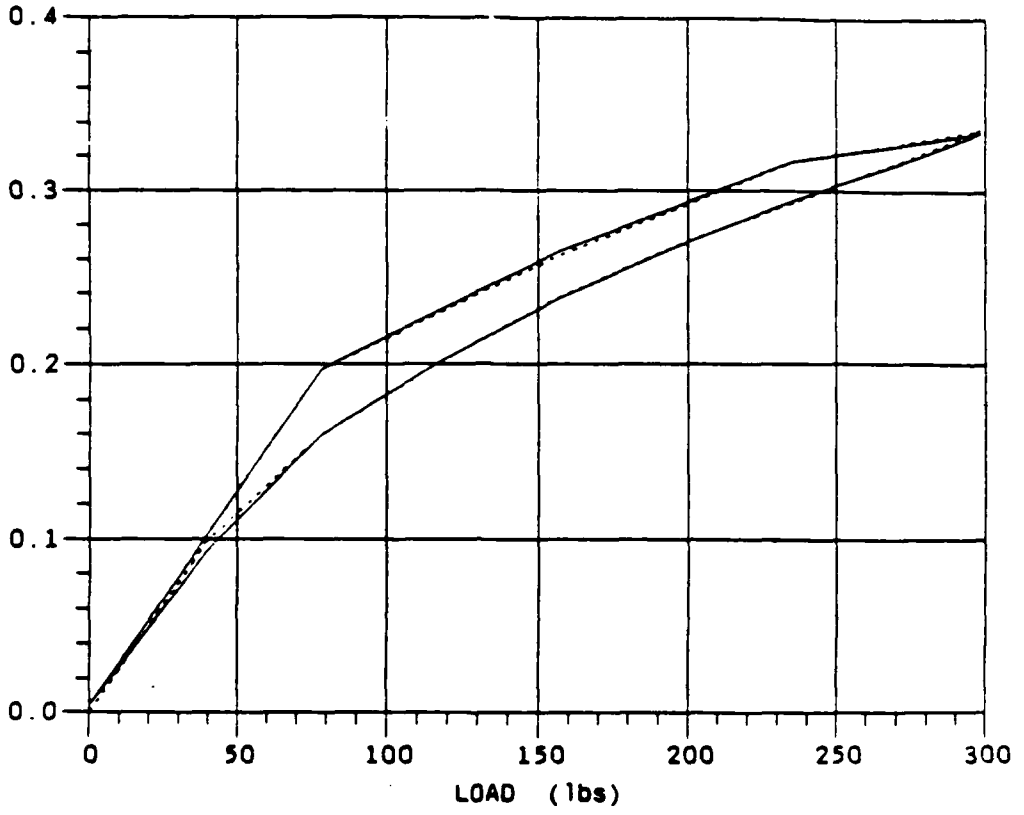

Figure 2.1. Deflection versus load curves for M61A1 Gatling gun (Ref. 11).

displacements as the unknowns, the applied loading and boundary conditions are translated into specific nodal values. Applying the nodal boundary conditions and forces, equation (2) relates the forces to the displacements through the stiffness matrix $[\mathbf{K}]$.

$$\{\mathbf{F}\} = [\mathbf{K}]\{\mathbf{X}\}. \tag{2}$$

For each individual element, there is an assumed solution to its governing

equation. The error incurred is a function of the element density and can be reduced by increasing the element density. Increasing the number of individual elements results in a monotonic convergence of the solution to the actual solution. A second source of error arises from numerically solving the governing equations. Ideally the finer the grid of elements, then the more accurate the model. However, a finer grid increases the size of the resulting stiffness matrices, creating CPU limitations. These tradeoffs must be considered in order to efficiently converge to a correct solution. (Ref. 12)

It is not important to build an exact geometric replica of the gun. It is the structure's mechanical behavior that is crucial. The FE engineer selects elements that represent the elastic and kinematic behavior of the structure and its associated mounting mechanisms.

B. ELEMENTS

1. Description

There are two broad categories of elements: structural and continuum. The structural elements in the gun model are beams and shells. The governing equations for these elements are derived directly from their respective beam and plate theories. Continuum elements are three dimensional solid elements. Their governing equations are derived directly from the theory of elasticity.

IDEAS has a library of element types from which to choose. These elements are categorized by family, order, and topology. The element family refers to the characteristics of geometry and the type of displacement that the element models. For further information on the element families and their formulations, consult the IDEAS MODEL SOLUTION and OPTIMIZATION manual.

The order of an element refers to the order of the shape equation used to interpolate strain between nodes. Specifically the equations can be linear,

parabolic, or cubic. Linear elements have two nodes along each edge, parabolic have three nodes and cubic four.

Topology is another classification of the elements. It refers to the overall shape of the elements; whether it is triangular or quadrilateral. In general, it is better to choose quadrilateral over triangular shapes, because the former has more degrees of freedom and will more accurately predict the true displacement. However, the geometry of the model often requires the use of triangular topology.(Ref. 13)

2. Beam Elements

Beams are elements whose length is much greater than its transverse dimension. A Beam can be modeled using individual elements of varying cross-sections along its length, and was important in the modeling of the gun barrels. It took approximately 3000 elements to model the barrels using solid elements. In order to simplify the problem and to maintain an acceptable number of DOF, the model used individual beam elements with a tubular cross-section of varying dimensions that mimic the inertial properties of the actual barrel along its length. IDEAS provides the user with a variety of standard cross-sectional shapes that can be customized with specific dimensions. For a tubular cross-section, the computer requires that an inner diameter and wall thickness be specified. With these two inputs IDEAS generates the cross-section, displays it for user approval, and stores it for potential future use.

The properties of the beam elements are 1) the cross-section is constant along the length of the individual element 2) the cross-section dimensions are small compared to the element length, and 3) the stress and strain vary linearly across the section depth. The finite element method simplifies calculations associated with a three dimensional beam of varying cross-section and varying orientations in space.

3. Thin Shell Elements

In a thin shell element, the lateral dimension is about the same size as its length, and both are large compared to the element thickness. Shells support loads in the same way as plates with the addition of a substantial in-plane support. The governing equations of shells are comparable to a three dimensional elasticity problem. The central idea of shell theory is that the shell thickness is so small that the load carrying capability due to shell bending is small. Therefore, only the displacement at the midsurface of the shell is of any significance. In order to compensate for this, the displacement at any point is a combination of the midsurface displacement and local nodal rotations. In the case of shells, nodes have three translational DOF and two rotational DOF in the plane tangent to the surface. Rotation in the plane of the shell is not allowed.

4. Solid Elements

Three dimensional solids elements describe all conceivable orientations in three space. The use in this thesis was limited to solid bricks and solid wedges. As implied by their respective names, the shapes in two dimensions are those of a rectangle and triangle, respectively. For a solid brick the minimum number of nodes is eight. For the wedge, it is six. In the formulation of these elements, the theory of elasticity provides the governing equations comprised of twelve independent partial-differential equations and six stress - strain relations. Solid elements are not appropriate for bending behavior, unless a large number of elements are used.

5. Node to Node Translational Springs

The node to node translational spring is an element that models a linear elastic spring between two nodes. These springs can be assigned a specific translational stiffness value in the three respective translational directions x, y,

and z. These represent the force required to separate the two nodes a unit distance in each respective direction. The units are force per unit distance.

6. Rigid Elements

Rigid elements restrict the motion of the nodes of an element. The nodes are related to each other as if they were connected by rigid mass less beams. A single rigid element can be defined by anywhere from two to 32 nodes, and all nodes have all six degrees of freedom. A unique feature of the rigid element is its end release code. The end release code is simply a series of six integer values (123456) corresponding to the six physical degrees of freedom, x translational through z rotational, respectively. These identify the degrees of freedom that are to be omitted from the rigid constraint, and apply to all nodes in the element except the first. This allows the simulation of different boundary conditions such as hinges or ball-socket joints. It is recommended that a simple model be built, in order to understand of the consequences of varying the end release code prior to applying it for a specific model application. The default value is 0. That is, no physical degrees of freedom are omitted. All applications of rigid elements in the gun used the default end release code. During analysis rigid elements are processed using a degree of freedom elimination method. The formulation is in the form of a multi-point constraint (MPC) equation. The MPC equation is a linear algebraic expression whose variables represent nodal displacement DOF. An MPC equation consists of nodal DOF, u_i, constant coefficients (real numbers), A_i, and a constant which represents the right hand side of the equation. The right hand side must be zero for normal modes of vibration. An example MPC follows:

$$A_1 u_1 + A_2 u_2 + A_3 u_3 = 0 \text{ (Ref. 14).}$$

C. EXAMPLE

To provide a better understanding of the formulation of a finite element, a simple two degree of freedom example is provided. A rod, shown in Figure 2.2, represents a continuously distributed mass of length L, mass density γ (mass / length), and stiffness proportional to the product $E\,A$, where E is Young's modulus and A is the cross-sectional area.

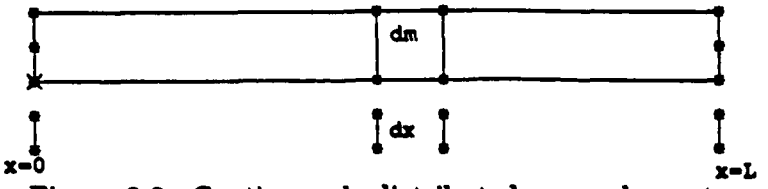

Figure 2.2. Continuously distributed mass element.

The approach will be to discretize the response of the rod in terms of its end-point values, or boundary conditions. In order to determine the displacement, use a function of location x and time t, u=u(x,t), along the rods length. The end-point values are u_1 and u_2 defined as

$$u_1 = u(0,t). \tag{3}$$

$$u_2 = u(L,t). \tag{4}$$

Shape functions will be used to relate the response of the rod anywhere along its length to the end point coordinates. The shape functions $\alpha_1(x)$ and $\alpha_2(x)$ are linear, so that the following restrictions apply:

$$\alpha_1(0) = 1. \quad \alpha_2(0) = 0.$$

$$\alpha_1(L) = 0. \quad \alpha_2(L) = 1.$$

Figures 2.3 and 2.4 are the resulting graphs showing the shape functions $\alpha_1(x)$ and $\alpha_2(x)$ respectively.

The resulting shape functions have the analytical form of

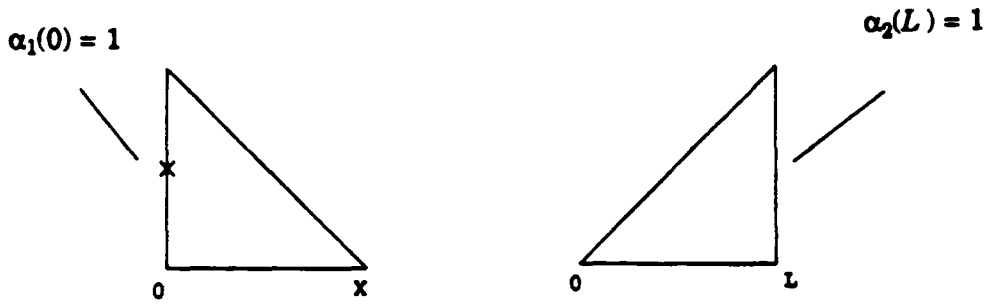

Figures 2.3 and 2.4. Shape functions.

$$\alpha_1(x) = 1 - \frac{x}{L} \ . \tag{5}$$

$$\alpha_2(x) = \frac{x}{L} \ . \tag{6}$$

The resulting displacement function for the rod is then

$$u(x,t) = \alpha_1(x)\, u_1(t) + \alpha_2(x)\, u_2(t) \ , \tag{7}$$

or

$$u(x,t) = \begin{bmatrix} \alpha_1(x) & \alpha_2(x) \end{bmatrix} \begin{Bmatrix} u_1(t) \\ u_2(t) \end{Bmatrix} \ . \tag{8}$$

The results of the two shape functions allow any response of the rod element to be described using linear combinations of the shape functions $\alpha_1(x)$ and $\alpha_2(x)$. The problem has been discretized with the variable q defined in (9).

$$\begin{Bmatrix} q \end{Bmatrix} = \begin{Bmatrix} u_1 \\ u_2 \end{Bmatrix} \ . \tag{9}$$

For deformations of a rod that do not have a linear shape, a second bending mode is shown in Figure 2.5.

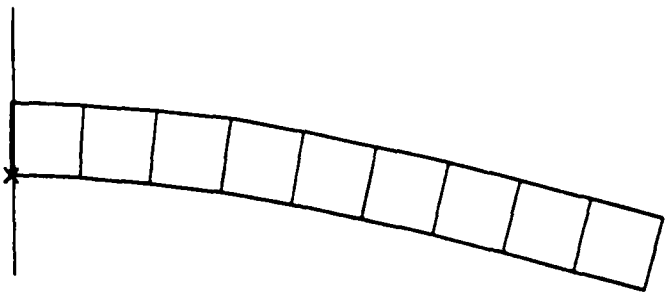

Figure 2.5. Deformed rod.

The response can be best approximated by dividing the rod up into several small segments so that the linear combination of each of these smaller elements can exactly represent this response. The higher the element density, the more exact is the solution. This illustrates the importance of the FE engineer's decisions, with regards to element density and its effect on the solution.

The equations of motion for the rod can be determined using Lagrange's method. It is a simple method to integrate the resulting kinetic energy, T, and strain energy, V, for each individual element over the length of the rod in (10) and (11). These equations can be substituted into Lagrange's equation, and solved for the equations of motion,

$$T = \frac{\gamma}{2} \int_0^L \left[\dot{u}(x,t)\right]^2 dx \quad , \tag{10}$$

$$V = \frac{E\,A}{2} \int_0^L \left[\frac{\delta u(x,t)}{\delta x}\right]^2 dx \quad . \tag{11}$$

Differentiating (7) with respect to time gives

$$\dot{u} = \alpha_1(x)\dot{u}_1(t) + \alpha_2(x)\dot{u}_2(t) \, . \tag{12}$$

Differentiating (7) with respect to x, and defining $\alpha'(x)$ as the differential of $\alpha(x)$ with respect to x, gives

$$\frac{\delta u(x,t)}{\delta x} = \alpha'_1(x)\, u_1(t) + \alpha'_2(x)\, u_2(t) \, . \tag{13}$$

Substituting (12) into (10) and (13) into (11) results in

$$T = \frac{\gamma}{2} \int_0^L \left[\alpha_1(x)\dot{u}_1(t) + \alpha_2(x)\dot{u}_2(t)\right]^2 dx \quad \text{,and} \tag{14}$$

$$V = \frac{E\,A}{2} \int_0^L \left[\alpha'_1(x)\,u_1(t) + \alpha'_2(x)\,u_2(t)\right]^2 dx \quad . \tag{15}$$

Define Lagrange's function L ,as

$$L = T - V. \tag{16}$$

Using Lagrange's method,

$$\frac{\delta}{\delta t}\left[\frac{\delta L}{\delta \dot{q}_i}\right] - \frac{\delta L}{\delta q_i} = Q_i \quad , \tag{17}$$

and (16), the equations of motion can be derived. In (17) i=1, 2, $\cdots$, n, where n is the number of degrees of freedom and Q_i , non-conservative work, is equal to zero.

In order to evaluate (17), we need

$$\frac{\delta L}{\delta \dot{u}_1} = \frac{\delta T}{\delta \dot{u}_1} = \gamma \int_0^L \left[\alpha_1(x)\dot{u}_1(t) + \alpha_2(x)\dot{u}_2(t)\right] \alpha_1(x)\; dx \quad , \tag{18}$$

$$\frac{\delta L}{\delta \dot{u}_2} = \frac{\delta T}{\delta \dot{u}_2} = \gamma \int_0^L \left[\alpha_1(x)\dot{u}_1(t) + \alpha_2(x)\dot{u}_2(t)\right] \alpha_2(x)\; dx \quad , \tag{19}$$

and

$$\frac{\delta L}{\delta u_1} = \frac{\delta V}{\delta u_1} = E\,A \int_0^L \left[\alpha'_1(x)\,u_1(t) + \alpha'_2(x)\,u_2(t)\right] \alpha'_1(x)\; dx \quad , \tag{20}$$

$$\frac{\delta L}{\delta u_2} = \frac{\delta V}{\delta u_2} = E\,A \int_0^L \left[\alpha'_1(x)\,u_1(t) + \alpha'_2(x)\,u_2(t)\right] \alpha'_2(x)\; dx \quad . \tag{21}$$

Define the mass and stiffness matrices as

$$m_{ij} = \gamma \int_0^L \alpha_i(x)\,\alpha_j(x)\,dx \quad \text{,and} \tag{22}$$

$$k_{ij} = E\,A \int_0^L \alpha'_i(x)\,\alpha'_j(x)\,dx \quad . \tag{23}$$

Collecting (18) to (23) into (17) results in Lagrange's equations of motion which can be recognized as Newton's Second Law

$$\left[m_{i\,j} \right] \begin{Bmatrix} \ddot{u}_1 \\ \ddot{u}_2 \end{Bmatrix} = \{F\} \quad . \tag{24}$$

and Hooke's Law

$$\left[k_{i\,j} \right] \begin{Bmatrix} u_1 \\ u_2 \end{Bmatrix} = \{F\} \quad . \tag{25}$$

As an example of the global stiffness and mass matrices, consider a simple case with four nodes defined along the rod's length. From Figure 2.6, it can be seen that node 2 has a stiffness contribution from element 1 and element 2.

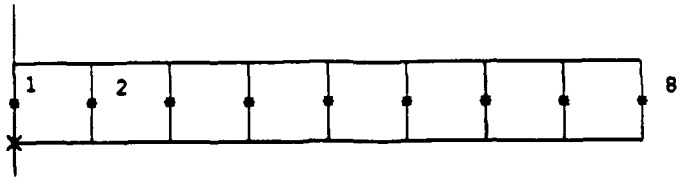

Figure 2.6. Rod with nodal points defined.

The assemblage of the global stiffness matrix, [K], results in the computation of each component in the matrix. In many cases, a component is comprised of the combinations of several individual element stiffness contributions The following illustrates an example (note that the subscripts on the global stiffness matrix components refer to the individual stiffness matrices of the finite elements)

$$\left[\mathbf{K}\right] = \begin{bmatrix} \begin{bmatrix} k_1 \end{bmatrix} & \cdot\cdot & \\ \cdot\cdot & \begin{bmatrix} k_2 \end{bmatrix} & \cdot\cdot \\ \cdot\cdot & \cdot\cdot & \begin{bmatrix} k_3 \end{bmatrix} \end{bmatrix} \quad . \tag{26}$$

for node 2,

$$\mathbf{K}_{22} = k_{22}^{\,1} + k_{11}^{\,2} \quad . \tag{27}$$

This can also be extrapolated for other nodes that have several stiffnesses associated with them.

The resulting general equation of motion is

$$[\mathbf{M}]\{\ddot{\mathbf{X}}\} + [\mathbf{K}]\{\mathbf{X}\} = 0. \tag{28}$$

From this global equation of motion stress analysis, linear static analysis, and normal mode dynamics can be solved to find the normal modes. The next chapter will describe the details of the gun model's development, and the solution of the eigenvalue problem of the normal modes.

III. MODEL DEVELOPMENT

A. INTRODUCTION

IDEAS is the cornerstone of parallel engineering, incorporating design, analysis, and manufacturing. Parallel engineering provides a project manager with early review of design alternatives and potential shortcomings. However, at the inception of the PHALANX project in the late 50's, finite element modeling (FEM) was no where near its current level of understanding and wide-spread use. Although FEM has been understood theoretically for many years, it was the technological advances in computer hardware that has expanded the horizons for FEM, allowing FEM to be performed with a desk top workstation. This new technology is being applied for the first time to investigate the performance of the PHALANX weapon system.

The layout of the model began with a site visit to the PHALANX gun at HUGHES MISSILE in Pomona, CA. Gun drawings and blueprints were studied to extract dimensions and the material types of individual components. Decisions were made as to which components of the gun would be critical in the ultimate dynamic analysis of the model.

Initially, the model was intended to focus on the six-barrels and clamps. However, on the advice of an outside consultant the double angular contact bearing, needle bearing and their support structure were included in the model. In addition to the bearings, the gun's mounting assemblies were critical to understanding the model dynamics. (Ref. 15)

With a budget of approximately 20,000 Degrees of Freedom (DOF), a model was developed in a logical fashion, much the same way the gun is built on an assembly line. Individual components were "built", quality checks performed, and

then a solution of their individual normal modes was found. Decisions were made as to which element types and element densities would best model the behavior of individual components.

This chapter discusses the functional description of the significant components of the M61A1 Gatling gun, followed by a discussion of the building of the model's components, the grouping of elements, model quality checks, boundary conditions, and finally the model solution. The development of the finite element (FE) model is the first step to solving for the normal modes and natural frequencies.

Mode shapes and natural frequencies are used to identify the excitation frequencies that may produce undesirably large structural responses. The response of the structure can be approximately represented, in many cases, by the lower frequency mode shapes. This allows the formation of modal components for future dynamic response analysis.

B. NODE CREATION

Nodes were created manually by keying in their coordinates, and by copying or reflecting existing nodes. Nodes are specified by their coordinates in an existing global coordinate system determined by the user. For the gun model, the coordinate system is predefined as global Cartesian. There is also the option to use a cylindrical or spherical coordinate system. A Computer Aided Design (CAD) of the entire gun was developed. The drawing was the result of information from the sight visit, technical manuals and blueprints. From the drawing, individual points were assigned to outline the various components. The coordinates of these points were keyed in as individual node coordinates. The model has 3750 nodes. The node points that were entered created a two dimensional model. The third dimension was generated by reflecting and copying the existing nodes.

C. ELEMENT CREATION

The manual method involves using the screen cursor to select nodes that define an individual element. For example, a solid linear brick was created by selecting 8 nodes in the proper sequence to form a single element. The building of all components could take advantage of the gun model's symmetry by creating a sector of a component, and then copying and rotating these elements to generate the remainder of the component. This results in fewer nodal coordinates having to be entered manually, and is an efficient way to build the model.

1. Element Attributes

Elements are described by a label, type, listing of nodes that form the element, display color, and the material and physical property table identification codes. These attributes can be modified after the element is created, with the exception of changing the element to a type described by a differing number of nodes. In conjunction with the creation of an element is the creation of its physical and material properties. In all cases the material properties were chosen to be isotropic steel. Physical property tables were tailored specifically to the individual elements, that is, a beam element's cross-section definition or a translational spring's stiffness value.

2. Element Compatibility

The gun model is made of several different element types. Therefore it is important to discuss element compatibility. The term compatibility applies specifically to the degrees of freedom (DOF) of the nodes of a respective element. Recall, the nodes of a beam element have six DOF, while the nodes of a solid linear brick have only three translational DOF. In order to ensure proper element behavior, nodes that are interconnecting between differing element types must be treated properly. In this case the incompatibility, 3 DOF versus 6 DOF, can be

overcome by constraint equations. The three rotational DOF of the beam must be constrained to the rotation of the edge of the brick element. This serves to force the beam's rotational DOF to be equal. The brick element's translational DOF normal to the edge would lie in the plane of the beam's rotated cross-section.

D. FUNCTIONAL DESCRIPTION

A brief functional description of the major components of the M61A1 will provide insight into the decisions made in the modeling of the individual components. Figure 3.1 is an assembly drawing of the M61A1 gun, and will be useful to visualize the interfacing of individual components. (Ref. 16)

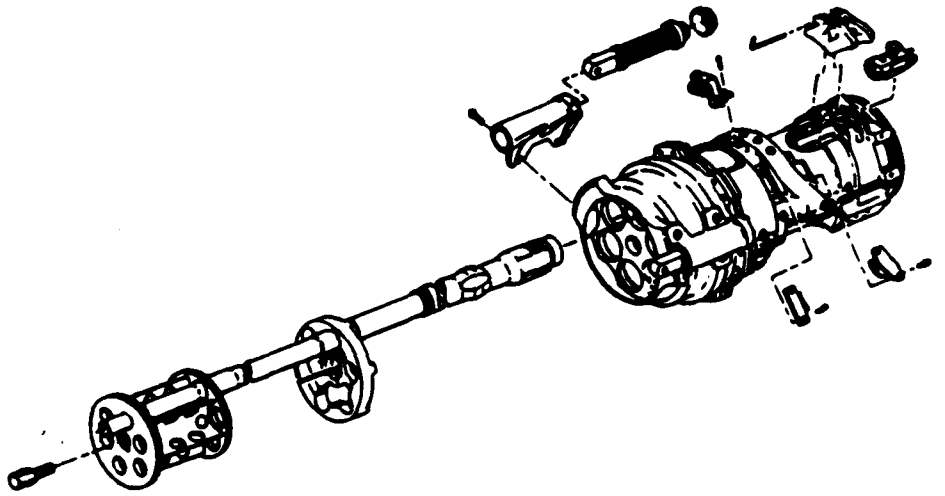

Figure 3.1. Assembly drawing of the M61A1.

1. Barrels

The gun incorporates six rifled barrels which are supported by a stub rotor enclosed in a bearing housing attached to the rotor assembly. Interrupted locking lugs on each barrel mate with similar interrupted locking lugs in the rotor body to secure the barrels. Knurled bands near the center of the barrels provide a convenient surface for handling the barrels during removal and installation. The barrels are designed to have a 0.8 degree inward cant.

2. Muzzle Clamp

The muzzle clamp assembly is positioned at the outer ends of the barrels. It sets the barrels' alignment and restricts barrel movement, thereby setting and maintaining projectile dispersion. The muzzle clamp assembly also aids the mid-barrel clamp in restraining individual barrel movement during firing. A self-locking nut assembly secures the muzzle clamp to the barrels.

3. Mid-barrel Clamp

The mid-barrel clamp is positioned near the center of the barrels, with the clamp tabs engaged in slots machined into the mid-point of the barrels. The clamp positions the six barrels for positive locking in the rotor assembly breech locking lugs and physically locks the six barrels together. This restrains individual barrel movement during firing.

4. Housing Assembly

The housing assembly is the primary unit of the gun and consists of an upper and lower section which are bolted and wire locked together. The housing and associated parts function to guide the breech through its correct fore and aft travel. The housing assembly consists of several components listed below.

a. Recoil Adapters

Recoil adapters reduce the amount of recoil and counter-recoil forces transmitted to the supporting structure when the gun is fired. There are two recoil mountings forward which are designed to transmit the recoil energy from the rounds being fired to "ground". The recoil adapters make up two of the gun's three point mounting system.

b. Ball Joint

The ball joint is the third mount. It supports the back of the gun, allowing the gun to translate axially with each round fired. A ball joint allows translation in the x direction and a limited range of rotations in all directions. The cup of the ball joint is an integrated part of the housing assembly cover plate. It is located on the gun's vertical center line 6.19 cm below the gun's horizontal center line. The cup is 4.3 cm deep, therefore it allows translation without the mount slamming into the housing assembly during firing.

c. Rotor

The rotor assembly is the major unit of the gun. It is hydraulically driven at a two speeds. At a firing rate of 3000 shots per minute (SPM), it rotates at 500 revolutions per minute (RPM) (8.3 Hz). At 4500 SPM, it rotates at 750 RPM (12.5 Hz). Theoretically, the maximum firing rate is 6000 SPM (100 Hz). The direction of rotation is counterclockwise, as viewed from the rear of the gun. The rotor functions to set the breech bolt assemblies into motion. This causes six basic actions: feeding, chambering, locking, unlocking, retracting, and ejecting of the MK 149 round.

d. Angular Contact Bearing and Needle Bearing

Front support of the rotor is provided by a double row angular contact bearing. Rear support is provided by a needle bearing. The needle bearing rides on an axle that is an integral part of the housing end-plate. The end-plate is attached to the aft end of the housing by a coupling clamp.

e. Stub Rotor

The stub rotor supports the breech end of the six barrels and permits easy alignment of the barrels to the rotor locking lugs. The stub rotor is welded to the rotor body.

f. Barrel Locking Lugs

Barrel locking lugs mate with the interrupted locking lugs on each barrel to physically lock the barrels to the rotor assembly.

E. MODEL COMPONENTS

In modeling the gun, there were necessary assumptions made to capture the gun in an "operating" condition. The recoil adapters allow translations and the ball joint allows rotations and translation. Therefore, it is necessary to choose initial displacement values for the nodes associated with these components.

The gun was modeled in a position consistent with displacements expected for a gun actually firing. Specifically, the ball joint was positioned at the geometric center of the cup, about 1.9 cm aft of the gun body. This assumption was based on the load deflection curve for the recoil adapters as shown in Figure 3.2. It is reasonable to presume that the design operating point would be in the center of the hysteresis loop. It is also known that the recoil adapters allow approximately 1.3 cm of gun travel. (Ref. 17)

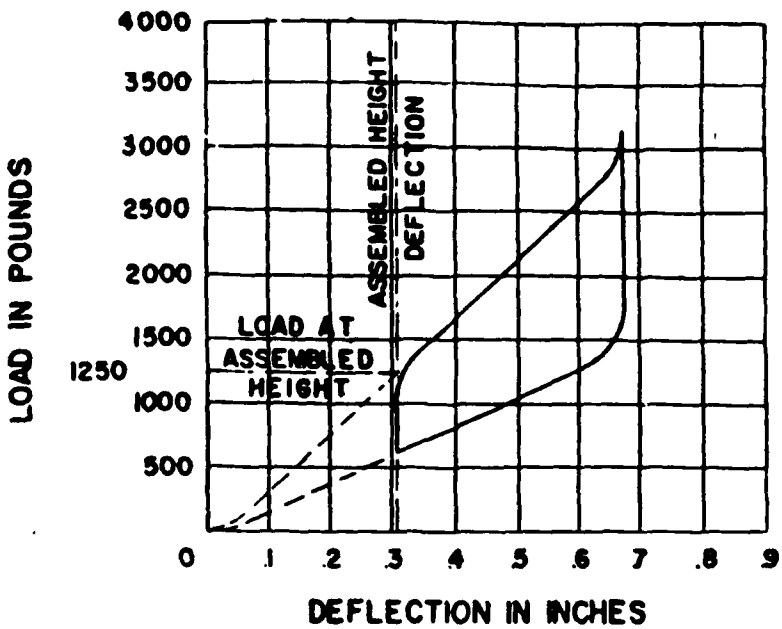

Figure 3.2. Load-deflection curve for M61A1 Recoil Adapters.

The gun model components are considered to be "new" with zero tolerance between them. Because of this assumption, the interconnection of certain components must be specifically addressed. The barrels' interrupted locking lugs are presumed to fit perfectly with those in the rotor. The interfaces between the barrels and the stub rotor, mid-barrel and muzzle clamps are connected with rigid elements. These rigid elements are connected from a barrel node, that lies halfway between the plates of the specific clamp, to six nodes on both the front and back sides of the respective plates as shown in Figure 3.3. Care was taken not to induce a moment at the interfaces so that the result is an ideal interface between the barrels and clamps.

The stiffness values for the bearings were derived for a specific load case. In order to get stiffness values from the bearing manufacturer, it is necessary to provide a specific loading of the bearing. The loading included the force of a single shot, gravity and a torque caused by a fluctuation of the rotor's rotational speed. This load condition is presumed to be a worse case. To determine the actual

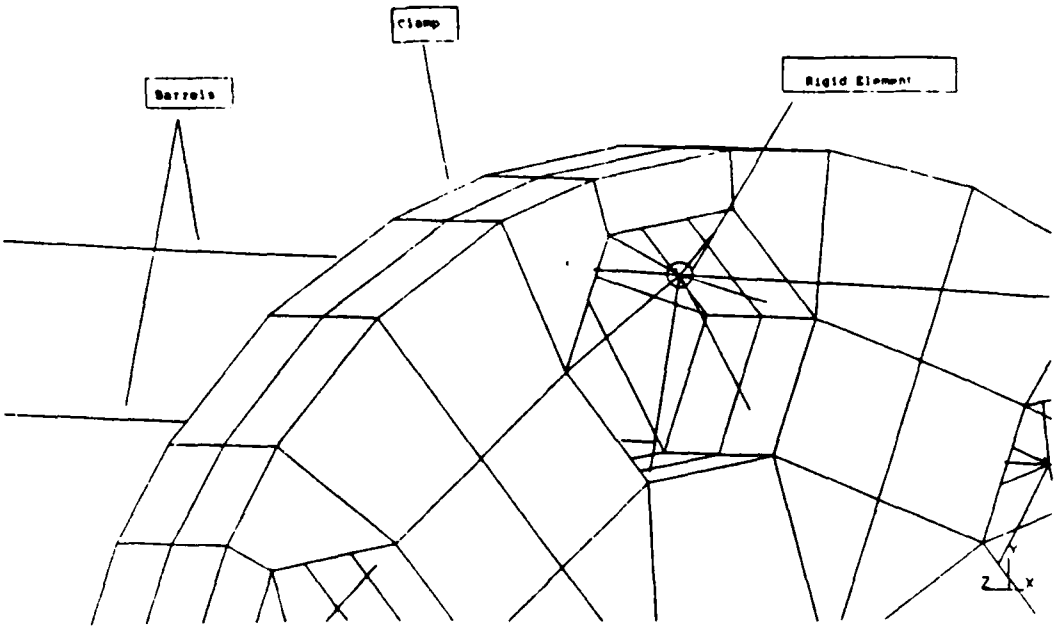

Figure 3.3. Barrel clamp interface.

loading of the bearing, the described load was applied to the gun model and reaction forces were measured at the respective bearing structures. The bearings were all assumed to be symmetrically loaded. This alleviated variations in stiffness and contact angle around the bearing's circumference.

The individual components of the gun were created and assembled, in a logical fashion, as they might be on an assembly line. The discussion below is a brief description of the "building" of these components, focusing on the element types selected for the representation. Figure 3.4 is an assembly drawing of the gun model.

1. Barrels

Two sets of barrels were created. The first set of barrels was created using solid linear bricks. A high element density was used, in order to capture the barrels exact geometric characteristics. However, the resulting barrel was

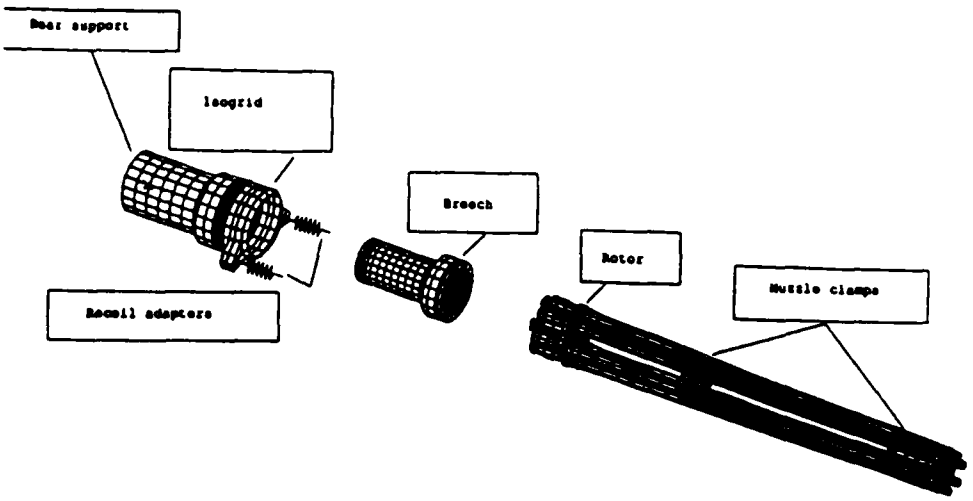

Figure 3.4. Assembly drawing of the PHALANX gun.

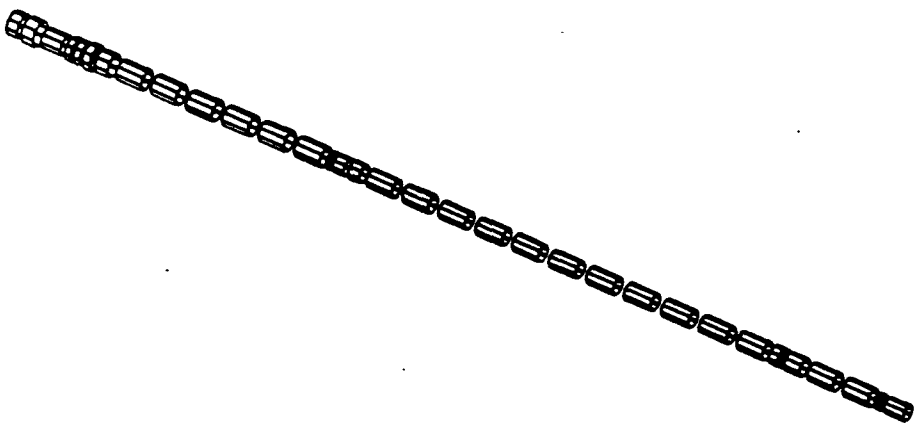

Figure 3.5. Single PHALANX barrel.

comprised of 400 elements. For a single component this was excessive. In order to stay within the DOF budget, an alternate approach was considered. The barrels were modeled using beam elements with various tubular cross-sections to represent the elasticity and structural mechanics of the actual barrel. The cross-section's parameters are the inner and outer diameters of the tube. There are 39 beam elements in a barrel with tubular cross-sections of varying thicknesses. It was

important to have a sufficient number of beam elements to ensure that the variations in the cross-sections of the original barrel were represented, and to have enough nodes to provide smooth mode shapes. For all cross sections of the barrel, the inner diameter was 2 cm. The outer diameter varied in each beam section consistent with the barrel's thickness at the respective length. There were eight different beam cross-sections representing the various changes in the barrels' thickness. TABLE 3.1 lists the eight different cross sections used. Figure 3.5 shows a single barrel using a special display option that shrinks the elements to allow inspection of individual elements. Another display option displays the tubular cross-section. In reality, a beam element is defined by only two nodes, and the element is normally displayed as a single line between the respective beam element's nodes.

TABLE 3.1. BARREL BEAM CROSS SECTIONS

Cross-Section Description
5.1 × 1.5
5.6 × 1.8
4.0 × 1.0
4.8 × 1.4
3.3 × 0.7
3.1 × 0.5
3.4 × 0.7
2.6 × 0.3

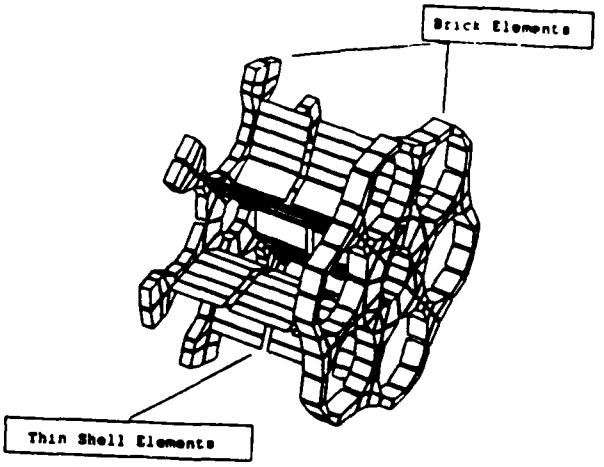

Figure 3.6. Stub Rotor.

2. Stub Rotor, Muzzle and Mid-barrel Clamps

The muzzle clamps, mid-barrel clamps, and stub rotor provide rigidity to the six barrel system. The clamps and the stub rotor themselves are relatively thick elements. It can be expected that their first flexible modes of vibration will be high. Their role in a dynamic analysis is strictly their mass and inertia contribution to the six-barrel system stiffness. The components themselves will not be excited based on the low frequency of the excitation force. The decision was made to use solid linear brick elements to model the thick sections and linear quadrilateral thin shell elements to model the webbing between the plates of the muzzle clamp and stub rotor as shown in Figures 3.6, 3.7, and 3.8. These figures also have the element shrink switch "on", in order to highlight the difference in element types.

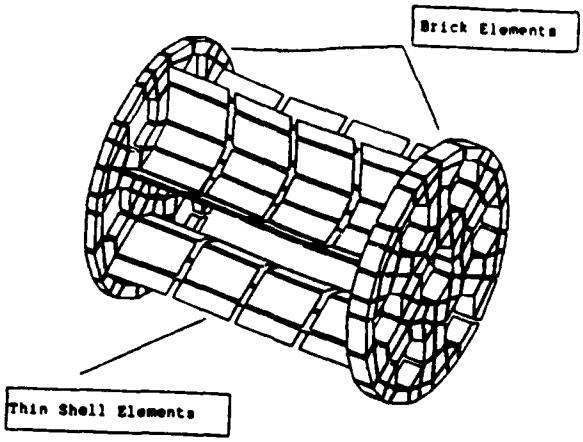

Figure 3.7. Muzzle Clamp.

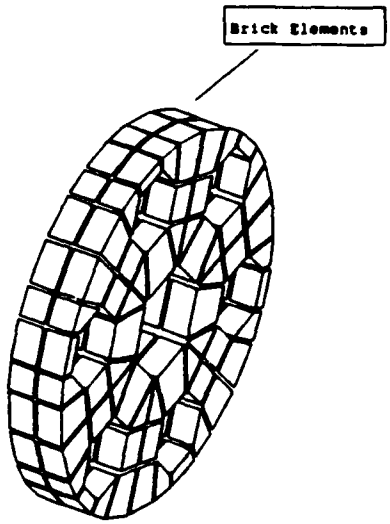

Figure 3.8. Mid-Barrel Clamp.

3. Housing Assembly

The model's housing assembly was constructed from linear quadrilateral thin shell elements. A value of 0.5 cm was entered in the physical property table to represent the thickness of the M61A1's casing. Figure 3.9 is an isometric view of the housing assembly. The additional housing assembly components are discussed below.

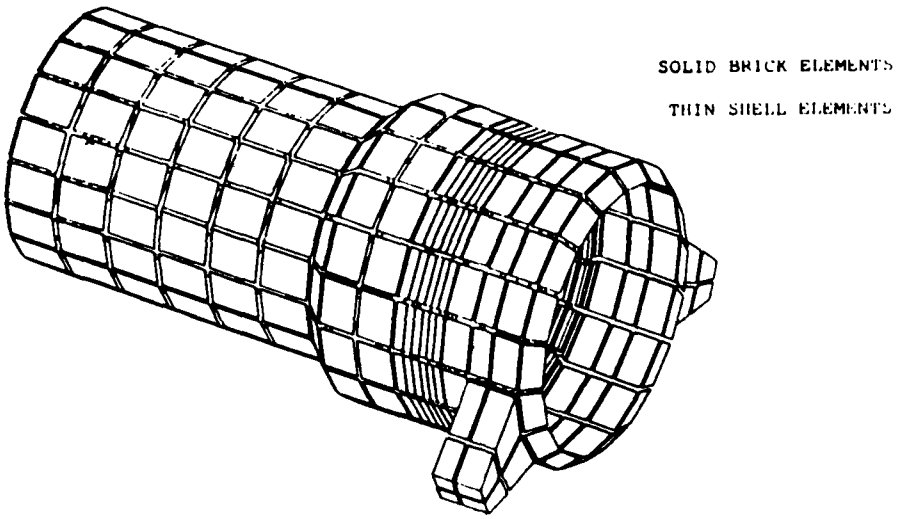

Figure 3.9. Housing Assembly.

a. Recoil Adapters

The recoil adapters were modeled using a variety of elements. The design emphasis was to properly model the recoil adapter stiffness and the geometry of its mounting. The stiffness was a simple matter. A node-to-node translational spring was created between two nodes. One node at a point representing the mounting point of the recoil adapter to the forward yoke. The other at an arbitrary point in-line with the gun attachment point. From this latter node a rigid element, representing the high stiffness value of the recoil adapter's shaft was created. The rigid element connected the node-to-node translational SPRING to five nodes on the recoil adapter support structure as shown in Figure 3.10. The support structure was created, using solid linear elements and provides the proper geometry for the line-of-action of the recoil adapters.

The stiffness value for the recoil adapters was calculated by taking the mean value of the two slopes of the hysteresis loop shown in Figure 3.2. The resulting value was $5.9 \times 10^5 N/m$.

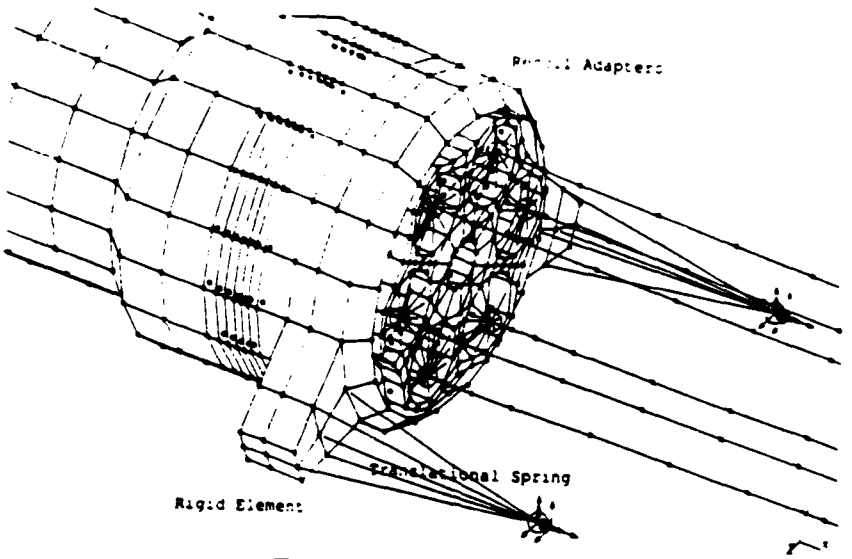

Figure 3.10. Recoil Adapters.

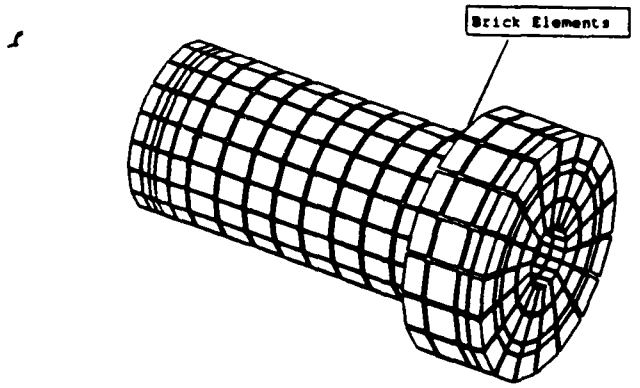

Figure 3.11. Rotor.

b. Rotor

The rotor shown in Figure 3.11 was created with solid linear brick elements. The rotor will not distort significantly from the low frequency excitation. However, the rotor does play an important role in providing a boundary condition for the six barrel system. All six barrels are locked into the rotor. The rotor is supported by two sets of bearings.

The bearings play an important role in understanding the behavior of the six-barrel system. By "eliminating" distortion of the rotor, the effects of the bearings can be fully realized.

c. Angular Contact Bearing and Needle Bearing

There are two sets of bearings in the gun contained in the housing assembly. The most important bearing in the gun is the double angular contact bearing. This bearing transmits the force of the firing rounds to ground via the recoil adapters. It also provides radial support to the forward portion of the rotor. The other bearing is a needle bearing located at the after end of the rotor. Its purpose is to provide radial support to the rotor as shown in Figure 3.12.

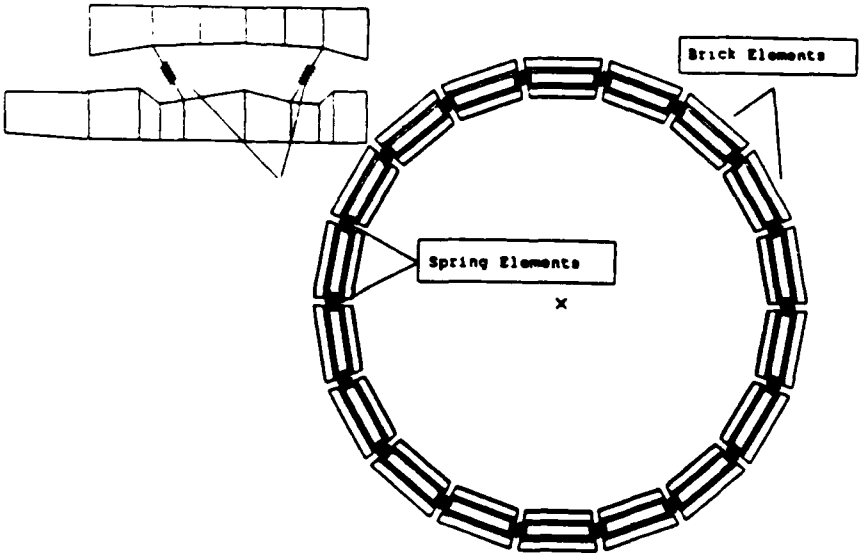

Figure 3.12. Double Row Angular Contact Bearing.

The angular contact bearing was modeled in great detail, because of its importance in the gun dynamics. The bearing's inner and outer races were modeled with solid linear brick elements. There are two rows of 18 elements around the circumference of the bearing. Eighteen elements was sufficient to maintain the bearing's round geometry and was a reasonable element density. The ball bearings were modeled using node-to-node translational springs connecting the

inner and outer races, representing the bearing's stiffness. The springs are oriented to accurately reflect the bearing's contact angle. The contact angle represents the line of action of the ball bearings between the inner and outer races.

All bearings have associated stiffness values depending on their loading. As discussed earlier, the bearing stiffnesses were computed for the gun in an operating condition and obtained from their respective manufacturers (Ref. 18 and 19).

A computer program was used to translate the actual bearing's axial and radial stiffness values provided by the manufacturer. The program iterated these two inputs to converge on a single stiffness value and contact angle for each of the 36 springs. The result is that the 36 springs represent the equivalent axial and radial stiffness values of the actual bearing. The actual stiffness value is $41.1 \times 10^9 \, N / m$, with a contact angle of 19.62 degrees (Ref. 20).

The needle bearing provides radial support to the after portion of the rotor. It was modeled with 18 node-to-node translational springs. The springs are evenly spaced around the circumference of the axle with a 20 degree angular separation. They are connected between the axle and the inner circumference of the aft portion of the rotor providing only radial support. Therefore, the springs are oriented in a vertical plane, with a contact angle of zero. Since, the needle bearing has no race, there was no attempt to model a needle bearing housing. The stiffness and support contributions were the important factors to model.

A simple hand calculation was used to translate the manufacturer's radial stiffness value to the model. The approach was to use Hooke's law and sum the forces around the circumference of the bearing. The variable **K** is the manufacturer's radial stiffness value and x is the displacement so that

$$\sum_{i=1}^{18} F_i = \mathbf{K}_i \, x \, .$$

From Figure 3.13, starting at the 12 o'clock position, the forces can be summed as follows:

$$F_1 = \frac{K}{\cos 0^o} x \quad ,$$

and

$$F_2 = \frac{K}{\cos 20^o} x \quad ,etc.$$

The effective stiffness value K_{EFF}, which is equal to

$$K_{EFF} = \frac{K}{f} \quad , \tag{3.1}$$

where f = Cos 0^o + Cos 20^o + Cos 40^o + Cos 60^o + Cos 80^o + Cos 100^o + ... Cos 340^o .

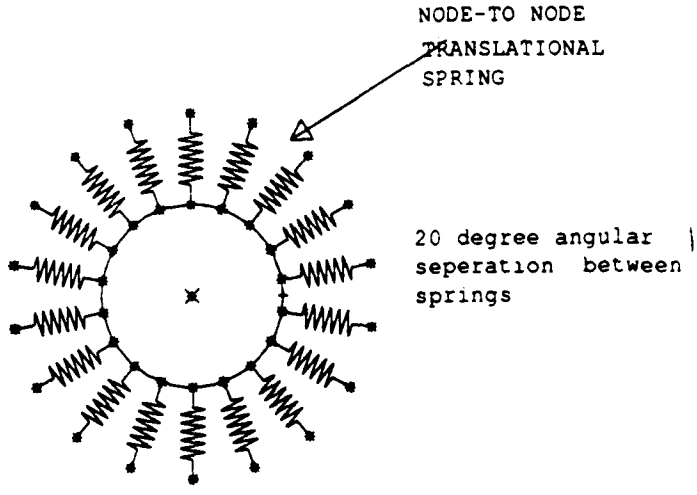

Figure 3.13. Needle Bearing Geometry.

The resulting stiffness value for the needle bearing springs is 21.2×10^6 N/m .

d. Barrel Locking Lugs

The barrel locking lugs were modeled using three nodes on the end of each barrel. The nodes are spaced consistent with the pitch of the locking lugs. These nodes have counterparts in the rotor. The barrels and rotor were aligned, and these nodes were merged. They are ideally fastened.

e. Ball Joint

The ball joint is a mounting or boundary condition. A decision was made to model the stiffness of the ball joint. The ball joint provides stiffness to the mounting equally in the Y and Z directions. It is not necessary to model the entire geometry. The stiffness of the ball joint is its significant contribution to the model. The local dynamics of the ball joint are unimportant. However, its kinematic contribution to the model is important.

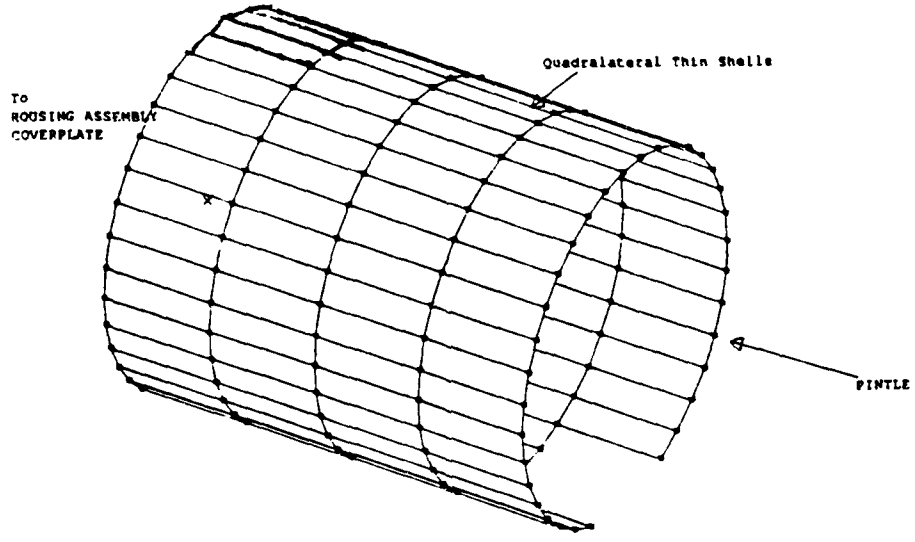

Figure 3.14. Finite element model of the ball joint cup.

A separate model of the ball joint cup was built using linear quadrilateral thin shells as shown in Figure 3.14. A linear static analysis was completed. A known force, F, was applied at a node, and the subsequent displacement, x, measured. The linear elastic stiffness of the cup, k_{cup}, was determined using

Hooke's Law, $F = k_{cup}\, x$, to find

$$k_{cup} = F/x \quad .$$

The resulting stiffness value, k_{cup} is 7.7×10^6 N/m.

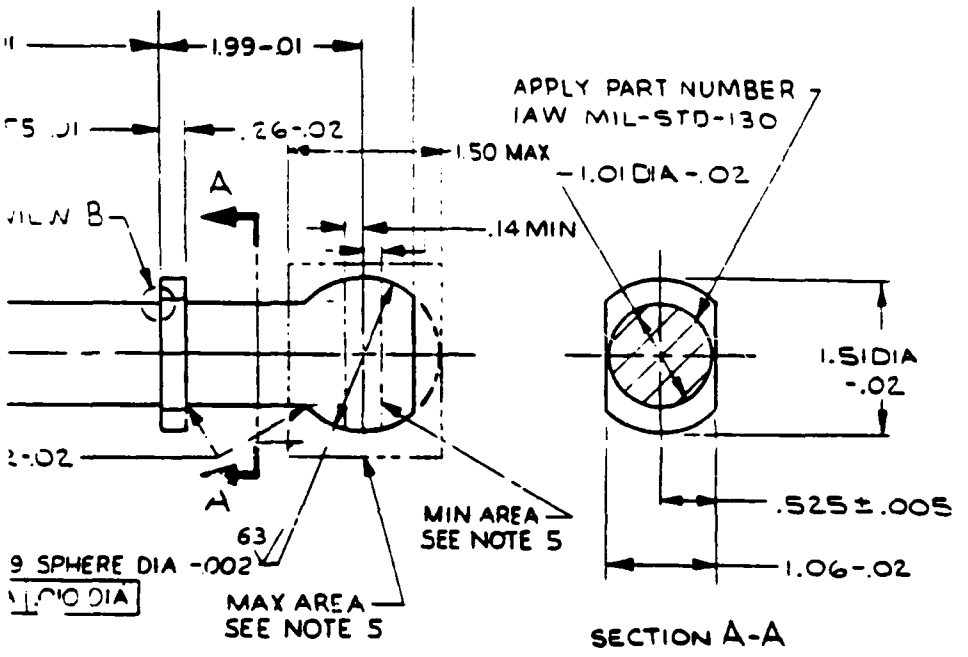

Figure 3.15. Ball Joint pintle.

It was also necessary to calculate the stiffness contribution of the pintle to the ball joint with a simple hand calculation. The pintle was approximated as a steel rod of length 4.4 cm and diameter 2.5 cm as shown in Figure 3.15. Using (3.2), the stiffness, k_{pintle}, was computed using a standard clamped-free cantilever beam equation,

$$k_{pintle} = \frac{3\,E\,I}{L^3} \quad , \tag{3.2}$$

where E is the modulus of elasticity of steel, I is the area moment of inertia about

an axis perpendicular to the pintle's length, and L is the length of the pintle. The resulting value of k_{pintle} is $155.5 \times 10^6 \text{N/m}$. The stiffnesses of the cup and the pintle were treated as two linear springs in parallel. Their stiffnesses are additive. The resulting equivalent stiffness for the ball joint is $163.0 \times 10^6\ N\ /\ m$ in both the y and z directions. The ball joint was simply modeled as a single node, two node-to-node translational springs, and a rigid element. The node is located at a position consistent with the gun in the "firing" position as discussed above in section E. This node was connected with a single rigid element to eight nodes on the back cover plate. This would simulate an even distribution of the load that the cup would impose on the housing assembly's cover plate. The two node-to-node translational springs have a stiffness value of $163.0 \times 10^6 \text{ N/m}$. The ball joint was simplified to one node and three elements as shown in Figure 3.16.

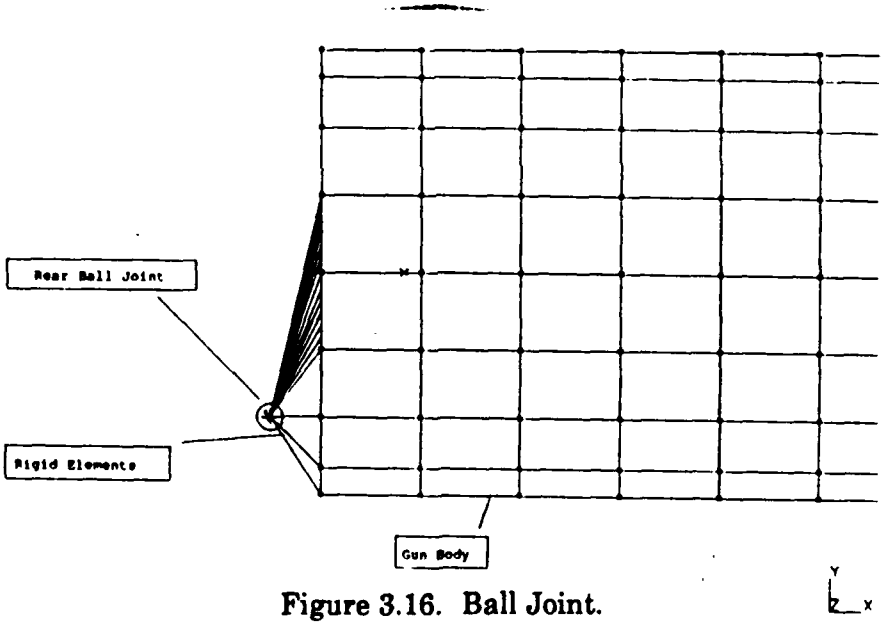

Figure 3.16. Ball Joint.

A comparison of some of the properties of the gun model to the actual M61A1 gun is summarized in TABLE 3.2.

These parameters are only a comparison of the solid properties. The model and the actual gun are geometrically in close agreement. However, this is important in determining the natural frequencies, there are an infinity of mass and

TABLE 3.2. MODEL COMPARISON.

	Mass (kg)	Center of Gravity (cm)			Moment of Inertia (kg-m^2)		
		$C.G._x$	$C.G._y$	$C.G._z$	I_{xx}	I_{yy}	I_{zz}
M61A1	113.5	53.83	0.04	0.0	6796	$2.38e^5$	$2.38e^5$
Model	120.5	55.2	-0.304	-0.053	7240	$2.59e^5$	$2.60e^5$
% Diff.	5.81	2.48	5.75	5.40	6.13	8.01	8.40

stiffness values that could result in a specific natural frequency. The correlation of these mass values is very important. It bounds the particular stiffness values that result in the natural frequencies from the eigenproblem. The ultimate comparison is in the mode shapes and frequencies between the model and the actual gun.

F. GROUPING

A group is a user defined subset of elements in the model. Groups are used to simplify selection of particular elements, for display flexibility and analysis. They provide a better understanding of an existing model. In the gun model, there are 21 groups that identify each individual component of the gun as well as subassemblies. The six barrels, the muzzle and mid-barrel clamps form the six-barrel system group seen in Figure 3.17. The use of groups allows the model to be easily modified and analyzed.

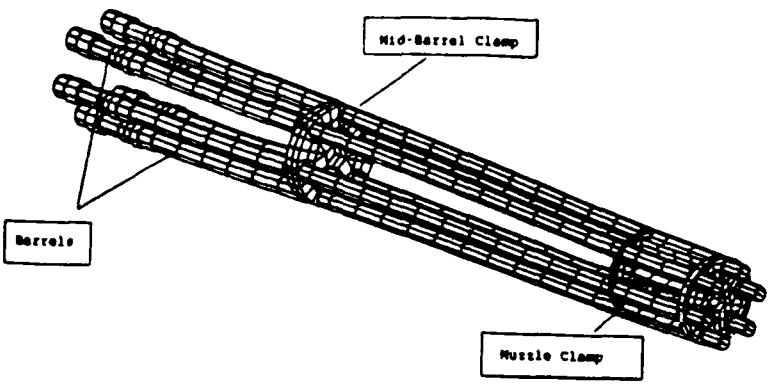

Figure 3.17. Six-Barrel System Group.

G. ELEMENT QUALITY CHECKS

I-DEAS has several features to help identify glaring modeling errors. It is important to realize that these checks will not reveal errors in the selection of elements or element density. They are designed to make sure the model is "clean". Typical problems that may arise are duplicate nodes, duplicate or missing elements, and element distortion. Consulting I-DEAS FINITE ELEMENT Manual under element quality checks will provide more details on these options. Below is a brief description of the quality checks that were used in forming the gun model. (Ref. 21)

1. Free Edge Check

The element free edge check displays the boundaries of a model. This can quickly alert the user to any missing elements or connectivity problems.

2. Element Distortion

Element distortion is another important check. The result of the check is a quantitative listing for each element in the model with values ranging from -1.0 to 1.0. A value of 1.0 represents a perfect square shape while values less than 0.0 are unsatisfactory. Acceptable values are between 0.5 and 1.0. Typical results for the gun model were between 0.6 and 1.0 with the majority around 1.0. Element distortion plays an important role in a stress analysis model so that highly distorted elements in areas of high stress concentration should be avoided. Some distorted elements can not be avoided due to the geometry being modeled. (Ref. 22)

3. Coincident Node Check

Coincident nodes can be identified and eliminated as a part of cleaning up the model. These extra nodes add unnecessary size to the stiffness matrix increasing the run time. A node is considered coincident, if it is within a user determined distance of another node. The nodes that are identified can be automatically deleted and the program will automatically merge adjacent elements to share the same nodes.

H. BANDWIDTH MINIMIZATION

A large model has many nodes and elements used to represent the system. This results in many system equations. It is difficult to find a numerical solution if the equation matrix is full. The accuracy will improve if the matrix has its non-zero terms clustered near the diagonal. This reduces the number of operations and the roundoff error carried along in each operation.

In FEM the node or element numbering pattern can strongly influence the bandwidth. A well planned numbering sequence can minimize the matrix bandwidth. The term bandwidth applies to the characteristic bandwidth of the global stiffness matrix. The elements of the stiffness matrix tend to lie along a

band centered about the matrix' diagonal. Outside the band the elements are zeroes. There are two general methods for setting up the order of the equations in assembly of the global stiffness matrix. One uses the node number numerical sequence and the other uses the element number numerical sequence.

1. Node Resequencing

Node resequencing is automatically conducted by the model solve command. The width of the band is determined by the sequence of the node numbers. If the size of the band can be minimized, the solution time will be reduced and the accuracy improved. Figure 3.18 shows two different node sequences for the same structure, and their resulting stiffness matrices. Notice the structure with resequenced nodes has a much narrower bandwidth, therefore shorter run time. (Ref. 23)

2. Wavefront Optimization

Wavefront optimization is a function of the element numbering and can also reduce run-time. Wavefront pertains specifically to the bandwidth of the stiffness matrix using an element numbering sequence. Figure 3.19 shows two different element sequences and their associated stiffness matrices. The structure with resequenced elements has a narrower wavefront. (Ref. 24)

I. BOUNDARY CONDITIONS

Boundary conditions are imposed conditions on the boundaries of the model. These imposed conditions can be in the form of an enforced displacement or an applied force on a specific nodes. The boundary conditions of the gun model are in the form of enforced displacements or restraints. Prior to solving any model, the boundary conditions must be specified such that rigid body motion is prevented. The gun model has three mounting points that hold it in space, preventing rigid

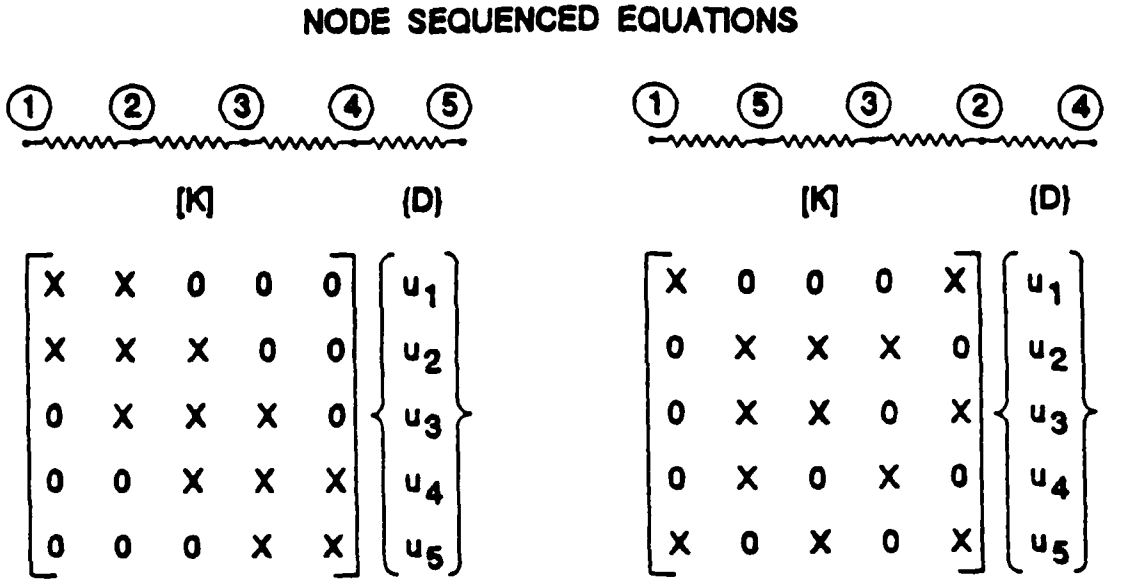

Figure 3.18. Bandwidth of Stiffness Matrices.

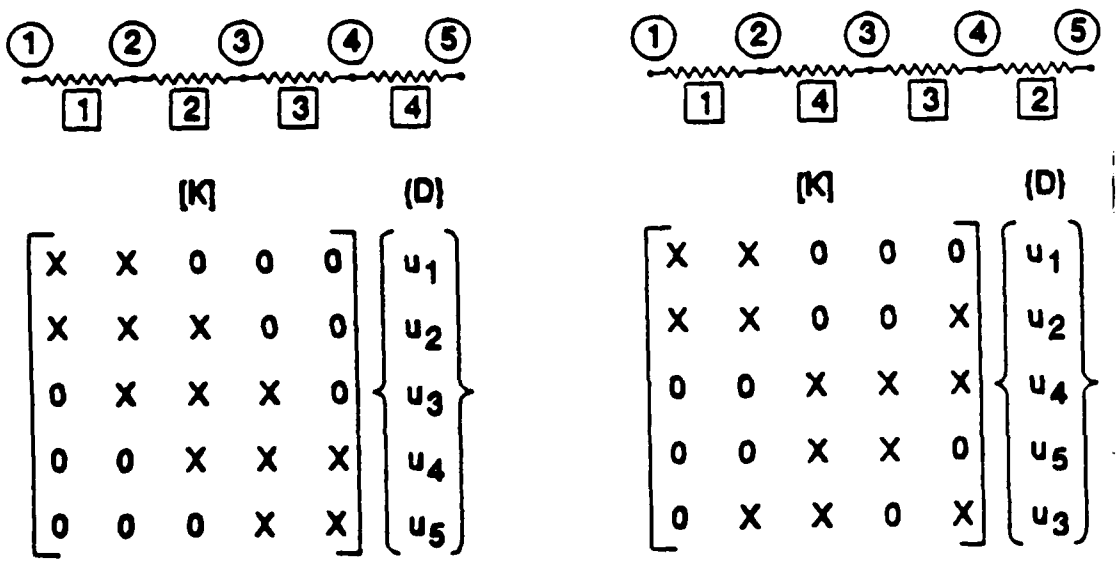

Figure 3.19. Wavefront of Stiffness Matrices.

body motion. However, the rotor and six-barrel system are free to rotate. This is a problem, because a solution for normal modes, with rigid body motion, will result in a singularity in the stiffness matrix and prevent the solution from converging. To ensure a converged solution, Kinematic Degrees of Freedom (KDOF) must be applied. This is discussed further in the Degrees of Freedom section below.

Boundary conditions also provide a means to model functions of certain components. Specifically, the muzzle clamp is designed to prevent rotations of three of the six barrels and allow three to be free. Deactivating a specific DOF can be used to represent this problem.

1. Restraints

Restraints serve to anchor the model to ground. Restraints at a particular node are determined by two inputs. First is the user enters one of two values, 0.0 for restrained displacement or "free" for the degree of freedom to move, for each of the six DOF. The gun model has one restraint set which consists of the restraints of several different nodes. The restraints applied to the gun model are at the nodes connecting the recoil adapters to ground. These nodes have all DOF restrained except for rotation about the z axis and x translation as shown in Figure 3.20. This mimics the pinned connection of the recoil adapters to the forward yoke, and allows the translations of the recoil adapters. The other restraints involved restraining the node-to-node translational springs used in the ball joint and recoil adapters to ground. These specific nodes have all DOF restrained.

The restraints at a particular node are indicated by single and double headed arrows. A single headed arrow indicates that the translation in the particular direction is restrained, and a double headed arrow indicates that the rotation is restrained.

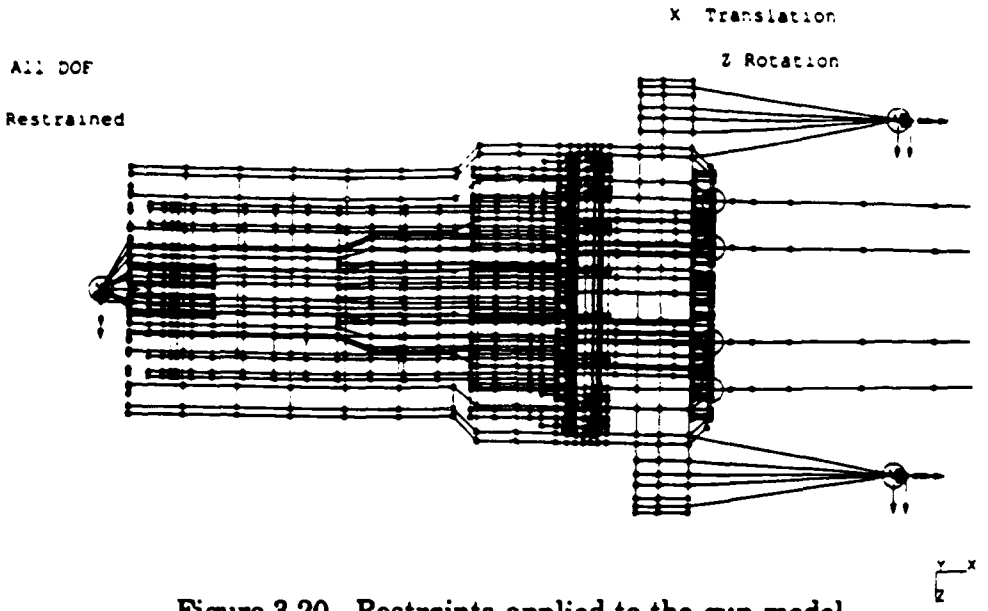

Figure 3.20. Restraints applied to the gun model.

2. Degrees of Freedom

Degrees of freedom sets are created to identify special DOF in a model, and the gun has 22,500 physical DOF. This number is a summation of the DOF of all the nodes in the model. The DOF a particular node has is determined by the element family.

In the model the gun bearings are formed using springs. Therefore, the rotating assembly does not have true rigid body motion. If the rotating assembly wants to rotate, the springs of the bearing generate strain energy. The rotating assembly is not allowed to rotate fully and freely. However, this quasi-rigid body motion is undesirable in the normal mode solution. There are four Kinematic DOF (KDOF) assigned in order to remove the quasi-rigid body mode of the rotor / barrel cluster assembly. This mode is valid in a dynamic system, but there must be enough KDOF assigned such that if they act as restraints they will "restrain" out the motion. Four nodes were chosen at the rotor's mid-point and 90 degrees relative to each other. In order to remove this rotational rigid body mode, two

nodes have the translation in the y direction and two have the translation in the z direction chosen, such that if they act as restraints the motion is eliminated.(Ref. 25)

The six nodes that represent the attachment point of three gun barrels to the muzzle clamp have their x rotation DOF deactivated. This prevents the rotation of three barrels about their longitudinal axis. This is a design condition that is imposed by the muzzle clamp. Every other barrel is free in this respective direction.

3. Case Set

Prior to solving a model, a case set must be defined. A case set identifies the DOF sets, restraint sets, and load sets as applicable. The gun model case set consists of one restraint set and one dof set, as described in the paragraphs above.

J. SOLUTION

The I-DEAS FEM module solves for the normal mode dynamics, which includes the mode shapes and natural frequencies. The mode shapes can be stored and later used for creating a modal representation of the gun model.

The Simultaneous Vector Iteration (SVI) method was used to solve for the normal mode dynamics. The SVI method is the most efficient method for large DOF models. It also allows for the solution of a model that has rigid body modes. Although the rigid body motion has been "restrained" out of the model, it is still considered to be a rigid body mode for solution purposes.

The SVI solution allows the user to select the number of flexible modes and to identify the number of rigid body modes. The solution algorithm has a fully automated iteration vector calculation. With the solution options set for one rigid body mode and 20 flexible modes, the program iterates the equations of motion until it converges on the solution. The gun model solution takes approximately 8

hours on a SUN MICROSYSTEMS MULTI-PROCESSOR WORKSTATION. The solution completes 10 iterations to converge on the 21 modes. A general outline of the SVI algorithm follows.

The solutions to eigenvalues, each with a natural frequency, can be formulated in terms of the stiffness matrix $[\mathbf{K}]$.

$$[\mathbf{M}^{-1}]\ [\mathbf{K}]\ \{\mathbf{X}\} = \lambda \{\mathbf{X}\} \tag{3.3}$$

where $\lambda = \omega^2$ is the eigenvalue. With this basic equation, the algorithm will iterate and converge on a value for the eigenvalue λ and the eigenvectors $\{\mathbf{X}\}$. The steps are below.

1. Arbitrarily assume a value for $\{\mathbf{X}\}$.

2. Substitute $\{\mathbf{X}\}$ into the following equation:

$$\lambda \{\mathbf{X}\} = \begin{Bmatrix} \lambda x_1 \\ \lambda x_2 \\ \lambda x_3 \end{Bmatrix}. \tag{3.3.a}$$

3. Normalize the vector from step 2.

4. Use the normalized vector as an imposed value of $\{\mathbf{X}\}$ and substitute into (3.3).

5. Carry out the matrix multiplication, approximating $\{X\}$

6. Repeat until two consecutive iterations converge to the same value for $\{X\}$, and the equation is satisfied.

The final normalizing factor to which the iteration process converges is the eigenvalue, λ, and $\{X\}$ is the associated eigenvector. (Ref. 26)

This method takes advantage of the orthogonality of the eigenvectors which represent mode shapes. After the first eigenvalue and eigenvector is found, the solution begins with an assumed vector that is orthogonal to the first. In addition, the eigenvector from the first solution is "swept" from the solution. This prevents the first eigenvector from influencing the second. This procedure is continued until the desired number of modes is solved.

K. FREE VIBRATION AND MODAL ANALYSIS

The solution of normal mode dynamics involves solving the eigenvalue problem for an entire system. An n DOF system has n natural frequencies, and for each natural frequency has a corresponding normal mode shape. The normal modes define a particular relationship between the amplitudes of oscillations of the coordinates. The squares of the natural frequencies and the corresponding coordinate values of the mode shapes are the eigenvalues and eigenvectors, respectively.

Consider 1 element from the discretized rod of Chapter I. Each element has two nodes and two DOF. The resulting stiffness and mass matrices are 2 x 2. The resulting equation of motion for free vibration is as follows.

$$[M]\{\ddot{X}\} + [K]\{X\} = 0. \tag{3.4}$$

Define the nodal displacement vector $\mathbf{x}(t)$

$$\mathbf{x}(t) = \begin{Bmatrix} x_1(t) \\ x_2(t) \end{Bmatrix} ,$$

and assume a solution of the form

$$\left\{\mathbf{x}(t)\right\} = C\ \phi(x)\, e^{i\omega t} ,$$

where C is a complex constant, ϕ is a spatial vector, and ω is proportional to the natural frequency. Taking the appropriate derivates and substituting into equation (3.4) yields

$$\left[-\omega^2 \left[\mathbf{M}\right] \left\{\phi\right\} + \left[\mathbf{K}\right] \left\{\phi\right\}\right] C\ e^{i\omega t} = 0 . \tag{3.5}$$

The problem is to find non-trivial values of ω (eigenvalues) and the corresponding eigenvectors, ϕ. The resulting set of linear homogeneous equations has solutions, if the determinant of the coefficients is zero. The values of ω satisfying this are the eigenvalues of the problem. Corresponding to each eigenvalue there is at least one eigenvector. The determinant is

$$Det\left(\left[\mathbf{K}\right] - \omega^2 \left[\mathbf{M}\right]\right) = 0 , \tag{3.6}$$

and the result is a polynomial in ω. The non-trivial solution of the eigenvalue problem is found by solving for the roots of the characteristic equation

$$\left(\left[\mathbf{K}\right] - \omega^2 \left[\mathbf{M}\right]\right) = 0.$$

In this case, since there are two DOF there will be two eigenvalues. To determine the respective eigenvectors, the eigenvalues are substituted back one at a time into (3.7) to find

$$\left[-\omega^2 \left[\mathbf{M}\right] + \left[\mathbf{K}\right]\right] \left\{\phi\right\} = 0 . \tag{3.7}$$

The resulting eigenvectors are a corresponding set of relationships between the unknown ϕ_i values. The eigenvectors describe the normal mode shapes, corresponding to the natural frequencies. For the first normal mode ω_1, the result is

$$\frac{x_2}{x_1} = \phi_1{}^1 \ ,$$

and for the second normal mode ω_2 the result is

$$\frac{x_2}{x_1} = \phi_1{}^2 \ .$$

The mode shape vector ϕ is typically normalized with respect to the maximum displacement component in the vector. For example if $x_1 = 1$, the resulting eigenvectors are

$$\phi^1 = \begin{Bmatrix} 1 \\ \phi^1 \end{Bmatrix} \quad \phi^2 = \begin{Bmatrix} 1 \\ \phi^2 \end{Bmatrix}.$$

There are alternative normalization methods. For example, the vectors could be normalized such that the resulting modal mass is equal to one.

$$\phi_i{}^T [\mathbf{M}] \, \phi_j = 1, \text{for} i = j.$$

where $\phi_i{}^T$ is the transpose of ϕ. The transpose of a matrix is defined as

$$A_{ij}{}^T = A_{ji} \ .$$

A unique feature of the eigenvectors is that they are orthogonal to one another. The SVI solution method takes advantage of this characteristic in the iteration of normal modes. Basically there are two orthogonality relationships involving the normal modes. One involves the mass matrix [M], the other the stiffness matrix [K]. The relationships are easily developed starting with (3.7) and the fact that [M] and [K] are real symmetric matrices, and are equal to their respective transposes. Consider two different mode shapes i and j, denoted on

their respective eigenvectors as superscripts. Substituting each of these one at a time into (3.7) results in

$$\left[\mathbf{K}\right]\left\{\phi^i\right\} = \omega_i{}^2 \left[\mathbf{M}\right]\left\{\phi^i\right\} , \qquad (3.8)$$

$$\left[\mathbf{K}\right]\left\{\phi^j\right\} = \omega_j{}^2 \left[\mathbf{M}\right]\left\{\phi^j\right\} . \qquad (3.9)$$

Multiply (3.8) by the transpose of $\left\{\phi^j\right\}$ and (3.9) by the transpose of $\left\{\phi^i\right\}$ giving

$$\left\{\phi^j\right\}^T \left[\mathbf{K}\right]\left\{\phi^i\right\} = \omega_i{}^2 \left[\mathbf{M}\right]\left\{\phi^i\right\}\left\{\phi^j\right\}^T , \qquad (3.10)$$

$$\left\{\phi^i\right\}^T \left[\mathbf{K}\right]\left\{\phi^j\right\} = \omega_j{}^2 \left[\mathbf{M}\right]\left\{\phi^j\right\}\left\{\phi^i\right\}^T . \qquad (3.11)$$

Rearranging, these become

$$\left\{\phi^j\right\}^T \left[\mathbf{K}\right]\left\{\phi^i\right\} = \omega_i{}^2 \left\{\phi^j\right\}^T \left[\mathbf{M}\right]\left\{\phi^i\right\} . \qquad (3.12)$$

$$\left\{\phi^i\right\}^T \left[\mathbf{K}\right]\left\{\phi^j\right\} = \omega_j{}^2 \left\{\phi^i\right\}^T \left[\mathbf{M}\right]\left\{\phi^j\right\}. \qquad (3.13)$$

Subtracting (3.13) from (3.12) results in

$$0 = \left[\omega_i{}^2 - \omega_j{}^2\right] \left\{\phi^j\right\}^T \left[\mathbf{M}\right]\left\{\phi^i\right\} . \qquad (3.14)$$

If $\omega_i{}^2 \neq \omega_j{}^2$ then $i \neq j$, and the result is

$$\left\{\phi^j\right\}^T \left[\mathbf{M}\right]\left\{\phi^i\right\} = 0 . \qquad (3.15)$$

Considering two modes $i = 2$ and $j = 1$, results in

$$[\phi_1{}^1 \quad \phi_2{}^1] \begin{bmatrix} m_{11} & m_{12} \\ m_{21} & m_{22} \end{bmatrix} \begin{Bmatrix} \phi_2{}^2 \\ \phi_2{}^2 \end{Bmatrix} = 0 .$$

The first mode is orthogonal to every other mode. The eigenvectors are basis vectors that represent a dynamic state of the system. The two conditions for orthogonality are summarized as follows:

$$\left\{\phi^j\right\}^T \left[\mathbf{M}\right] \left\{\phi^i\right\} = 0 \quad \text{for } i \neq j, \text{ and} \tag{3.16}$$

$$= M \qquad \text{for } i = j . \tag{3.16.a}$$

Similarly, it can be shown that

$$\left\{\phi^j\right\}^T \left[\mathbf{K}\right] \left\{\phi^i\right\} = 0 \quad \text{for } i \neq j, \text{ and} \tag{3.17}$$

$$= K \qquad \text{for } i = j . \tag{3.17.a}$$

where M is modal mass, and K is modal stiffness.

The orthogonality relationships are fundamental to decoupling equations of motion. Considering the entire continuous rod element as a system, the resulting equations of motion are coupled. In the case of the continuous rod, the system is considered to be statically coupled. The global stiffness matrix [K] is nondiagonal. To decouple these equations of motion, it is necessary to perform a linear transformation. The transformation involves the creation of a modal matrix, [Φ]. The modal matrix is a square matrix, in which the columns correspond to the eigenvectors of the system. For a system with n DOF

$$[\Phi] = \left[\left\{\phi\right\}_1 \cdots \left\{\phi\right\}_n \right] .$$

The uncoupling of the equations of motion in terms of the mode shapes simplifies the analysis of a multiple-degree-of-freedom system. The process is called modal analysis.

Solving the eigenvalue problem for free vibration, results in the solution of the normal modes and natural frequencies. The eigenvalues are proportional to the natural frequencies f_i

$$f_i = \frac{\omega_i}{2\pi}$$

Where $\omega_i{}^2$ is the eigenvalue equal to

$$\omega_i{}^2 = \frac{\mathbf{K}_i}{\mathbf{M}_i} \quad .$$

The corresponding mode shapes are the eigenvectors.

Starting with the free vibration equation of motion

$$\left[\mathbf{M}\right]\left\{\ddot{\mathbf{X}}\right\} + \left[\mathbf{K}\right]\left\{\mathbf{X}\right\} = 0 \quad , \tag{3.18}$$

assume a solution of the form

$$\left\{\mathbf{X}\right\} = \left[\Phi\right]\left\{q\right\} \quad , \tag{3.19}$$

where $\left\{q\right\}$ is a sinusoidal temporal term. For an elastic mode q has the form

$$q = A\cos\omega t + B\sin\omega t \quad .$$

For a rigid body mode, q has the form of a polynomial. ω is the square root of the eigenvalue. Taking the appropriate derivatives of (3.19) and substituting into (3.18) results in

$$\left[\mathbf{M}\right]\left[\Phi\right]\left\{\ddot{q}\right\} + \left[\mathbf{K}\right]\left[\Phi\right]\left\{q\right\} = 0 \quad . \tag{3.20}$$

Multiplying by the transpose of the modal matrix gives

$$\left[\Phi\right]^T \left[\mathbf{M}\right] \left[\Phi\right] \left\{\ddot{q}\right\} + \left[\Phi\right]^T \left[\mathbf{K}\right] \left[\Phi\right] \left\{q\right\} = 0 \ . \tag{3.21}$$

The result is the following diagonalized matrices:

$$\left[\Phi\right]^T \left[\mathbf{M}\right] \left[\Phi\right] = \begin{bmatrix} \mathbf{M}_i & 0 \\ 0 & \mathbf{M}_j \end{bmatrix} = \left[\mathbf{M}\right]$$

the diagonalized mass matrix, and the diagonalized stiffness matrix

$$\left[\Phi\right]^T \left[\mathbf{K}\right] \left[\Phi\right] = \begin{bmatrix} \mathbf{K}_i & 0 \\ 0 & \mathbf{K}_j \end{bmatrix} = \left[\mathbf{K}\right] \ .$$

The result is a set of uncoupled second-order ordinary differential equations,

$$\left[\mathbf{M}\right] \left\{\ddot{q}\right\} + \left[\mathbf{K}\right] \left\{q\right\} = 0 \ . \tag{3.22}$$

The equation representing the ith row is a scalar second-order ordinary differential equation,

$$M_{ii} \ \ddot{q}_i + K_i \ q_i = 0 \ . \tag{3.23}$$

Multiplying by $1/M_{ii}$ gives

$$\ddot{q}_i + \frac{K_i}{M_{ii}} \ q_i = 0, \text{ and} \tag{3.24}$$

$$\ddot{q}_i + \omega_i^{\,2} \ q_i = 0 \ . \tag{3.25}$$

If the eigenvectors had been normalized according to unit modal mass, (3.25) would have resulted directly.

The result is an equation of motion for a one DOF simple harmonic oscillator with angular frequency ω_i. The resulting natural frequency, f, is

$$f_i = \frac{1}{2\,\pi} \sqrt{\omega_i^{\,2}} \ . \tag{3.26}$$

The associated column of the modal matrix is the corresponding mode shape. For a system of n DOF there are n such equations. It follows that the undamped free vibration of an n DOF system can be described using

$$\begin{Bmatrix} x_1 \\ x_2 \\ x_3 \\ . \\ . \\ . \\ x_n \end{Bmatrix} = [\Phi] \begin{Bmatrix} q_1 \\ q_2 \\ q_3 \\ . \\ . \\ . \\ q_n \end{Bmatrix},$$

where x_i are generalized coordinates used to describe the vibratory motion.

The greatest advantage of modal analysis is its use to determine the response of forced systems. This topic will be discussed in the following chapter. The same approach is used, but the right-hand-side term in the equation of motion is no longer zero.

IV. DYNAMIC ANALYSIS

A. INTRODUCTION

A structure that experiences a time varying load will also have a time varying response. For time varying loads at low frequency, the response is approximated by the static solution in proportion to the load. Low frequency is considered to be less than one third of the lowest natural frequency of the structure (Ref. 27).

However, when the load varies more rapidly, inertial effects and damping effects must be considered. This chapter presents the types of dynamic analyses that can be done, and the factors involved in performing a finite element analysis for the dynamic problem. The element structural formulations and classifications remain valid.

The response of a forced system depends primarily upon the system's natural frequencies, the damping present and the characteristics of the excitation. If a periodic excitation contains a frequency component that has the same frequency as one of the system's natural frequencies, a condition of resonance occurs. The displacement amplitude response of a system excited at one of its natural resonant frequencies, becomes infinite for an undamped mode. The corresponding stresses and strains will ultimately lead to nonlinear behavior and material failure of the structure.

Dynamic analysis allows for a quantitative understanding of the response of a system subjected to various load conditions. Specifically, I-DEAS allows the user to apply excitation forces in either the time or frequency domain to obtain zero, first, or second order responses of displacement, velocity, or acceleration for any or all nodes. The response can be displayed either in the time or frequency domain, consistent with the excitation force. The particular application for the M61A1

model involved the zero-order displacement response in both the time and frequency domains. The next chapter will address the specific results of the forced response of the model.

The foundation of dynamic analysis is the creation of an analytical modal component. An analytical modal component is a numerical representation of the model using its natural mode shapes. The model is transformed from the physical to the modal domain. In the physical domain, the model has 22,500 DOF. In the modal domain, the number of DOF is chosen by the user based on specific criteria to ensure the model's behavior is properly represented. The criteria for selecting modes is discussed in Section E. The M61A1 will use 21 modal DOF. Reducing the number of DOF makes the computation of a response a more manageable task for the computer's algorithm.

The frequency content of the excitation force determines the range of modes used to form the analytical modal component. The modes that are within this range must be carefully analyzed through animation to ensure that they reflect reasonable gun behavior. Problems in displaying a mode's animation may result in modifications to the model's mesh or boundary conditions.

The theory of modal analysis in both the time and frequency domains will be outlined in the final section of the chapter. The most common type of dynamic analysis is the natural frequency analysis, or the normal mode dynamics discussed in Chapter III. This is the undamped free vibration response of the structure caused by an initial disturbance from the static equilibrium position. Theoretically, if any structure is initially deformed into one of its mode shapes, when released, it would continue to vibrate in that mode shape indefinitely.

This chapter will focus on the steady-state response of the structure to a harmonic force. In frequency response analysis, the displacement, velocity, and acceleration responses of the structure to a harmonic input are also harmonic and occur at the same frequency. The displacement amplitudes define the deformed

structural shape. It is generally not the same shape as one of the natural mode shapes unless the frequency of the input coincides with the natural frequency.

If the input loading is not harmonic, but an arbitrary time dependent function, then a transient response analysis must be performed. One approach is simply a direct integration of the equations of motion, and another is modal analysis. The latter is the preferred method and the one used by I-DEAS. The basis of this approach is an assumption that the superposition of the mode shapes corresponding to the lower natural frequencies adequately represents the dynamic response of the structure. The complete response is found by the summation of linear combinations of the low frequency mode shapes.

Included in this chapter is a modal comparison of two single barrel computer models and an actual PHALANX gun barrel. Receipt of an actual single barrel provided the opportunity to conduct a modal test. Although, only a single barrel was tested, it provided an understanding into the importance of modeling decisions.

B. ANALYTICAL MODE SHAPES

The mode shapes are simply a set of relative node displacements, arbitrarily normalized with respect to the maximum displacement component of the individual eigenvectors. For I-DEAS, the maximum displacement is assigned 1 SI unit of displacement. (Ref. 28)

A mode shape can not be pictured simply from the frequency values. The graphic data file of mode shapes will consist of displacements and rotations, for every node in every DOF, for each of the natural frequencies. Each deformed mode shape must be examined for its ability to accurately predict the behavior of the mesh being used (Ref. 29).

In addition to a static display of mode shapes, I-DEAS has the ability to animate individual mode shapes. The animation of mode shapes provides insight into the model's behavior, and provides direct feedback for element selection and density.

Prior to solving the model for its normal modes, it is important to anticipate expected results using analytical solutions. Two vibrational modes and their are accompanying analytical solutions to their equations of motion evident based on the gun's mounting and bearing locations are described below.

The first example considers the simple recoiling of the entire gun with a single DOF. This problem can be reduced to a mass supported by two springs. The second example is more complex and considers the rotating assembly of the gun including barrels, clamps, rotor, stub rotor, and bearings. It is anticipated that there will be some coupled motion involving a translation perpendicular to the longitudinal axis of the gun and a pitching motion in the same direction. This would couple 2 DOF. Later in this section, several mode shapes from the model will be discussed. A comparison of these analytic solutions will be made to actual modes of the model. The SDOF calculation has a correlation to mode 3 and the lower frequency. The coupled 2 DOF problem, has a correlation to mode 9. The higher frequency in the 2 DOF problem was not matched. The frequency at 704 Hz was out of the range of interest. These calculations do not completely validate the model. Because of the assumptions made for the analytical solutions and the complexity of the model's dynamics, these calculations are estimated solutions. But, agreement between the analytical solutions and the simple modes is important to establish and gives insight to the solution.

1. Single Degree-of-Freedom

The schematic in Figure 4.1 is a simple representation of the gun recoiling where M = 120.5 kg is the mass of the entire gun, and $K_R = 5.9\times10^5$N/m is the elastic stiffness of a recoil adapter.

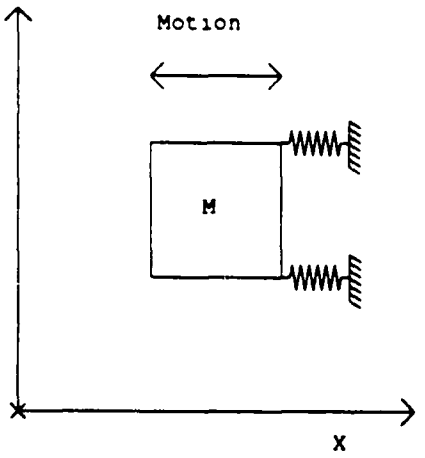

Figure 4.1. Schematic of a simple harmonic oscillator.

Starting with Lagrange's equation, the undamped free equation of motion can be developed using the actual gun's parameters. The goal is to predict the natural frequency of the mode. Lagrange's function L is shown in (4.1) where T is the kinetic energy and V the potential energy of the body of mass M.

$$L = T - V \ , \tag{4.1}$$

$$T = \frac{1}{2} M \dot{X}^2 . \tag{4.2}$$

Treating the two recoil adapters as two springs in parallel, their stiffness values are additive. The resulting potential energy is

$$V = \frac{1}{2} (K_R + K_R) X^2 . \tag{4.3}$$

Substituting into Lagrange's function gives

$$L = \left[\frac{1}{2} M \dot{X}^2\right] - \left[\frac{1}{2} (K_R + K_R) X^2\right] \quad . \tag{4.4}$$

Lagrange's equation of motion is

$$\frac{d}{dt}\left[\frac{\delta L}{\delta \dot{q}_i}\right] - \frac{\delta L}{\delta q_i} = 0 \quad . \tag{4.5}$$

where q_i and $\dot{q}_i$ are the generalized coordinates representing X and $\dot{X}$, respectively. Substituting (4.4) into (4.5), the resulting equation of motion is

$$M \ddot{X} + 2 K_R X = 0 \quad , \tag{4.6}$$

where the frequency of oscillation is seen to be

$$\omega = \left[\frac{2K_R}{M}\right]^{\frac{1}{2}} \quad .$$

Equation (4.6) represents the equation of motion for a single DOF harmonic oscillator. The angular frequency of oscillation is ω and the corresponding natural frequency is f

$$f = \frac{\omega}{2\pi}.$$

Substituting in the actual gun parameters, the natural frequency is found to be

$$f = 15.8 \text{ Hz} \quad .$$

2. Coupled Two Degrees-of-Freedom

The coupled two DOF problem depicts the motion of the gun pitching and translating in the x-y plane. The problem can be treated as a rigid mass that is supported by two springs and is allowed to translate and rotate about its center of gravity (CG). The motion of the mass couples 2 DOF because any vertical displacement in x results in a rotational displacement θ. To consider this motion, it is only necessary to examine the effects of the gun's rotating assembly of six

barrels, barrel clamps, rotor, stub rotor, and both bearings. It is assumed that it is rigid with a constant cross-section, and the mass that is evenly distributed. A schematic is provided in Figure 4.2 where M = 100 kg is now the mass of the rotating assembly, I_{zz} = 2.4×10^5 cm^2 kg is the mass moment of inertia about the Z axis with respect to the CG. L_1 = 25.6 cm and L_2 = 57.1 cm are the distances from the CG to the thrust and needle bearings, respectively. Assuming that displacements in θ are small, the small angle approximation is used and sin θ = θ.

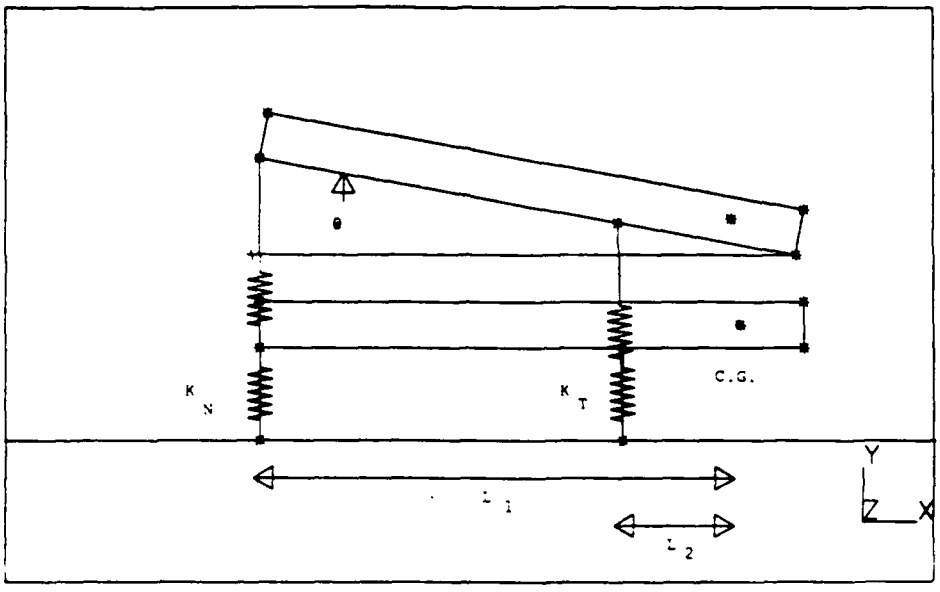

Figure 4.2. Coupled two DOF system.

Again returning to Lagrange's equation, the kinetic energy is

$$T = \frac{1}{2} M \dot{x}^2 + \frac{1}{2} I_{zz} \dot{\theta}^2 .$$

The potential energy contains the coupling of the rotational and translational generalized coordinates X and θ,

$$V = \frac{1}{2} K_N (L_2 \theta + X)^2 + \frac{1}{2} K_T (X + L_1 \theta)^2 ,$$

Where K_N = 507.4×10^6 N/m, and K_T = 654×10^6 N/m, are the equivalent radial stiffnesses of the needle and thrust bearings, respectively. The resulting equations of motion are

$$M\,\ddot{X} + K_T\,(L_1\,\theta + X) + K_N\,(X + L_2\theta) = 0 \quad \text{,and}$$

$$I_{zz}\,\ddot{\theta} + K_T\,L_1(L_1\,\theta + X) + K_N\,L_2(X + L_2\theta) = 0 \ .$$

Rearranging and collecting like terms gives

$$M\,\ddot{X} + X\,(K_N + K_T) + \theta\,(K_T\,L_1 + K_N\,L_2) \ , \tag{4.7}$$

and

$$I_{zz}\,\ddot{\theta} + X\,(K_T L_1 + K_N L_2) + \theta\,(K_T L_1^{\,2} + K_N L_2^{\,2}) \ . \tag{4.8}$$

The term proportional to $(K_T\,L_1 + K_N\,L_2)$ present in both (4.7) and (4.8) is referred to as the coupling term, coupling the θ and X displacements.

Using the following form for the time dependence of X and θ

$$X(t) = A\,\sin\omega\,t \ ,$$

gives

$$\ddot{X}(t) = -\,\omega^2\,X\,(t) \ ,$$

and

$$\theta(t) = B\,\sin\omega\,t \ ,$$

gives

$$\ddot{\theta}(t) = -\,\omega^2\,\theta\,(t) \ .$$

Substituting into (4.7) and (4.8) results in

$$A\,\sin\omega\,t\,(-\omega^2\,M + (K_T + K_N)) + B\,\sin\omega\,t\,(K_T L_1 + K_N L_2) = 0 \tag{4.9a}$$

$$A\,\sin\omega\,t\,(K_T\,L_1 + K_N\,L_2) + B\,\sin\omega\,t\,(-\omega^2\,I_{zz} + (K_T L_1^{\,2} + K_N L_2^{\,2})) = 0 \tag{4.9b}$$

Taking the determinant of the above system of equations gives

$$\begin{vmatrix} (-\omega^2\,M + (K_T + K_N)) & (K_T\,L_1 + K_N\,L_2) \\ (K_T\,L_1 + K_N\,L_2) & (-\omega^2\,I_{zz} + (K_T L_1^{\,2} + K_N L_2^{\,2})) \end{vmatrix} = 0 \ ,$$

which is quadratic in ω^2. Defining

$$K_S = (K_T L_1^2 + K_N L_2^2),\ K_E = (K_T + K_N),\ K_C = (K_T\ L_1 + K_N\ L_2),$$

the quadratic equation, (4.10), can be simplified so that

$$\omega^4 - \omega^2 \left[\frac{K_S}{I_{zz}} + \frac{K_E}{M} \right] + \frac{1}{M\ I_{zz}} \left[K_E\ \ K_S - K_C^2 \right] = 0 \ . \qquad (4.10)$$

The roots of (4.10) have positive and negative values of ω^2, but only the positive values of ω^2 have physical significance. Using the gun parameters, the results are

$$\omega_1^2 = 6.9\times10^5 \left[\frac{\text{rad}}{\text{sec}} \right]^2 ,$$

and

$$\omega_2^2 = 19.6\times10^6 \left[\frac{\text{rad}}{\text{sec}} \right]^2 .$$

The corresponding natural frequencies are:

$$f_1 = \frac{\omega_1}{2\pi} = 132 \text{ Hz} \ ,$$

and

$$f_2 = \frac{\omega_2}{2\pi} = 704 \text{ Hz} \ .$$

The mode shapes associated with these frequencies can be easily determined. Substituting ω_1^2 back into (4.9a) and (4.9b) results in

$$\begin{bmatrix} (-\omega_1^2 M + (K_T + K_N)) & (K_T\ L_1 + K_N\ L_2) \\ (K_T\ L_1 + K_N\ L_2) & (-\omega_1^2 I_{zz} + (K_T L_1^2 + K_N L_2^2)) \end{bmatrix} \begin{Bmatrix} X \\ \theta \end{Bmatrix} = 0$$

Substituting in values results in

$$\frac{\theta}{X} = 0.01 \ ,$$

for the first mode. Similarly for ω_2^2, the second mode is

$$\frac{\theta}{X} = -0.02 \ .$$

Normalizing these ratios by letting $X = 1$, the resulting eigenvectors or mode shapes are

$$\left\{\begin{matrix} X \\ \theta \end{matrix}\right\}_1 = \left\{\begin{matrix} 1 \\ 0.01 \end{matrix}\right\} ,$$

and

$$\left\{\begin{matrix} X \\ \theta \end{matrix}\right\}_2 = \left\{\begin{matrix} 1 \\ -0.02 \end{matrix}\right\} .$$

The first mode shape describes the system for undamped free-vibration at 132 Hz. Since the ratio is positive the system is pitching and heaving in phase. The second mode shape describes the system for undamped free-vibration at 704 Hz. Since the ratio is negative the pitching and heaving are 180 degrees out of phase.

These hand calculations have simplified the complexity of the actual gun dynamics. However, they still provide a crucial reference to compare the computer's results. The actual motion of this complex system will not be purely in any one mode, because the recoil adapters and bearings provide for extensive coupling of motion for all modes.

C. MODE SHAPES FOR THE M61A1 FINITE ELEMENT MODEL

With an understanding of two anticipated mode shapes and quantitative results for expected natural frequencies, the computer results for the gun model can be studied with more confidence. In all, 21 flexible modes were solved, with a range of frequencies from 14 to 308 Hz. Appendix B contains a set of all 21 modes, in ascending order by frequency, with x-y or side view. TABLE 4.1 is a listing of the frequencies of all modes in ascending order of frequency. A description of some of the lower order modes is discussed below including displays of the individual

mode shapes. All are isometric views with the maximum deformation represented as eight percent of the computer screen dimension. The dashed lines outline the boundaries of the undeformed model. These deformations are exaggerated for clarity and no attempt should be made to derive quantitative results from these mode shapes. Only the relative nodal displacements are accurate. Note also that the descriptive comments for each mode are provided through the benefit of viewing the animation of these modes.

TABLE 4.1. MODES 1-21 FOR THE M61A1 FINITE ELEMENT MODEL

Mode No.	Frequency (Hz)	Mode No.	Frequency (Hz)
1	3.3	11	179
2	14.4	12	231
3	15.5	13	243
4	16.0	14	246
5	35.3	15	254
6	55.3	16	255
7	111	17	274
8	116	18	274
9	129	19	289
10	165	20	308
		21	309

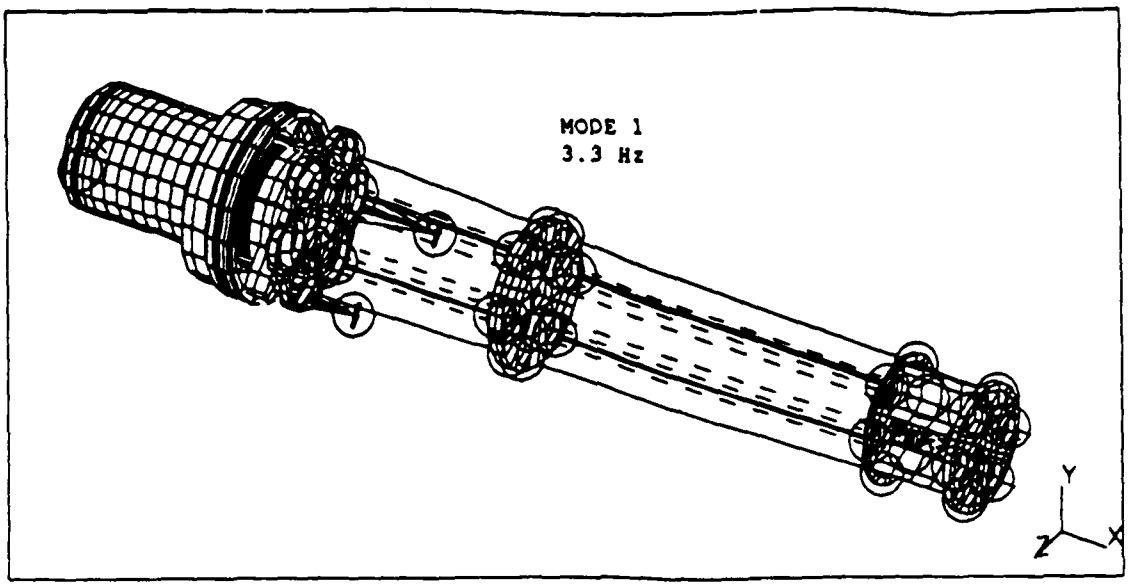

Figure 4.3. Isometric view of MODE 1.

1. MODE 1

Mode 1 at 3.3 Hz represents the rotation of the six-barrel assembly and is a computational artifact. Rotational motion should not generate any strain energy; it should be a rigid body motion of the rotating assembly. The use of translational springs to model the ball bearings in the gun's bearings introduces an artificial second order effect. As the rotating assembly rotates strain energy is being generated which results in a non-zero quasi-rigid body mode. In order to prevent this undesirable mode from corrupting the higher order flexible modes, it was restrained out using KDOF as discussed in Chapter III, Section I.2. The mode is treated as a rigid body mode for purposes of the solution.

Figure 4.3 is misleading. The computer's graphic interpretation has made it appear that the rotating assembly has swelled out of the housing. With the benefit of animation, the actual motion is depicted as a rotational oscillation of the rotating assembly about the gun's longitudinal axis.

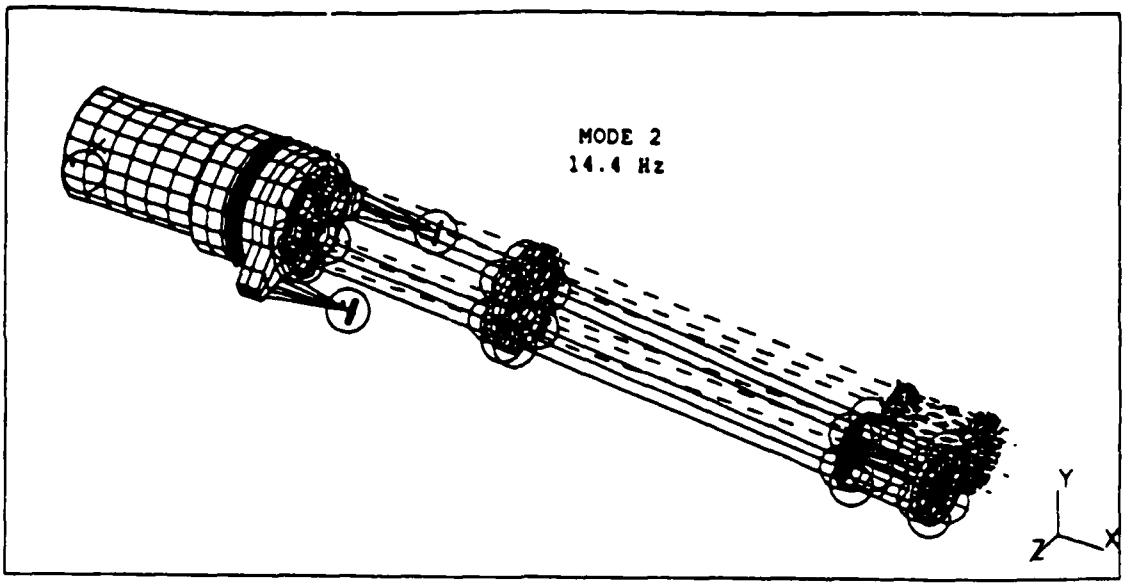

Figure 4.4. Isometric view of MODE 2.

2. MODE 2

Mode 2 the yawing mode at 14.4 Hz, and is the first actual flexible mode of the gun. The overall motion is the six-barrel system yawing in the x-z plane. The recoil adapters are not being exercised. There is localized deformation of the cover plate and the six barrels have no local deformation. It appears that the bearing stiffnesses play a significant role in this mode shape. Figure 4.4 shows the deformed geometry of mode 2.

3. MODE 3

Mode 3 is the recoil mode at 15.5 Hz, and exercises the recoil adapters in translation. The gun is translating in the fore and aft directions. However, the motion is not purely in the x direction. There is also a coupled pitching motion in the Y direction that is pronounced at the extremity of the recoil mode's translation. The rear cover plate is deformed as is the ball joint. The six-barrel system shows no deformation. This natural frequency is in close agreement with the hand calculation for the single DOF problem calculated above, at 15.8 Hz. Animation of

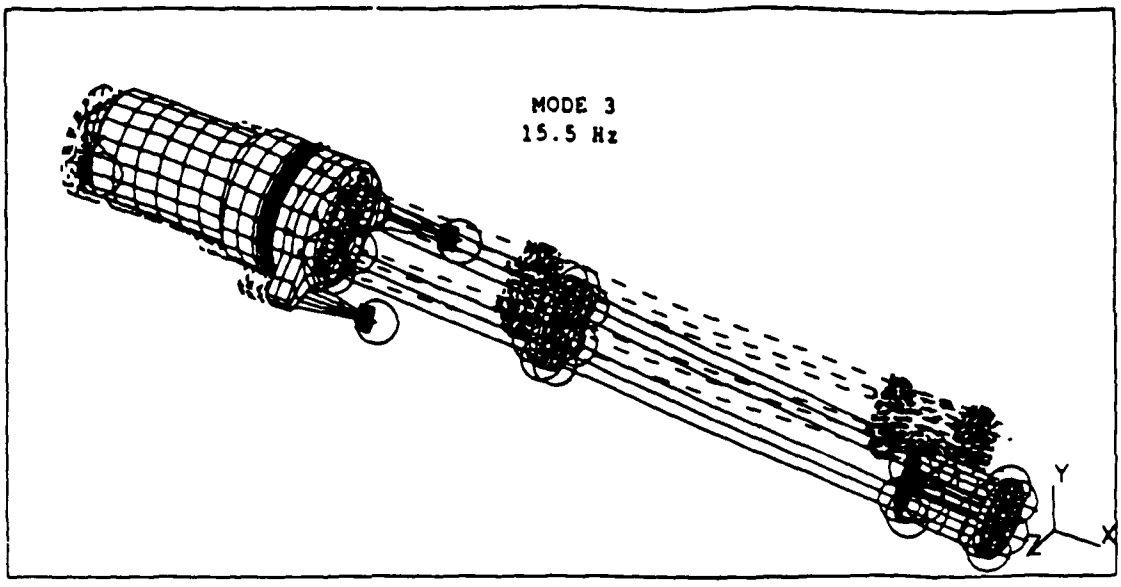

Figure 4.5. Isometric view of MODE 3.

mode 3 also verifies the recoil motion with a slight pitching of the six-barrel system as shown in Figure 4.5. This mode is a result of the way the gun is mounted.

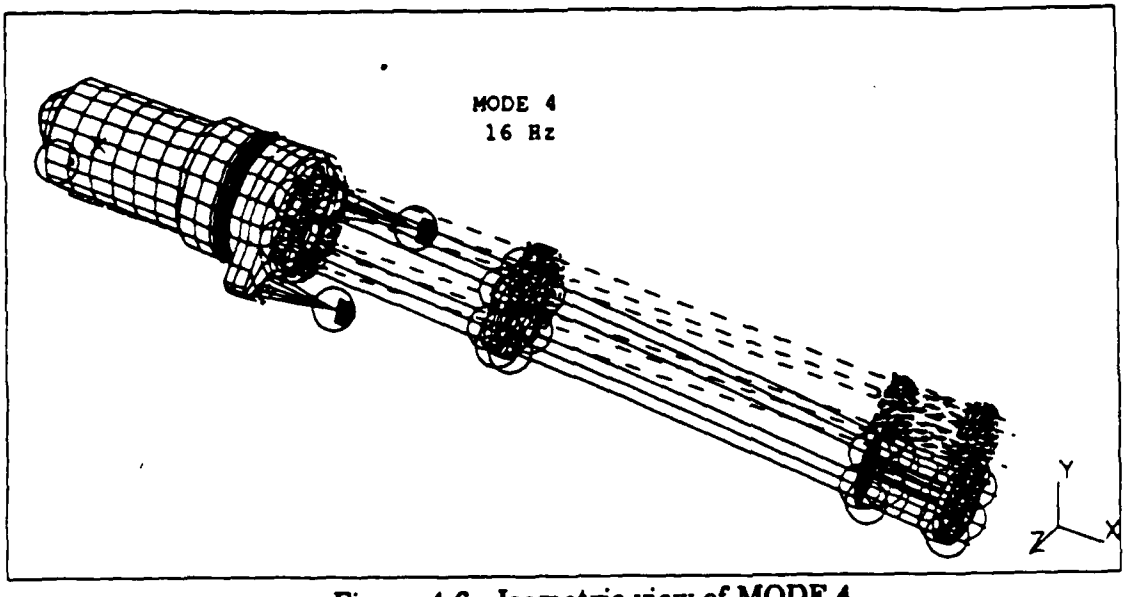

Figure 4.6. Isometric view of MODE 4.

4. MODE 4

Mode 4 is the pitching mode at 16.0 Hz, and is a rigid body pitching of the gun in the y direction. The recoil adapters are exercised moderately while the rear cover plate appears to be experiencing some plate bending. The six barrels show no local deformation as seen in Figure 4.6. It appears that this mode can also be attributed to the way the gun is mounted.

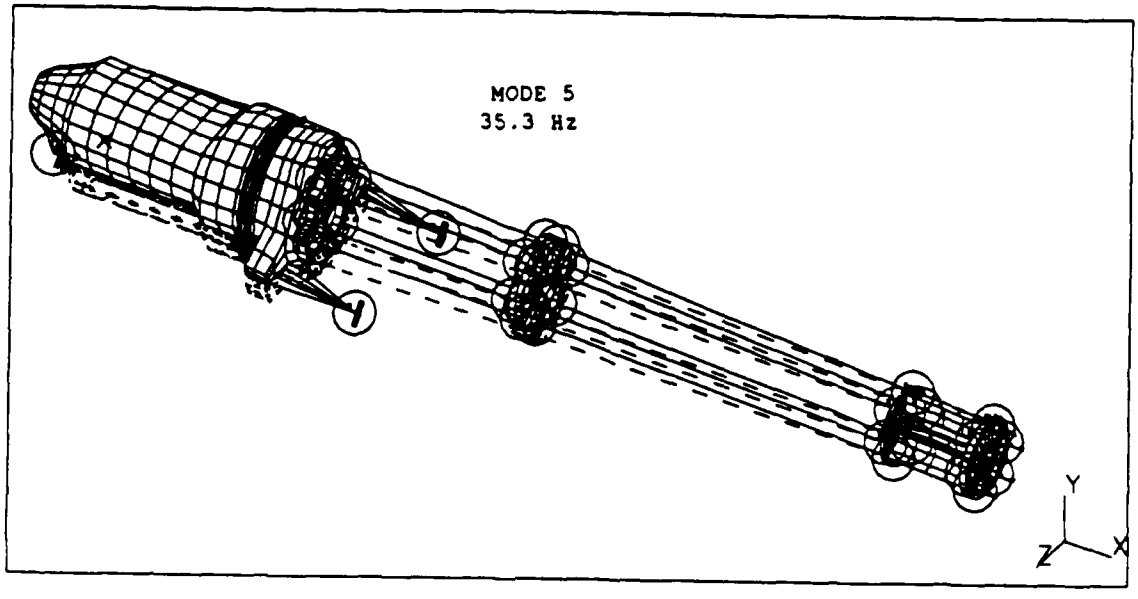

Figure 4.7. Isometric view of MODE 5.

5. MODE 5

Mode 5 is the rocking mode at 35.3 Hz, and is an overall rocking of the gun about the z axis at the center of gravity. The needle bearing and the rear cover plate are experiencing significant deformation. The recoil adapters are exercised as the pitching reaches the extremity of its range of motion. This mode involves the entire gun pitching in the x-y plane. Mode 4 involved pitching in a plane that was slightly rotated with respect to the y axis. The six barrels remain undeformed as seen in Figure 4.7. This mode can be also be attributed to the gun's mounting.

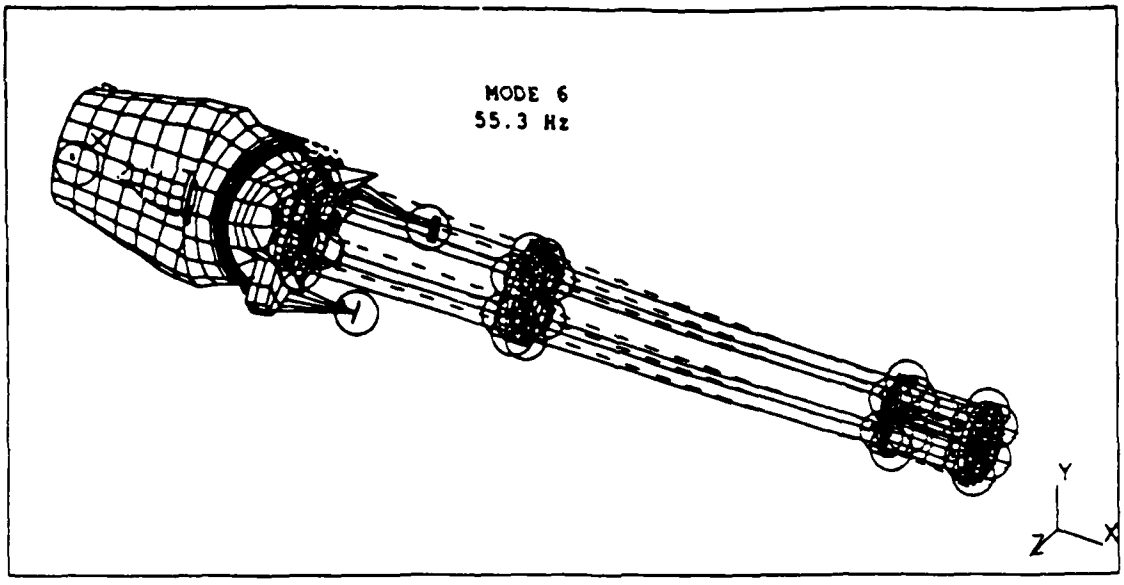

Figure 4.8. Isometric view of MODE 6.

6. MODE 6

Mode 6 is the ovalization mode at 55.3 Hz, and is an ovalization of the housing assembly. The recoil adapters are asymmetrically loaded and there is a significant bending of the rear cover plate. The six barrels show no local deformation as seen in Figure 4.8. This mode is attributed to the structural design of the housing assembly and its interface with the angular contact bearing.

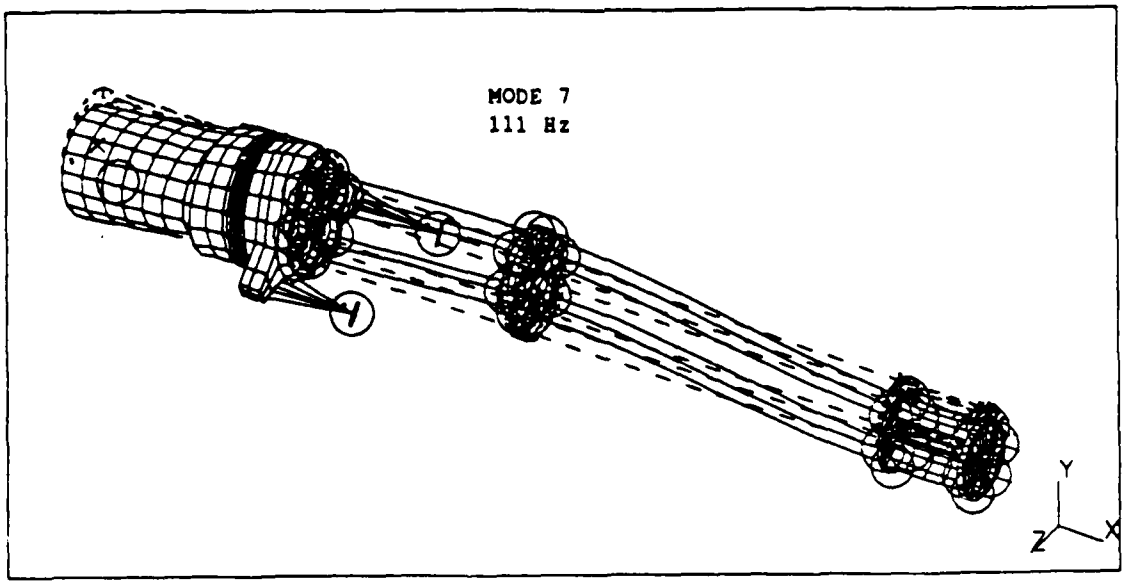

Figure 4.9. Isometric view of MODE 7.

7. MODE 7

Mode 7 at 110 Hz is the first mode to involve bending of the six barrels. The barrel clamps cause the six-barrel system to behave as a deep-flanged beam. The six-barrel system's first bending mode is a shear deformation. The significant deformation takes place forward of the mid-barrel clamp, and the muzzle clamp serves to maintain the relative positions of all six muzzle tips as seen in Figure 4.9. It is important to note that the first bending mode of the six-barrel system is at 110 Hz when they are attached to the gun system. If the six barrels and clamps are treated separately in a clamped-free condition, they have a natural frequency of only 35 Hz. The clamped-free condition represents the classic cantilever beam. One end of the beam is fully restrained in all DOF, and the other end is free in all DOF. This significant change in natural frequencies highlights the effect of the bearings and mountings on the six-barrel system. It confirms the decision to include the bearings and mountings in the analysis. The bearing structure and mountings have a profound impact on the modes of vibration of the six-barrel system. Mode 7 can be attributed to the stiffnesses of the barrel cluster and bearings.

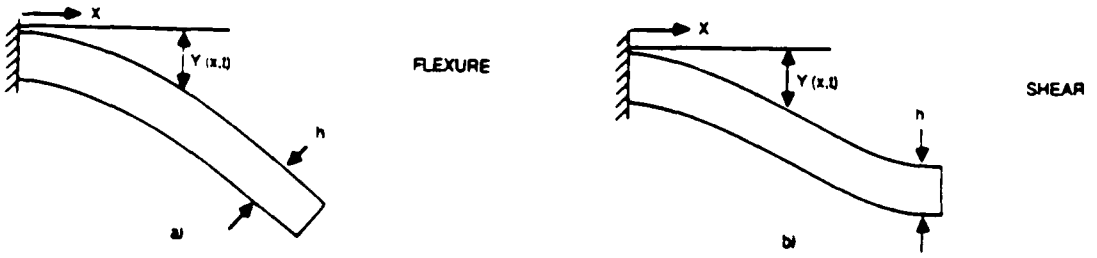

Figure 4.10. First mode of a clamped-free deep beam in a) flexure and in b) shear.

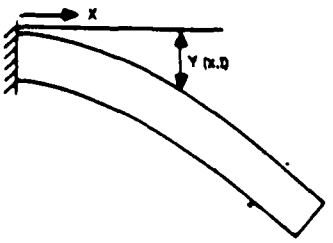

Figure 4.11. First bending mode of a clamped-free slender beam.

To elaborate on the comments above, a brief discussion is provided describing the deep-flanged versus slender beams, and the mechanisms of bending. Deep beams are those whose ratio of span length L to the depth H in the direction of vibrational deformation is not much greater than one, or maybe less than one. Shear deformation becomes important in deep beams, and is more dominant than flexural deformation. Figure 4.10 shows the first mode of a clamped-free deep beam in flexure and in shear. Notice the significant difference in the deep beam's bending mode due to shear versus flexure. The behavior of the deep beam is strongly dependent on the relative distance from the restraint. A slender beam's deformation is due to bending or flexing. A single barrel can be thought of as a slender beam with a tubular cross-section. Figure 4.11 shows the first bending mode of a single clamped-free slender beam due to flexure. (Ref. 30)

Figures 4.12 and 4.13 are the first bending modes of a clamped-free single barrel and clamped-free six-barrel system. Notice the similarity to the slender beam and deep-flange beam respectively.

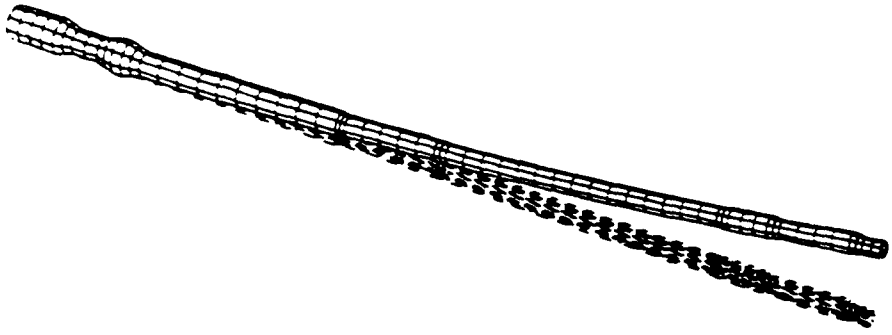

Figure 4.12. First bending mode of a clamped-free single barrel.

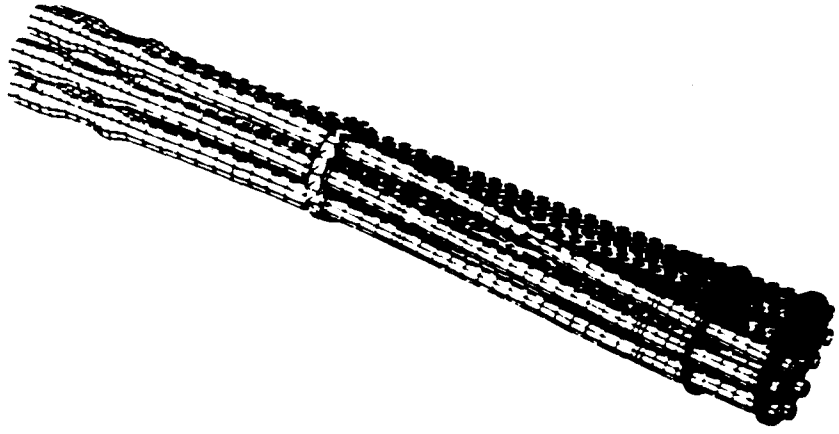

Figure 4.13. First bending mode of clamped-free six-barrel system.

8. MODE 8

Mode 8 at 116 Hz shows increased deformation of the six-barrel system. The recoil adapters are asymmetrically loaded and animation reveals pitching in the x-y plane. The line-of-motion is slightly rotated in the counter-clockwise direction from the y axis. The muzzle clamp maintains all six barrels in the horizontal plane. An increased amount of flexure is evident in the barrel group

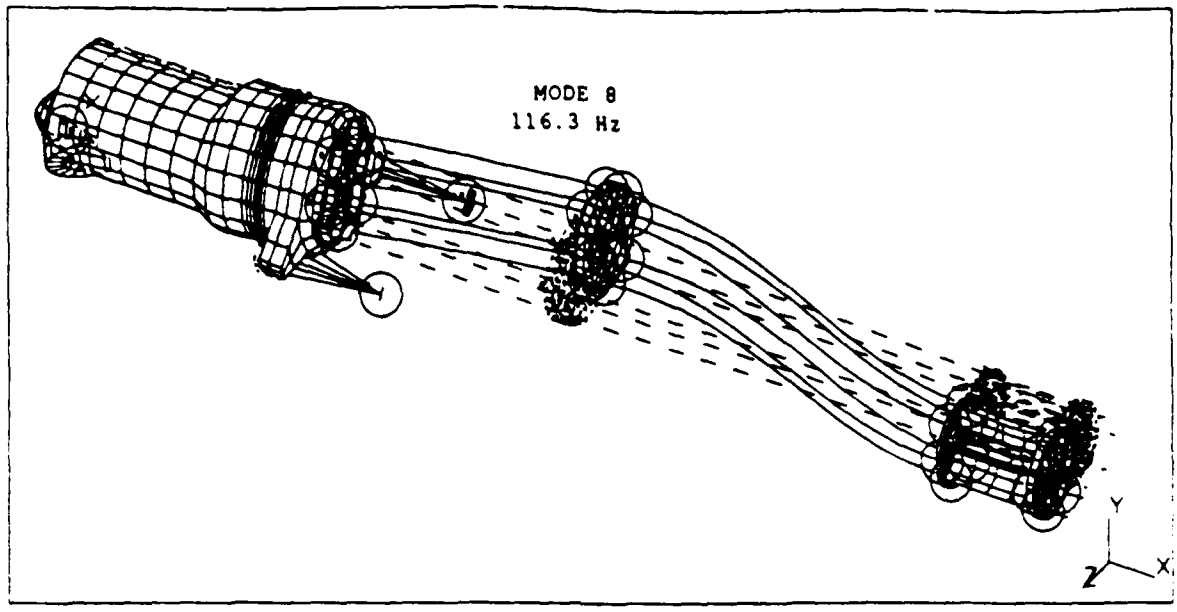

Figure 4.14. Isometric view of MODE 8.

while the housing has only slight deformation. However, the needle bearing axle has significant deformation. Mode 8 can be attributed to the barrel cluster characteristics, and the needle bearing stiffness.

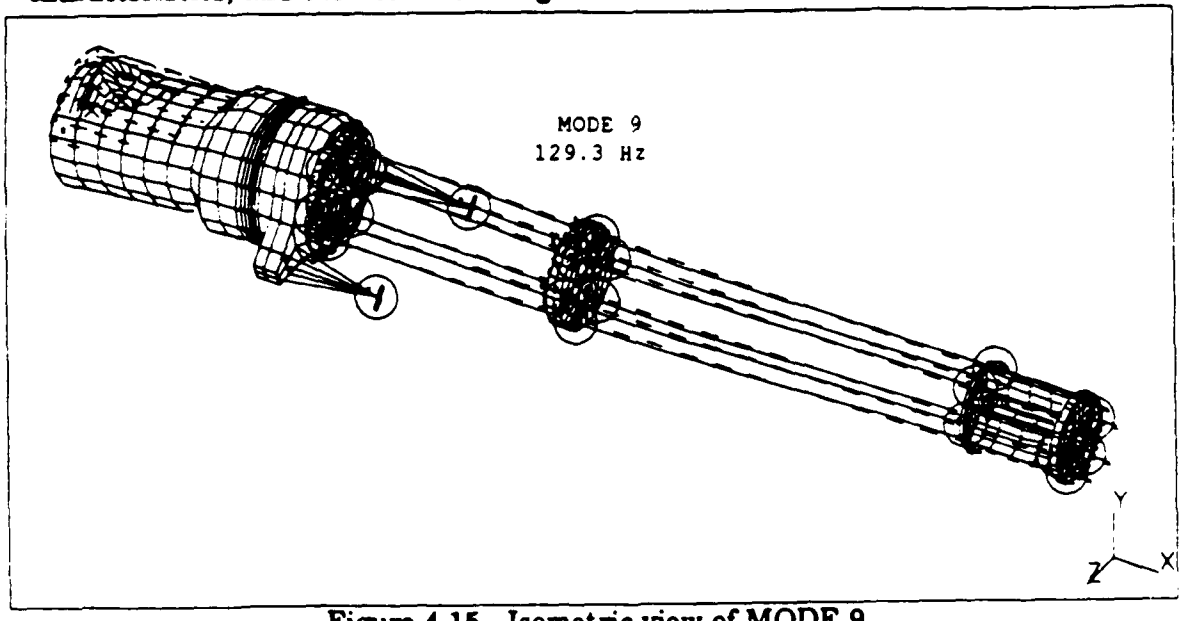

Figure 4.15. Isometric view of MODE 9.

9. MODE 9

Mode 9 at 129 Hz closely resembles the analytical coupled 2 DOF problem. The analytical solution has one of its frequencies at 132 Hz. This frequency corresponds to an in phase pitching and heaving of the rotating assembly within the bearing structure. Animation of mode 9 displays this same motion. However, in mode 9 the six-barrel group appears to have slight deformation. Animation reveals this deformation as a ripple down the barrel, as it pitches and heaves. This effect is not accounted for in the analytic solution. In the calculation, the rotating assembly was treated as an evenly distributed mass with constant cross-section. Mode 9 can be attributed to the stiffness values of the angular contact and needle bearings.

TABLE 4.2 provides a summary of the first nine modes of the M61A1 model with a brief description of each mode.

TABLE 4.2. LOWEST ORDER MODE SUMMARY

Mode No.	Description	Freq. (Hz.)
1	Rotation of the six barrel system	3.3
2	Yaw of the six-barrel system within the housing	14.4
3	Recoil of the gun	15.5
4	Moderate recoil with pitching	16.0
5	Rocking of the entire gun about its CG	35.3
6	Housing deformation	55.3
7	First bending of the six-barrel system	110
8	Increased bending of the six-barrel system	116
9	In Phase pitching/ heaving	129

D. SIMPLE AND COMPLEX SINGLE BARREL COMPARISON

As mentioned earlier in this chapter, there were two different FEM representations of a gun barrel. Initially, a complex barrel was built comprised of solid linear bricks as shown in Figure 4.16. However, the number of elements for the single complex barrel was excessive. In order to reduce the number of elements and to stay within a reasonable DOF budget, a simple barrel was created from beam elements as shown in Figure 4.17.

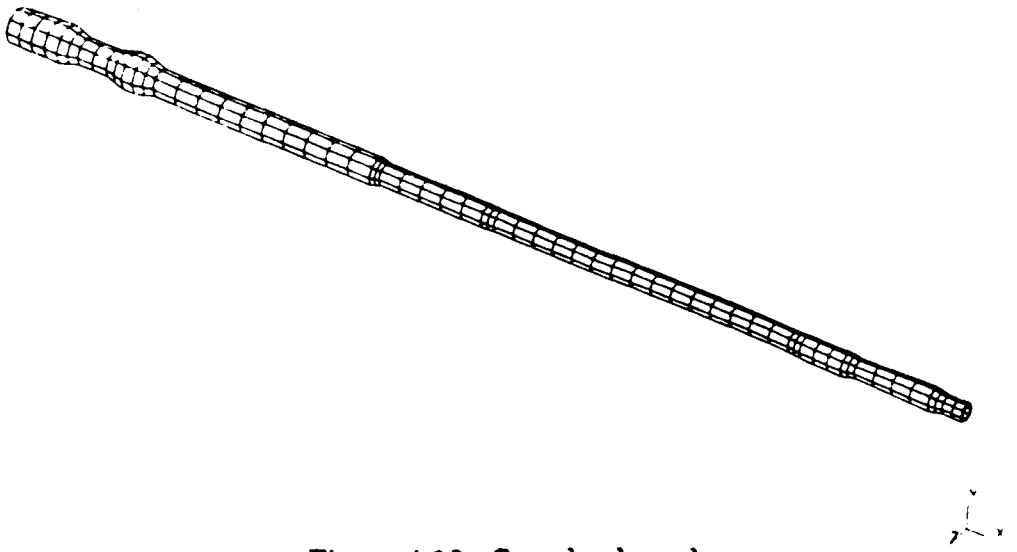

Figure 4.16. Complex barrel.

At the same time, an actual barrel from a PHALANX system was received from Naval Surface Warfare Center (NSWC), Point Hueneme, CA.. The barrel provided an opportunity to conduct a modal test and compare the computer model to the actual gun barrel. An impact point modal test was conducted on the actual barrel in a free-free condition (Ref. 31). The free-free condition refers to the ends of the barrel having no restraints. The free-free condition was attained using light springs or bungee cords attached to the barrel at its quarter points. Figure 4.18 shows is the graphical output from the frequency spectrum analyzer used in the modal test. Note the peak at 72 Hz indicating the first flexible mode of the actual barrel in the free-free condition. The free-free condition represents the most

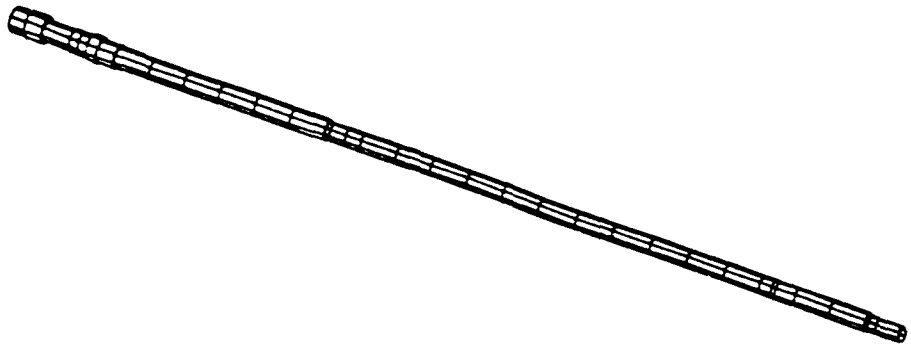

Figure 4.17. Simple barrel.

pristine condition for a modal test where the barrel is essentially free to deform in any manner. This same condition can be easily achieved in I-DEAS. The natural modes for the two computer models, in the free-free condition, were obtained. The first modes of both the simple and complex barrel are shown in Figures 4.19.A and 4.19.B, respectively. TABLE 4.3 is a summary of the natural frequencies of all three barrels.

A graphical comparison of the three barrels' frequencies, simple, complex, and actual is shown in Figure 4.20. There is excellent agreement of all three sets of data from zero through 500 Hz. The range of modes retained for the analytical modal system has frequencies only through 308 Hz. Therefore, agreement through 500 Hz is acceptable. This demonstrates the importance of element selection to represent proper dynamic behavior. In this case, the beam elements have better dynamic behavior, with respect to bending, than the solid linear bricks. As a result the decision to use beam elements for the barrels reduces the overall number of DOF and gives proper dynamical behavior.

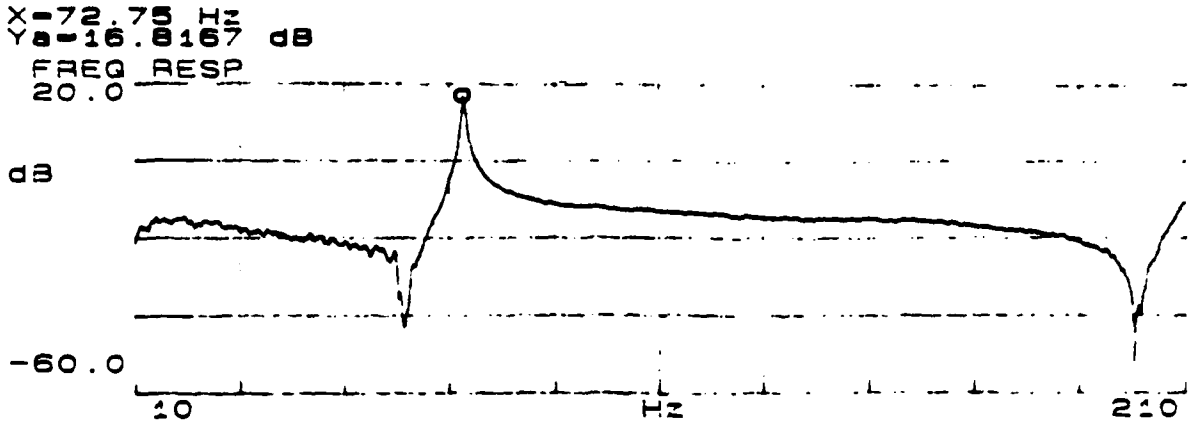

Figure 4.18. First flexible mode frequency response of an actual PHALANX gun barrel in a free-free condition.

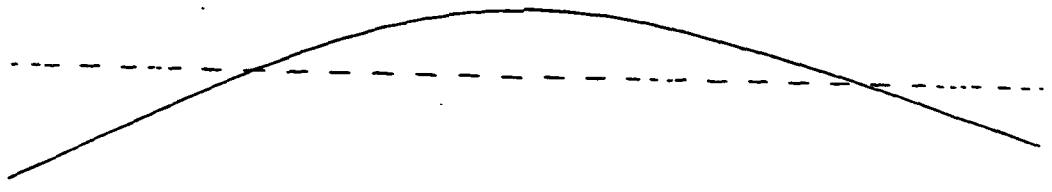

Figure 4.19.A. First mode of the simple barrel in a free-free condition.

It is important to state that this is a validation of only a single barrel. Validation of the entire gun system is not implied. However, this demonstrates that the procedure can eventually be scaled up to include the entire gun.

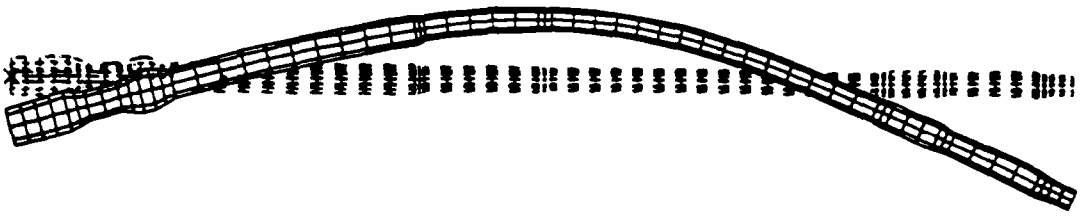

Figure 4.19.B. First mode of the complex barrel in a free-free condition.

TABLE 4.3. MODAL SUMMARY OF SIMPLE, COMPLEX, AND EXPERIMENTAL BARRELS.

	FREQUENCY (Hz)		
Mode No.	Simple	Complex	Experimental
1	71.6	64.7	72.8
2	223.9	200.9	217
3	455.3	399.8	431
4	743.8	652.3	694
5	873.6	809.2	1040
6	1111.4	982.2	1428
7	1515	1357.1	1848

E. MODAL TRUNCATION / SELECTION

When solving for the normal modes of a system, the maximum number of modes is equal to the number of physical DOF. The number of DOF is 22,500 for the gun model, so that there are actually 22,500 normal modes for the system.

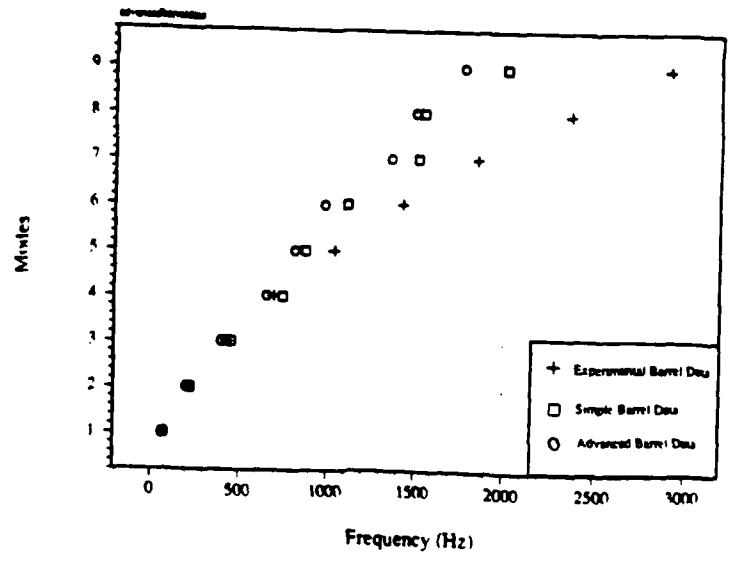

Figure 4.20. Comparison of the model and actual barrels.

Any solution using less than the number of physical DOF is approximated and truncated. The primary advantage in creating an analytical modal component is that the number of modal DOF are significantly less in number than the physical DOF. As discussed in Chapter III, the modal matrix allows transformations between the two domains, and the results of a modal analysis have physical significance upon transforming back to the physical domain.

An important decision made in modal analysis is MODAL TRUNCATION / SELECTION. For the modal system, the number of normal modes determines the number of degrees of freedom or possible responses of the system. The response of a modal component is a summation of linear combinations of the mode shapes used to define it. An analogy to the three primary colors provides insight into modal analysis. Just as every color in the spectrum can be produced by mixing the three primary colors, in modal analysis any response can be described as a linear combination or mixing of the normal mode shapes. If modal truncation is not done carefully, then the results of the dynamic response will be inaccurate. The FEM must retain the primary colors necessary to create the colors of interest.

There are no hard and fast rules for modal truncation. It is based on sound engineering judgement and a consideration for the ultimate analysis. However, there are a few rules-of-thumb that can assist in retaining an appropriate range of frequencies.

To aid in the modal truncation, it is essential to have an understanding of the excitation force that will be applied. In the case of the gun, the highest firing rate has a fundamental frequency of 75 Hz. The recoil from a single shot should be considered to be essentially an impulse. The bullet takes only about 1 millisecond to travel down the barrel. In terms of frequency content, an impulse can be described as a broad band of excitation frequencies. Understanding the frequency content of the excitation is the basis for modal truncation.

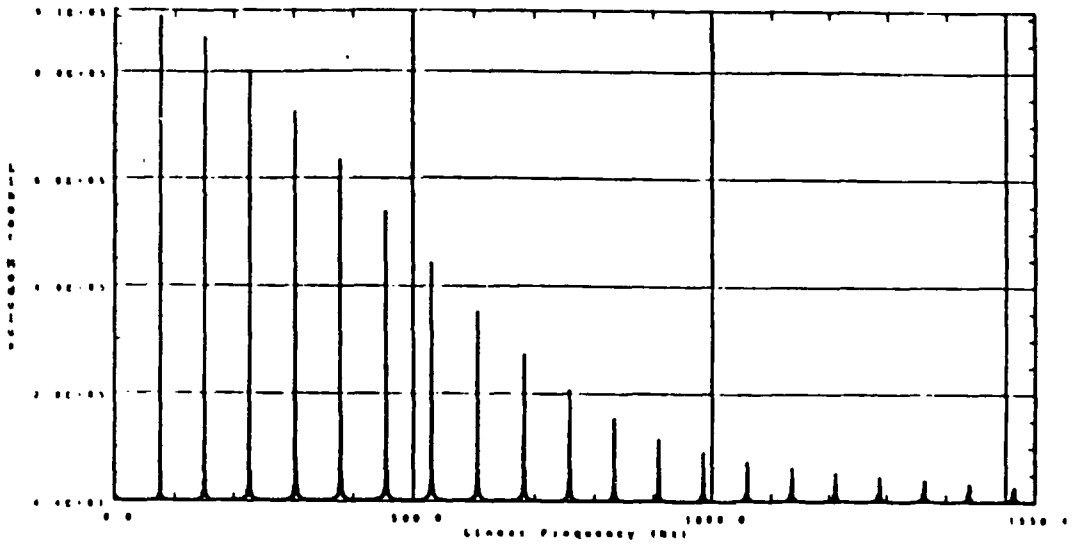

Figure 4.21. Power Spectral Density of 100 Shot Burst at 4500 SPM.

One rule that can be applied is to use the power spectral density of the excitation force. Figure 4.21 is the power spectral density of a 100 shot burst at a firing rate of 4500 SPM.

The specific point of interest is the 3 dB or half-power point in the spectrum. The corresponding range of frequencies, consistent with the half-power point, may

be considered as a valid estimate to be used in modal truncation. From Figure 4.21, the corresponding half-power frequency range is approximately 400 Hz. However, this range of frequencies alone is not a sufficient condition for retention. The mode shapes that fall within this range should be carefully studied in order to ensure that their motion is reasonable and consistent with the properties of the mesh. This allows the user to truncate those specific modes in the range that may not be important to the system response. A particular mode may have only localized deformations, and therefore, would not be significant in the system analysis, and can be truncated. It is more important to satisfy this latter requirement, than to satisfy the half-power range of frequencies. For the gun model a range of frequencies was taken up through 308 Hz and all modes 2-21 were retained. Mode 1, the quasi-rigid body mode, is truncated in order to remove the false rigid body motion from the response.

The truncation of higher order modes is appropriate, because the effects of higher natural frequencies are small localized deformations in many specific components in the system. Since the goal of the analysis is to gain insight into the dispersion problem, the displacement of the barrel muzzle tip is important. These higher order modes will have only a small displacement amplitude when the 75 Hz excitation force is applied with modal damping, and will contribute little to the ultimate analysis. Figure 4.22 shows mode 21 at the cutoff frequency of 308 Hz. Notice the deformation of the barrel group. The overall effect does not vary much from mode 7 shown in Figure 4.9. Each higher frequency mode has one extra node in the barrels mode shape. The significant change is the increased local deformation of the housing.

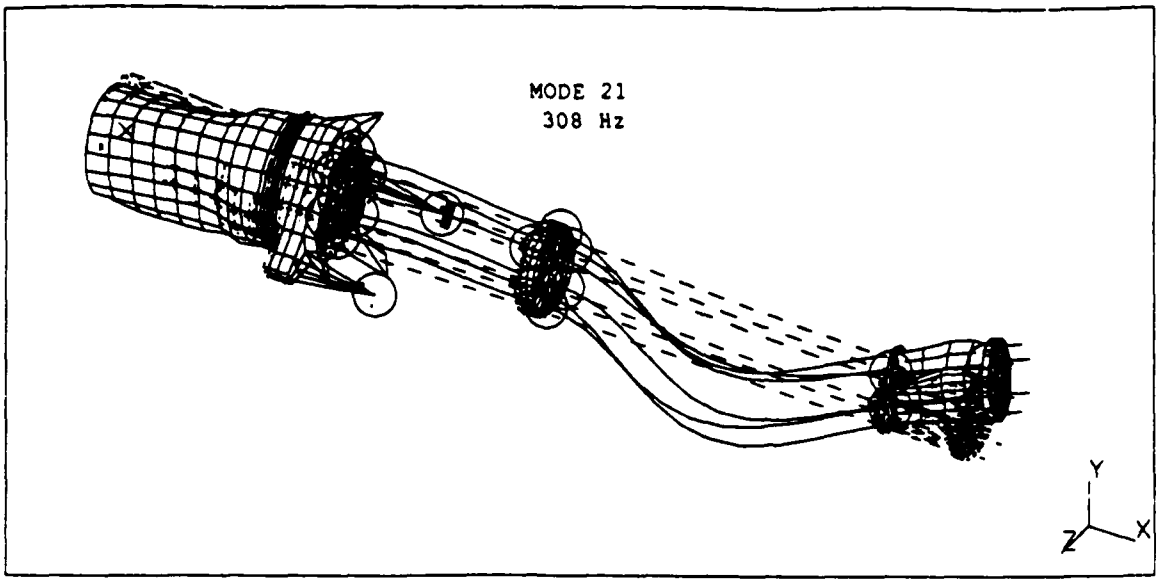

Figure 4.22. M61A1 mode 21.

F. CREATING AN ANALYTICAL MODAL COMPONENT

Modal analysis involves the uncoupling of the many differential equations of motion describing the system. The resulting independent equations of motion facilitate the response analysis of the multiple-degree-of-freedom system. This procedure was demonstrated at the end of Chapter III. The equations of motion were uncoupled through a transformation involving the modal matrix. The resulting independent equations are expressed in terms of modal mass, the mode shapes and modal frequencies. These equations can each be treated as single DOF equation of motion. A system response is described by the superposition of the responses of the individual normal modes.

In the SYSTEM DYNAMICS MODULE the analytical modal component is simply created by referring to the title of the specific FEM solved. The corresponding modes and frequencies are used to form the analytical model. There is no geometry created, although the nodes and elements created in the FEM module are displayed for presentation purposes. The model is a numerical representation of the mode shapes.

Decisions must be made as to which modes are to be retained and what damping value is assigned to each retained mode. The issue of damping will be discussed in more detail in the next chapter. The actual values become significant when the results of a forced response are desired.

G. FORCED RESPONSE IN THE TIME AND FREQUENCY DOMAINS

As a prelude to the next chapter, the analysis of a forced response in both the time and frequency domains is discussed here. The total response of a system can be considered to consist of two distinct components. The first is the forced response which resembles the excitation force. The second is the free response. The free response, or natural response, was discussed earlier in the solution of the natural frequencies and normal modes. This response depends only on the characteristics of the system. However, the forced response component depends on the specific forcing function as well as the system's modal characteristics.

Mathematically these responses are found separately as the *particular* and *homogeneous* solutions,

$$X(t) = X(t)_{Homogeneous} + X(t)_{particular} .$$

The sum of these results are the total response, $X(t)$, of the system. The free response is often referred to as the transient response, because it decays with time. The forced response is referred to as the steady-state response (Ref. 32).

1. Time Response.

As an example of a forced response analysis, consider the multi-degree-of-freedom system shown in Figure 4.23 with N physical DOF, damping matrix [C], stiffness matrix [K], and mass matrix $[M]$. An arbitrary time varying force $F(t)$ shown in Figure 4.24 is applied in the X direction,

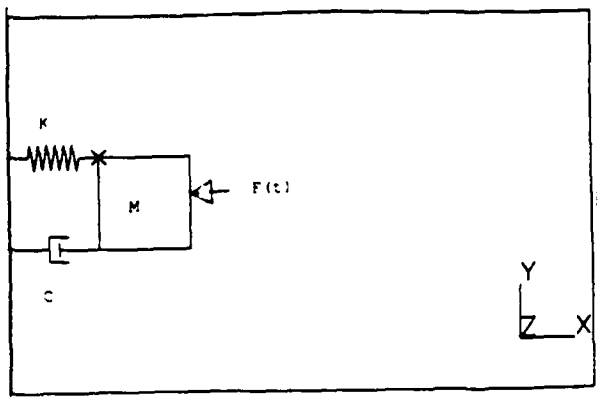

Figure 4.23. System with a time varying excitation force.

$$\left\{F\ (t)\right\} = \begin{Bmatrix} F_x(t) \\ 0 \\ 0 \end{Bmatrix},$$

with initial conditions, $X(t) = \dot{X}(\ t\ ) = 0$.

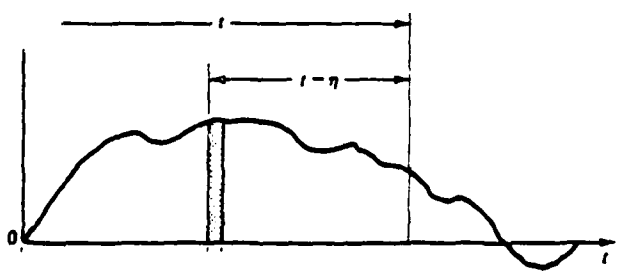

Figure 4.24. Arbitrary time varying excitation force.

The resulting equation of motion is

$$\left[\mathbf{M}\right]\left\{\ddot{\mathbf{X}}\right\} + \left[\mathbf{C}\right]\left\{\dot{\mathbf{X}}\right\} + \left[\mathbf{K}\right]\left\{\mathbf{X}\right\} = F(t) \ . \tag{4.11}$$

Where all matrices are $N \times N$ and the vectors are N components long. The system can be transformed into a modal component, with n modes retained, or n modal DOF. The transformation is the same approach as in Chapter III. However, the modal matrix is partitioned as a result of modal truncation. The columns of the modal matrix, $[\phi]$, represent individual mode shapes. When modes are truncated, columns are removed from the modal matrix. The equations of motion are uncoupled using the partitioned $N \times n$ modal matrix, $[\Phi']$. The assumed solution is of the form in (4.12) where q is the sinusoidal temporal term, and $[\Phi']$ is a partitioned spatial term,

$$\left\{\mathbf{X}\right\} = \left[\Phi'\right]\left\{q\right\} \ . \tag{4.12}$$

Substituting the assumed solution into (4.11) results in a set of coupled second-order ordinary differential equations of motion.

$$\left[\mathbf{M}\right]\left[\Phi'\right]\left\{\ddot{q}\right\} + \left[\mathbf{C}\right]\left[\Phi'\right]\left\{\dot{q}\right\} + \left[\mathbf{K}\right]\left[\Phi'\right]\left\{q\right\} = \left\{F(t)\right\} \ .$$

Multiplying by the transpose of the partitioned modal matrix gives

$$\left[\Phi'\right]^T\left[\mathbf{M}\right]\left[\Phi'\right]\left\{\ddot{q}\right\} + \left[\Phi'\right]^T\left[\mathbf{C}\right]\left[\Phi'\right]\left\{\dot{q}\right\} + \left[\Phi'\right]^T\left[\mathbf{K}\right]\left[\Phi'\right]\left\{q\right\} = \left[\Phi'\right]^T\left\{F(t)\right\},$$

which diagonalizes the mass and stiffness matrices. However, the damping matrix [C] does not usually reduce to a diagonal matrix. In order to completely uncouple the damped vibration, the concept of proportional damping is introduced.

The damping matrix [C] is assumed to be proportional to the mass matrix [M], the stiffness matrix [K], or a linear combination of the two. This latter

proportionality is referred to as Rayleigh damping (Ref. 33). Lord Rayleigh considered damping to have the form

$$[\mathbf{C}] = \alpha\,[\mathbf{M}] + \beta\,[\mathbf{K}] \ .$$

Where α and β are constants. First consider [C] as being proportional to [M]. Upon modal transformation it follows that

$$\left[\Phi'\right]^T \left[\mathbf{C}\right] \left[\Phi'\right] = \alpha \left[\Phi'\right]^T \left[\mathbf{M}\right] \left[\Phi'\right] \ .$$

It is common practice to assume modal damping of the form

$$2\,\gamma_i\,\omega_i\,M_i = \alpha\,M_i \ ,$$

where γ_i is the modal damping factor of the i^{th} mode, ω_i is the natural circular frequency of the i^{th} mode, and M_i is the modal mass of the i^{th} mode. Similarly the same can be shown for

$$[\mathbf{C}] = \beta\,[\mathbf{K}] \ .$$

In this case, the modal damping is typically represented as

$$2\,\gamma_i\,\omega_i\,M_i = \beta\,\omega_i^{\,2}\,M_i \ .$$

Using the above results, Rayleigh damping assumes the form of

$$2\,\gamma_i\,\omega_i\,M_i = (\,\alpha + \beta\,\omega_i^2\,)\,M_i \ .$$

The resulting modal transformation is

$$\left[\Phi'\right]^T \left[\mathbf{C}\right] \left[\Phi'\right] = \alpha \left[\Phi'\right]^T \left[\mathbf{M}\right] \left[\Phi'\right] + \beta \left[\Phi'\right]^T \left[\mathbf{M}\right] \left[\Phi'\right] \ ,$$

$$\left[\Phi'\right]^T \left[\mathbf{C}\right] \left[\Phi'\right] = \alpha \left[\mathbf{M}\right] + \beta \left[\mathbf{K}\right] \ .$$

The result is a set of uncoupled second-order ordinary differential equations. Defining f as a "modal force", results in

$$f = \left\{F\,(t)\right\} \left[\Phi'\right]^T \ ,$$

$$\left[\mathbf{M}\right]\left\{\ddot{q}\right\} + \left(\alpha\left[\mathbf{M}\right] + \beta\left[\mathbf{K}\right]\right)\left\{\dot{q}\right\} + \left[\mathbf{K}\right]\left\{q\right\} = \left\{f\right\} \ .$$

The resulting equation of motion is then

$$\left\{\ddot{q}\right\} + \frac{1}{[\mathbf{M}]}\left(\alpha\left[\mathbf{M}\right] + \beta\left[\mathbf{K}\right]\right)\left\{\dot{q}\right\} + \frac{1}{[\mathbf{M}]}\left[\mathbf{K}\right]\left\{q\right\} = \frac{1}{[\mathbf{M}]}\left\{f\right\} \ .$$

Defining $\omega_i{}^2$ as the natural frequency of the i^{th} mode, results in

$$\omega_i{}^2 = \frac{K_{ii}}{M_{ii}} \ .$$

The resulting single DOF equation of motion is then

$$\ddot{q}_i + (\alpha + \beta\ \omega_i{}^2)\ \dot{q}_i + \omega_i{}^2 q_i = \frac{f_i}{M_{ii}} \ .$$

Using the relation

$$2\ \gamma\ \omega_i = (\alpha + \beta\ \omega^2{}_i) \ ,$$

the resulting single DOF equation of motion is

$$\ddot{q} + 2\ \gamma_i\ \omega_i\ \dot{q} + \omega_i{}^2\ q = \frac{1}{M_{ii}}\ f_i \ . \qquad (4.13)$$

The response of a linear system to an arbitrary force can be obtained by considering the arbitrary force to be the sum of a sequence of impulses. An arbitrary force in the time domain can be represented by a summation of delta functions (Ref. 34). The solution is simply in the form of a summation or integration of these delta functions. Equation (4.13) is solved using Laplace transforms and the convolution integral. An outline of the particular solution follows.

Taking the Laplace transform of (4.13) results in the following

$$s^2\ X(s) - s\ x(0) - \dot{x}\ (0) + 2\ \gamma\ \omega_i\ \ (s\ X(s) - x\ (0)) + \omega_i{}^2\ X\ (s) = \frac{1}{M_{ii}}\ F(s) \ .$$

Applying initial conditions, $X(t) = \dot{X}(t) = 0$ gives

$$s^2 X(s) + 2\gamma\omega_i \; s \; X(s) + \omega_i^2 X(s) = \frac{1}{M_{ii}} F(s) \; .$$

The result is the generalized product solved for the response $X(s)$

$$X(s) = \frac{1}{M_{ii}} \frac{F(s)}{\left[s^2 + 2\gamma\omega_i \; s + \omega_i^2\right]} \; .$$

Taking the inverse Laplace transform gives

$$q_i(t) = \frac{\sin \omega_i \sqrt{1-\gamma^2}\, e^{-\gamma\omega_i t} \; F(s)}{M_{ii} \; \omega_i \sqrt{1-\gamma^2}} \; .$$

Applying the convolution integral to the generalized product results in the following:

$$q_i(t) = \frac{1}{M_{ii} \; \omega_i \sqrt{1-\gamma^2}} \int_0^t \sin \omega_i \sqrt{1-\gamma^2}\,(t-\tau)\, e^{-\gamma\omega_i (t-\tau)} \; F(\tau) d\tau \; .$$

The total displacement $q_i(t)$ at any time t is the integral from $0 \rightarrow t$ of all impulses $F(\tau)$. The solution is a convolution of an impulse response and the forcing function. As long as $F(\tau)$ is a simple function, such as a step function, the integral can be easily solved. More complex excitation forces must be solved using numerical methods. Convolution integrals account for the behavior of a system at time t which depends not only on its state at time t, but also its past history (Ref. 35).

The result $q_i(t)$ is the time response for a DOF in the system. In order to solve for the displacement value, it is only necessary to substitute the solution for the generalized coordinate q into the transformation (4.13)

$$\begin{Bmatrix} x_1(t) \\ x_2(t) \\ x_3(t) \\ . \\ . \\ . \\ x_N(t) \end{Bmatrix} = [\Phi'] \begin{Bmatrix} q_1(t) \\ q_2(t) \\ q_3(t) \\ . \\ . \\ . \\ q_n(t) \end{Bmatrix} .$$

where x_i are generalized coordinates used to describe the vibratory motion.

2. Frequency Response

For a frequency response, the solution proceeds in much the same way. A particular application of a frequency response is the development of a transfer function. In I-DEAS, the transfer function is developed by applying a unit amplitude sinusoid to the right-hand-side of (4.11) at any allowable DOF. For this case, damping will be ignored so that [C] = [0].

The equation of motion for an excitation in the X direction at any node has the form

$$[\mathbf{M}]\{\ddot{\mathbf{X}}\} + [\mathbf{K}]\{\mathbf{X}\} = \{F(\Omega,t)\} , \tag{4.14}$$

where $\{F(\Omega,t)\}$ represents the force applied at the p DOF and, has the form

$$\begin{Bmatrix} 0 \\ . \\ 0 \\ F_p \sin(\Omega t) \\ 0 \\ 0 \end{Bmatrix} .$$

For other DOF, the force term appears in the appropriate row of the force vector $F(t)$ where $|F_p| = 1$.

Assume the solution to (4.14) is of the form:

$$\left\{X(t)\right\} = [\phi]\left\{q(t)\right\} \ ,$$

where the temporal term $q(t)$, is of the form $q(t) = \sin(\Omega t)$. The frequency Ω is the frequency of excitation. For convenience, the modal matrix, $[\phi]$, is unity mass normalized so that

$$[\phi^i]^T\ [\mathbf{M}]\ [\phi^j] = 1, \text{ for } i = j$$

$$= 0, \text{ for } i \neq j \ .$$

Taking the appropriate derivative and substituting into (4.14) results in

$$\left[-\Omega^2\left[\mathbf{M}\right] + \left[\mathbf{K}\right]\right]\ [\phi]\left\{q(t)\right\} = \left\{F\right\} \ .$$

Multiplying by $[\phi]^T$ gives

$$[\phi]^T\ \left[\mathbf{K}-\Omega^2\mathbf{M}\right][\phi]\left\{q\right\} = [\phi]^T\left\{F(\Omega t)\right\} \ ,$$

and defining the modal force as f,

$$[\phi]^T\left\{F\right\} = \left\{f\right\} \ .$$

the natural frequency of mode i, f_i, is

$$f_i = \frac{1}{2\,\pi}\ \omega_i \ ,$$

where

$$\omega_i{}^2 = \frac{K_{ii}}{M_{ii}} \ .$$

The resulting equation is

$$\left[\left[\omega^2\,\mathbf{I} - \Omega^2\,\mathbf{I}\right]\left\{q\right\} = \left\{f\right\}\right. , \tag{4.15}$$

$$(\,\omega^2 - \Omega^2\,)\,[\mathbf{I}]\left\{q\right\} = \left\{f\right\} ,$$

where [I] is the identity matrix. Note that the natural frequency matrix is diagonalized. Inverting the result gives the modal frequency response function (FRF)

$$\left\{q\right\} = \left[\;\omega_i{}^2 - \Omega^2\;\right]^{-1}\left\{f\right\} .$$

To convert from the modal FRF to the physical, the following relations are used

$$\left\{f\right\} = [\phi]^T\left\{F\right\} ,$$

and

$$\left\{X\right\} = [\phi]\left\{q\right\} .$$

Multiplying by [ϕ], (4.15) can be written as

$$[\phi]\left\{q\right\} = [\phi]\left[\;\omega^2 - \Omega^2\;\right]^{-1}[\phi]^T\left\{F\right\} ,$$

and resulting in

$$\left\{X\right\} = [\phi]\;\left[\;\omega^2 - \Omega^2\;\right]^{-1}\;[\phi]^T\left\{F\right\} .$$

It can be shown that the above can be written as a summation over all DOF with the result

$$\left\{X\right\} = \sum_{i=1}^{n}\;\frac{\left\{\phi^{(i)}\right\}\left\{\phi^{(i)}\right\}^T}{\omega_i{}^2 - \Omega^2}\;\left\{F\right\}.$$

Define the frequency response function (FRF), [H(Ω)], as

$$[\mathbf{H}(\Omega)] = \sum_{i=1}^{n} \frac{\left\{\phi^{(i)}\right\}\left\{\phi^{(i)}\right\}^{T}}{\omega_i{}^2 - \Omega^2} ,$$

where n is the number of nodes, and the superscript on $\phi^{(i)}$ is the i^{th} column of the modal matrix which indicates a particular mode shape.

The displacement transfer function represents the ratio of the displacement response of a point on the system divided by the input force at another point plotted as a function of frequency. The magnitude of this function will have peaks at the natural frequencies of the system. The height of each peak relative to other FRF's is proportional to the mode shape. The width of each peak is proportional to the damping. The higher the damping for a particular mode, the wider is the peak.

A component of the response matrix [H(Ω)] is defined in terms of components (p ,q) where p represents the DOF of application of the force, and q is the DOF of the response. Therefore, an individual component is defined as

$$H_{p,q}(\Omega) = \left[\frac{\phi_p{}^{(i)}\,\phi_q{}^{(i)}}{\omega_i{}^2 - \Omega^2}\right]$$

At resonance, $\omega_i{}^2 = \Omega^2$, the response matrix component for an undamped system becomes infinite unless the system is being driven at, or observed, at a node of the mode i, whereby the amplitude becomes zero.

Ideally a transfer function for every DOF in the system could be used to reconstruct the mode shapes for a wide range of frequencies. They provide a means to quickly gain insight into a system.

V. FORCED RESPONSE

A. INTRODUCTION

The response of a forced system depends primarily on the system's natural frequencies, the damping in each mode, and the characteristics of the excitation force. The response contains a full description of a structure's dynamics. This chapter will discuss the specifics of these parameters as they pertain to the gun model. The forced response plots are derived from the results of the modal analysis. The first section will discuss damping and the decisions made regarding damping of the retained modes in the gun model. The second section will discuss the modeling of the excitation force: a 100 shot burst at 4500 shots per minute (SPM). The final section will discuss the forced response plots in the time and frequency domains. The response is analyzed at the tip of the firing barrel in the x, y, and z directions. The behavior of the firing barrel muzzle tip provides insight into aim point errors and contributions to dispersion. Although the forced response plots in the two domains are discussed separately, their analyses must be integrated. The time response provides the analyst with a visualization of what the barrel tip is doing. Although time is a convenient dimension to understand the effects of response, the frequency domain provides insight into specific mode participation in the response.

The modal system is created by a set of orthogonal normalized mode shapes. For the gun model, 21 mode shapes were considered to provide a sufficient range of frequencies based on an excitation force with a fundamental frequency of 75 Hz.

The response of the gun model is limited to linear combinations of these 21 normal modes and natural frequencies. The result of modal analysis is a set of uncoupled equations of motion.

The uncoupled equations of motion developed in the modal analysis are expressed in terms of mode shapes, modal damping factors, and natural frequencies. Each uncoupled equation has the form of a forced, single-degree-of-freedom system.

The effect of the individual modes on the total response of the system can be expressed in terms of the n retained modes,

$$\begin{Bmatrix} x_1 \\ x_2 \\ x_3 \\ \cdot \\ \cdot \\ \cdot \\ x_n \end{Bmatrix} = q_1 \begin{Bmatrix} \phi_1 \\ \phi_2 \\ \phi_3 \\ \cdot \\ \cdot \\ \cdot \\ \phi_n \end{Bmatrix}_1 + q_2 \begin{Bmatrix} \phi_1 \\ \phi_2 \\ \phi_3 \\ \cdot \\ \cdot \\ \cdot \\ \phi_n \end{Bmatrix}_2 + \ldots + q_n \begin{Bmatrix} \phi_1 \\ \phi_2 \\ \phi_3 \\ \cdot \\ \cdot \\ \cdot \\ \phi_n \end{Bmatrix}_n .$$

where $i = 1 \cdots n$. Here the x values represent the total displacements, the ϕ 's represent the components of a particular (eigenvector) mode shape, and the q_i's represent the sinusoidally varying temporal terms. The subscripts on the q_i's and ϕ 's denote a specific natural frequency of the sinusoidal term.

B. DAMPING

Vibrations in a system are a result of energy being transferred back and forth between the kinetic energy of the mass motion and the potential energy stored in the material stiffness. Vibration amplitude is limited by system damping, specifically viscous damping which is proportional to velocity. All physical systems have some inherent mechanism to dissipate energy, or damping. Damping causes

the amplitude of vibration to diminish with time with no excitation force. However, the magnitude of damping has little effect on the natural frequencies of a system (Ref. 36).

There is no analytic method to determine the elements of the damping matrix [C] which specifies the system damping. However, the effect of damping on systems is readily included when using modal analysis. Physically realistic values can only be obtained from experimental data.

In general, there are three distinct cases of damping strength. Their characterizations can be described based upon their impact on the single-degree-of-freedom differential equation of motion for free vibration,

$$m\,\ddot{x} + c\,\dot{x} + k\,x = 0 \ , \tag{5.1}$$

where m is the mass, c is the damping coefficient, and k is the spring constant. Assume a solution of the form

$$x = e^{\gamma t} \ ,$$

where γ is an arbitrary variable. Substituting into equation of motion results in the following auxiliary equation

$$m\,\gamma^2 + c\,\gamma + k = 0 \ .$$

If γ satisfies this auxiliary equation, then the assumed solution will satisfy (5.1). The roots to the auxiliary equation are found by using the quadratic formula

$$\gamma = \frac{-c \pm \sqrt{(c^2 - 4mk)}}{2m} \ .$$

The specific case of damping is determined by the value of the discriminant $(c^2 - 4\,m\,k)$. The three cases are below:

I. $(c^2 - 4\,m\,k) < 0$ underdamping

Underdamping is the case that c is small. The roots of the auxiliary equation are complex. The physical motion is best described as the product of an

exponential decay and a sinusoidal oscillation. The presence of damping causes the frequency of oscillation to be slightly less than it would be in the absence of damping. The sinusoidally varying displacement has an exponentially decaying amplitude as shown in Figure 5.1 (a) (Ref. 37).

II. $(c^2-4mk) > 0$ overdamping

The roots of the auxiliary equation are real, negative and distinct. The physical motion is an exponential decay with two different decay constants. The system, given an initial displacement, returns to the equilibrium position without oscillating. The damping force dominates and prevents any periodic motion as shown in Figure 5.1 (b) (Ref. 38).

III. $(c^2-4\ m\ k) = 0$ critical damping

The roots of the auxiliary equation are equal. The result is one function which is an exponential decay, and a second function which is the product of time t and the exponential decay function. The resulting motion is non-oscillatory. With an initial displacement, the system returns asymptotically to the equilibrium position. Critical damping provides an optimum return to equilibrium as shown in Figure 5.1 (c). It is the limiting case of the non-oscillatory mode of return to equilibrium (Ref. 39).

In I-DEAS, the user assigns damping ratios for each normal mode retained in the analytical modal component. The damping ratio represents a percentage of critical damping. A damping ratio of 1.0 means the particular mode is critically damped.

As mentioned above, there is no analytic way to determine actual damping values. The only meaningful results are obtained from experimental data from the actual system. The damping factor can be determined experimentally by obtaining frequency response data for a system. By studying the variation of the amplitude of vibration with time, the damping factor can be determined. Ultimately, an experimental modal analysis is conducted on the actual system and

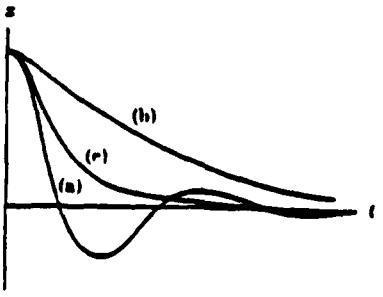

Return of harmonic oscillator to equilibrium. (a) Underdamped. (b) Overdamped. (c) Critically damped.

Figure 5.1. Three general cases of damping.

the damping values are determined. These values, in turn, can be used in subsequent analyses.

The individual modes for the gun system were assumed to be underdamped, and each was assigned a value of 0.02, or two percent of critical damping. These values are accepted in industry as a first estimate. The only exception to this is mode 3, the recoil mode. It was determined that the recoil mode is characterized by the properties of the recoil adapters. Therefore, the recoil adapter's force deflection curve can be used to determine the damping factor. The force deflection curve has a hysteresis loop and from this the damping factor can be calculated.

The area enclosed by a hysteresis loop represents the amount of energy dissipated each cycle by the recoil adapter.

$$E_D = \pi C_H \mid x \mid^2 \omega \ ,$$

where E_D is the energy dissipated per cycle of the recoil adapter, C_H is the equivalent viscous damping factor, x is the amplitude of displacement for the recoil adapter, and ω is the frequency of the recoil adapter's motion (Ref. 40). The

dissipated energy value was computed by estimating the area enclosed by the hysteresis loop in Figure 5.2 (Ref. 41). The result is 384 lbf in or 43.3×10^4 N m. The displacement amplitude is presumed to be 0.2 in, or 0.6 cm, by assuming that the recoil adapter's equilibrium position is at the center of the hysteresis loop or 0.5 inches. The boundaries of the loop are approximately 0.2 inches on both sides of equilibrium. The particular mode shape that this damping value is applied to is mode 3 at $f = 15.5\ Hz$. The resulting value for the equivalent viscous damping is

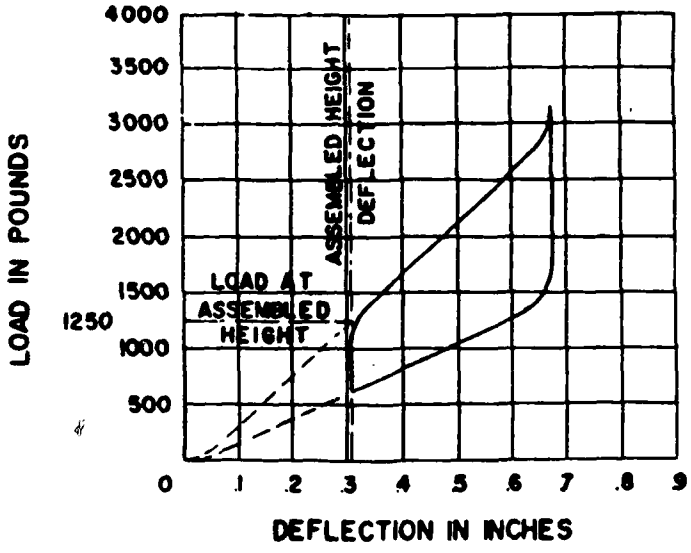

Figure 5.2. Recoil adapter force deflection curve.

$$C_H = \frac{E_D}{\pi \mid x \mid^2 2\,\pi f} = 8351 \text{ kg / s} \quad .$$

The value of critical damping for the gun system is

$$C_{crit} = 2\sqrt{M\,K_R} = 23{,}900 \text{ kg/s} \quad .$$

where $M = 120.5$ kg is the mass of the gun system, and $K_R = 5.9 \times 10^5$ N / m is the recoil adapter stiffness. The resulting damping ratio is

$$\gamma = \frac{C_H}{C_{crit}} = 0.35 \quad .$$

This value was entered as the viscous damping ratio for mode 3 in the gun model. The value is in agreement with the value used by the gun manufacturer in their recoil adapter simulations and calculations.

In forced harmonic motion, the effect of damping is important. The equation of motion (5.1) is modified by adding a sinusoidal driving term to the right hand side,

$$m\,\ddot{x} + c\,\dot{x} + k\,x = F_o \sin(\omega t + \phi) ,$$

where F_o is the magnitude of the force, ω is the frequency of excitation, and ϕ is a phase angle. The solution of this linear differential equation is given by the sum of the homogeneous solution and the particular solution. The resulting particular solution relates the amplitude and phase in response to the driving force. If the driving force is driven near a natural frequency, ω_0, the result is a maximum in the response's amplitude. In the case of weak damping, there is a slight reduction in the resonant frequency from that of the freely running undamped oscillator. For strong damping, there is no amplitude resonance and the amplitude becomes a monotonically decreasing function of frequency as shown in Figure 5.3 (Ref. 42).

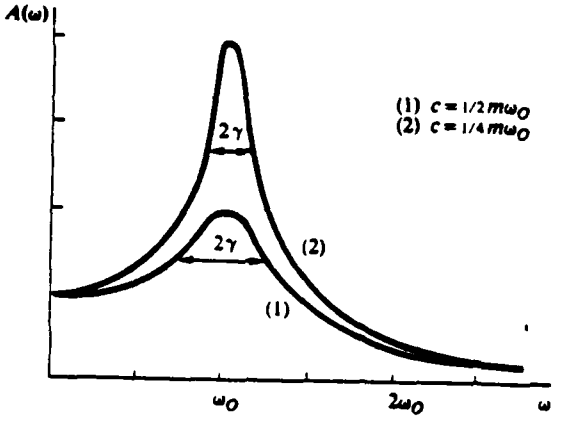

Figure 5.3. Effect of damping on the resonance peak.

The sharpness of the resonant peak is directly proportional to the amount of damping. The quality factor Q determines the sharpness of the peak. The quality factor is expressed in terms of the natural frequency and the corresponding half-energy point frequencies. Let f_1 and f_2 represent the frequencies, below and above the resonant frequency, f_n, that correspond to the half-energy points (Ref. 43), then the quality factor is given by

$$Q = \frac{f_n}{f_2 - f_1} .$$

The phase angle difference, ϕ, between the applied driving force and the steady-state response is proportional to the driving frequency, ω, and the resonant frequency, ω_o.

$$\phi = \tan^{-1}\left[\frac{2 \mid \omega_o - \omega \mid \omega}{(\omega_0^2 - \omega^2)}\right] .$$

At $\omega = 0$, the driving force is static, and the phase difference is zero. The phase difference remains small for small ω, so that the response is in phase with the driving force. Near resonance, $\omega = \omega_o$, the phase angle ϕ increases to 90 degrees so that the response and driving force are 90 degrees out of phase. For large values of ω, the value of ϕ approaches 180 degrees and the response and driving force are 180 degrees out of phase. See Figure 5.4 (Ref. 44).

C. EXCITATION FORCE

The excitation force applied to the gun model represents a 100 shot burst at a rate of 4500 SPM. Typical PHALANX engagements are 60 - 100 shot bursts at the gun's maximum rate of fire of 4500 SPM. Therefore, this excitation is reasonable. The force was developed from analytical data provided by the gun manufacturer. The data was computed using an interior ballistics computer simulation, PRODAS VERSION 5.6, to compute breech pressure versus time for a

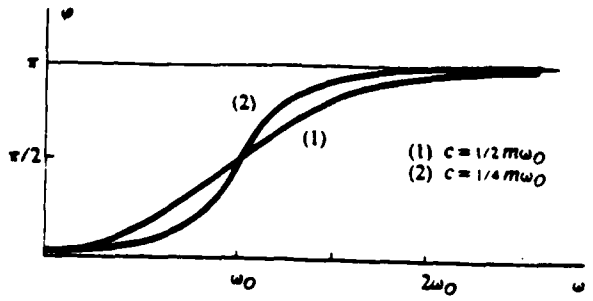

Figure 5.4. Plot of phase difference versus frequency.

single shot (Ref. 45). The breech pressure was converted to a force by using a cross-sectional area of a 20 mm diameter circle

$$F = \frac{P}{A} ,$$

where P is the analytical breech pressure and A is the cross-sectional area of the circular breech chamber,

$$A = \pi r^2 .$$

TABLE 5.1 lists the breech pressure values as a function of time for a single shot of a MK149 20 mm round.

The force is exerted on the breech as the bullet travels down the barrel. The shots are separated at an interval of 0.0133 seconds at 75 Hz, simulating 100 successive shots. Because the model's rotating assembly does not rotate, the point of application of the force is from the same barrel for all shots. The six-barrel system is oriented such that the "firing" barrel is located approximately 12.5 degrees prior to top dead center (TDC). This represents the initiation of the firing of a round. In the gun's operating schedule, all rounds are fired at 12.5 degrees

TABLE 5.1. BREECH PRESSURE VERSUS TIME FOR THE MK-149 PROJECTILE.

TIME(mSec)	PRESS (PSI)	TIME(mSec)	PRESS (PSI)
0.05	1700	0.800	56900
0.10	2500	0.850	60100
0.15	3400	0.900	62200
0.20	4700	0.950	63000
0.25	6200	1.000	62400
0.30	8300	1.050	60200
0.35	10800	1.150	51600
0.40	14000	1.250	40200
0.45	18000	1.450	23200
0.50	23000	1.650	15300
0.55	29000	1.850	11100
0.60	35000	2.050	8560
0.65	41000	2.250	6900
0.70	47000	2.312	6500
0.75	53000		

prior to TDC. If the firing rate is 3000 SPM, then the round exits the barrel at TDC. If the firing rate is 4500 SPM then the round exits the barrel at 14 degrees past TDC. The rotation of the gun is counter-clockwise as viewed from the rear. There are no interior ballistic effects taken into account; the torque exerted on the barrel by the spinning round as it travels down the barrel.

In I-DEAS, the excitation force is created using a universal file representing evenly spaced force values. The excitation force has negative values, because the line-of-action of the firing rounds is in the negative x direction. The data consists of 26400 data points that are evenly spaced at 0.05 milliseconds. This is a convenient method for data to be entered. The excitation force may be created easily allowing flexibility for exploring various forcing functions. The force is applied to the model by designating a specific direction and DOF. In this case, node 1165 in the x translational DOF.

Figure 5.5 shows the plot of force versus time for a single shot. Figure 5.6 shows the fast Fourier transform (FFT) of a single shot consists of a wide spectrum of frequencies (0-10,000 Hz). The FFT used 512 data points, which provided the best presentation.

The FFT of a 100 shot burst fired at 4500 SPM has a fundamental frequency of 75 Hz, and is harmonic. The FFT has 1024 data points, which provides the best presentation. See Figure 5.7. The single shot is essentially an impulse or delta-function. The frequency spectrum is expected to be broad. The envelope of the 100 shot burst has the profile of a single shot. Comparing Figures 5.6 and 5.7, the amplitude of the FFT of the force for a single shot is reduced by a factor of 10 in about 2000 Hz as is the 100 shot burst profile. This is expected because the 100 shot burst is comprised of 100 individual single shots fired at 75 Hz. The fundamental frequency is determined by the firing rate of the gun.

D. TIME RESPONSE

Figures 5.8 - 5.10 are the culmination of the model development and subsequent forced response analysis. The three figures represent the time response of the firing barrel's muzzle (node 3748) in the x, y, and z directions respectively. From $t = 0$ to $t = 1.3$ seconds, the gun is firing the 100 shot burst. From $t = 1.3$ seconds to $t = 5.0$ seconds, the excited normal modes decay due to

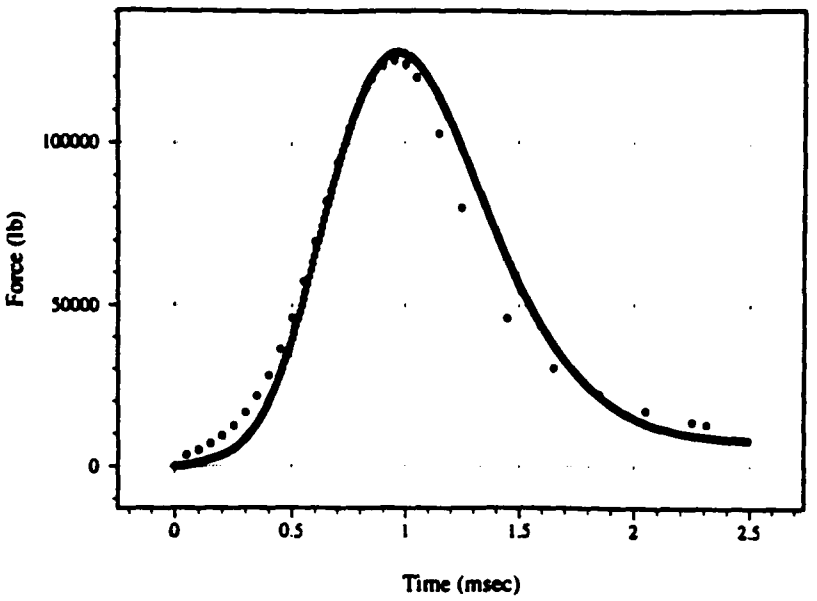

Figure 5.5. Force versus time for a single shot.

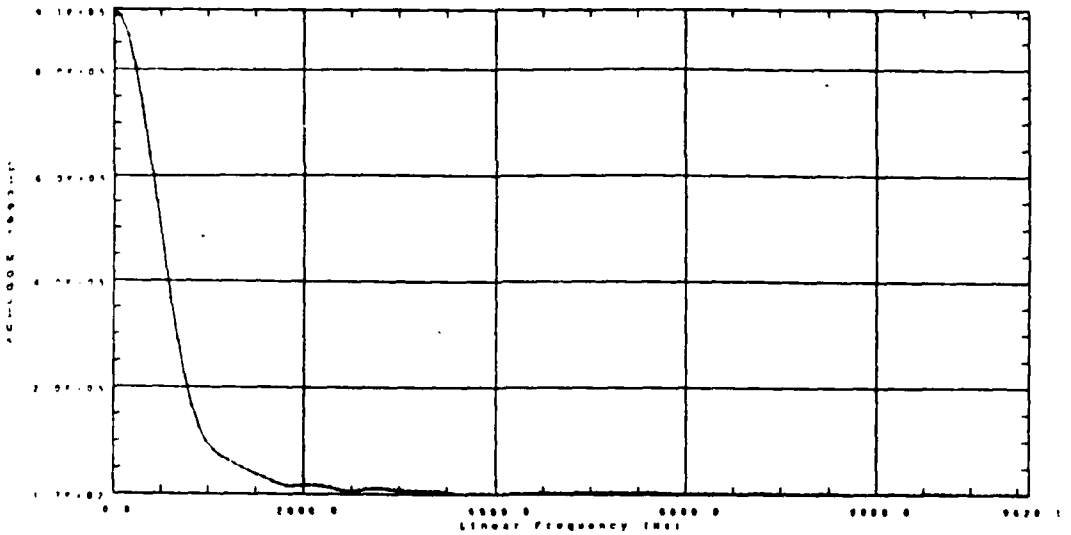

Figure 5.6. FFT of a single shot.

damping. The overall behavior of the three plots is encouraging with respect to model behavior. At the initiation of the excitation force, $t = 0$, all displacements are zero. Upon completion of the 100 shot burst, time 1.3 seconds, all displacements decay to their original zero displacement values.

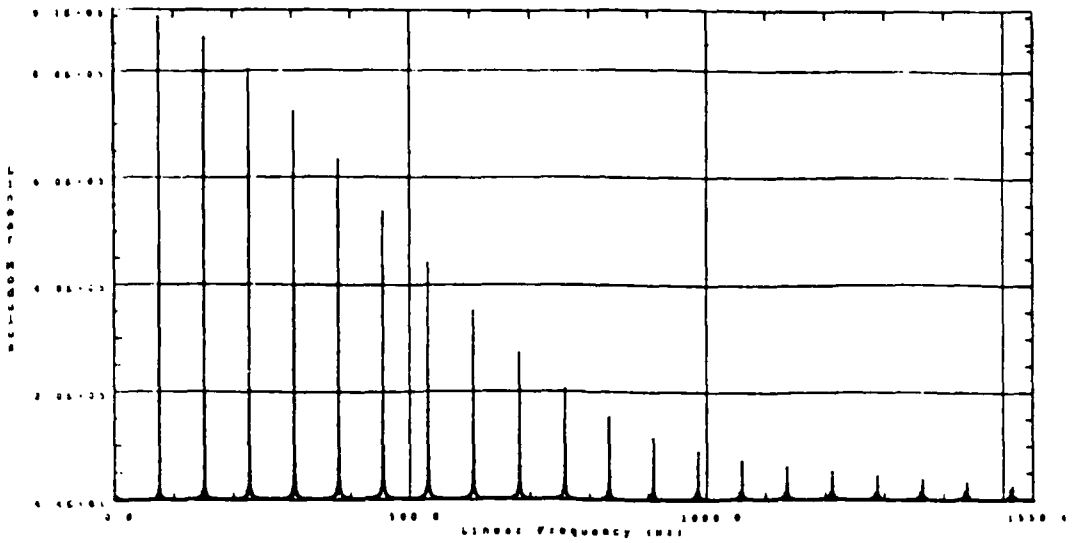

Figure 5.7. FFT of a 100 shot burst.

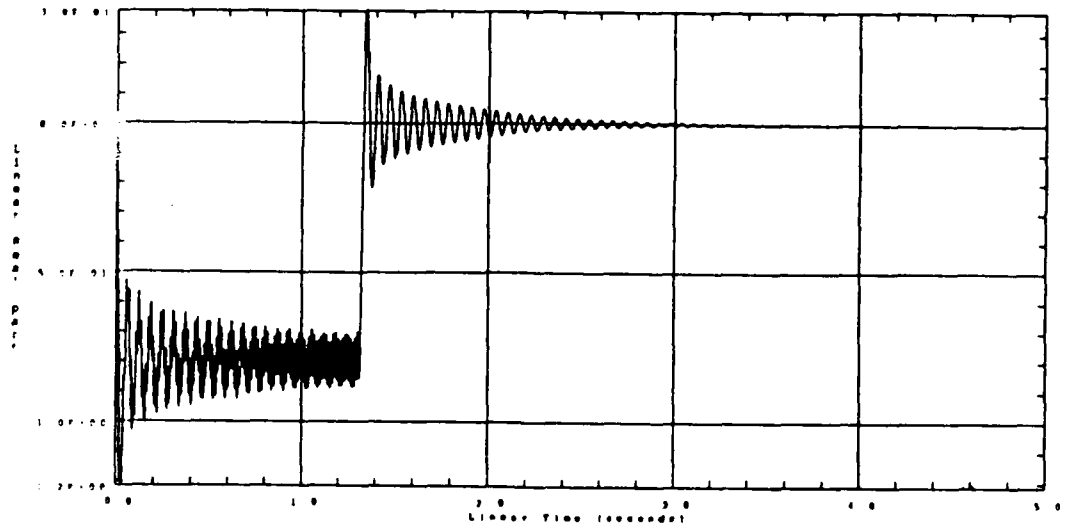

Figure 5.8. Firing barrel time response in the x direction.

In the x direction the barrel tip is displaced in the negative direction by approximately 0.96 cm. This is consistent with the displacement behavior of the recoil adapters. In the gun's firing sequence, the first shot causes the entire gun to set back, and then the gun begins to return to battery. The short period of the

firing causes the gun to recoil before it returns an appreciable distance. The result is the first shot establishes a new equilibrium position for the recoil adapters to oscillate. The recoil adapters allow the gun to oscillate approximately 0.6 cm. The establishment of a new equilibrium position is representative of the D.C. or 0 Hz component of the excitation force.

Mode 3, the recoil mode, is assigned a damping ratio of 0.35. It is sensible that the response in the x direction is comprised almost entirely of mode 3. Reviewing the lowest order modes, mode 3 is the only mode that has significant x translation. However, inspection of Figure 5.8 shows the combination of two modes. The steady-state region has jagged peaks, indicative of the combination of two modes of different frequencies. Close inspection reveals the jagged peaks of the oscillation. Mode 2, the yawing mode, also has moderate x translation, as does mode 4. The second mode could be mode 2 or mode 4. The FRF will confirm which modes are participating.

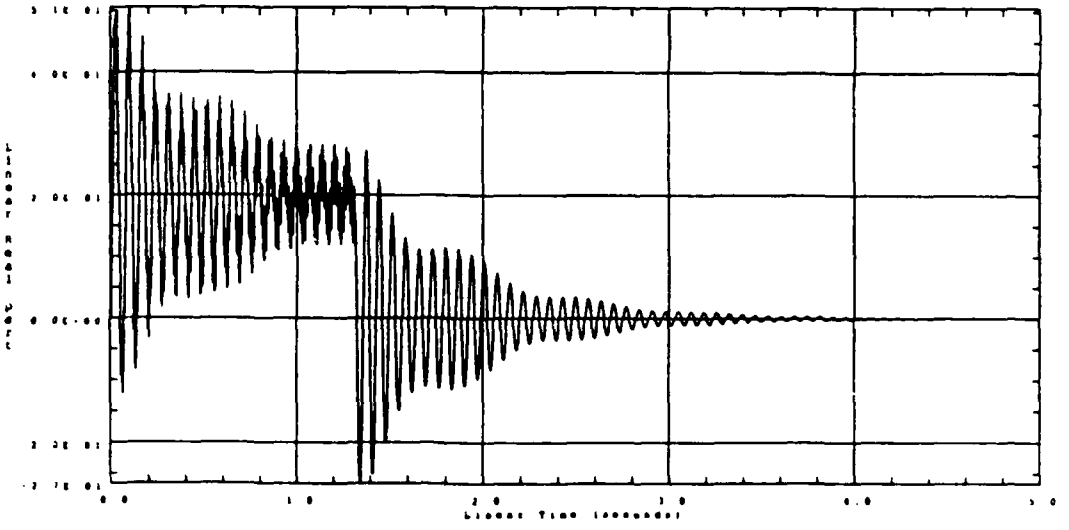

Figure 5.9. Firing barrel time response in the z direction.

The z displacement also shows appropriate behavior. Since the shot is fired at 12.5 degrees prior to TDC, it can be expected that the shots will create a moment about the gun's vertical axis. As a result, the barrel tip will yaw in the positive z

direction, establish a new equilibrium and begin to oscillate about this new equilibrium until the shots are completed. Inspection of the z response clearly indicates the presence of two modes. The damping envelope of the response has a profile indicative of a beat frequency. The beat frequency results in a periodic variation of the amplitude. It is the result of two functions of slightly different frequencies. The beat frequency is much less than either of the frequencies of the two contributing modes. Inspection of Figure 5.9 shows that the beat period is approximately 0.9 seconds corresponding to 1.1 Hz. This frequency separation is consistent with the separation between modes 2 and 3 of 1.05 Hz. It is apparent that mode 2, the yawing mode is a participant, and the beat frequency provides the means to determine the other participating mode, mode 3. Modes 2 and 3 have drastically different damping ratios. Mode 2 has a ratio of 0.02 and mode 3 has a damping ratio of 0.35. This difference is evident in the peculiar profile of the oscillation envelope. Upon completion of the shots, the response is transient and returns to the original equilibrium position. The displacement FRF in the z translation DOF will provide more evidence to support this analysis.

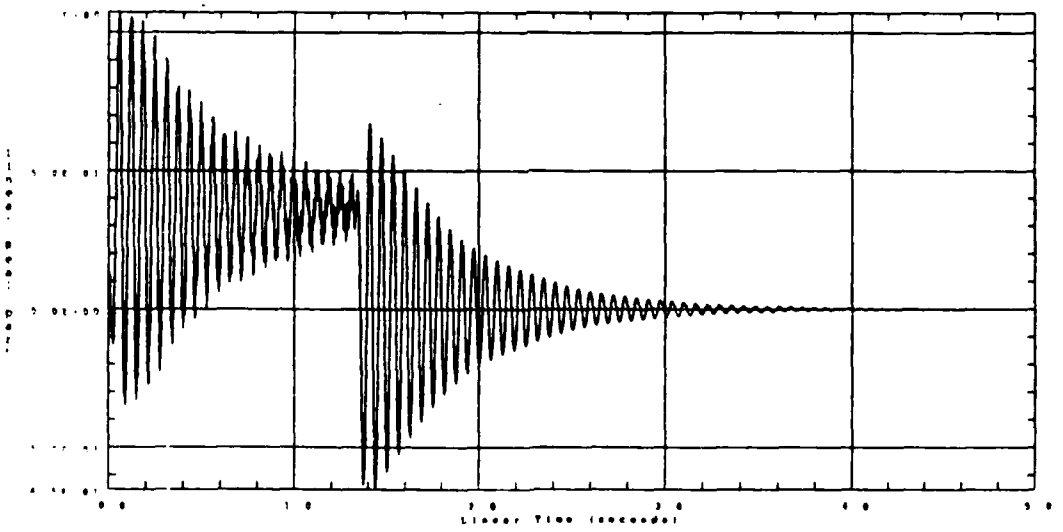

Figure 5.10. Firing barrel time response in the y direction.

The y response is the most important with respect to dispersion. The barrel length determines that a three millimeter barrel deflection in the vertical direction would account for an aim-point error of 1.6 mradians of angular dispersion. The resulting forced response causes the muzzle tip to displace positively in the y direction. The reason the barrel tip establishes a positive y equilibrium value is due to the eccentricities of the firing barrel, the gun mountings, and the gun's CG. The gun's mountings are in a plane that is below the gun's vertical CG. The barrels act in a plane above the gun's vertical CG. The result is that the excitation force causes a moment about a horizontal axis through the CG, and the barrel tip pitches upward. The steady-state response establishes an equilibrium position at about 3 mm displacement. This creates an aim-point error that is consistent with a dispersion value of approximately 1.6 or 1.7 mradians.

Inspection of Figure 5.10 indicates the presence of two modes, but there is no pronounced beat frequency. Review of the lowest order modes indicate that mode 4, the pitching mode, at 16.0 Hz, is the logical participant. Animation of mode 4 depicts the behavior that is consistent with the response described above. However, the second mode that is participating is not so obvious. The FRF is needed to completely understand the response.

E. FREQUENCY RESPONSE

The results of the time response curves are valuable and insightful. However, in order to gain a more significant understanding of the gun dynamics, the results of the frequency response must be studied. The frequency response function (FRF), or transfer function, can be defined for any node at any of its defined DOF, for an excitation applied at any node in any defined DOF. The output is a plot of normalized displacement versus linear frequency. The displacement is normalized per unit excitation. The peaks in the plot coincide with the natural frequencies of retained modes that are participating in the particular DOF's response. The

sharpness of these peaks is a function of the amount of damping for that particular mode. The peak amplitude provides a relative measure of the amount that an individual mode is participating in the response. The frequency response is able to quantify and confirm the participation of the mode shapes in a particular response.

Reviewing the mode shapes from Chapter IV, there are only five retained modes under 100 Hz. Of these five modes, review of their mode shapes reveals that only modes 2, 3, and 4 have barrel tip displacements. Therefore, it is sensible that only these three modes, or combinations of these modes, are evident in the displacement FRF's of the barrel tip displacements.

An important part of a FRF is the associated phase plot. The phase plot represents the phase difference between the excitation force and the response. The significant characteristics of the phase plot are discussed above in Section C. It is important to recognize that a response at a natural frequency corresponds to a phase shift of 90 degrees at resonance and 180 degrees through resonance. Phase relationships between the response and excitation provide insight into understanding system dynamics. Phasing problems can contribute to undesirable responses.

In the discussion above, it was mentioned that the x translation of the gun could be attributed to mode 3, or the recoil mode, and possibly mode 2, the yawing mode. For an excitation applied at the breech of the firing barrel, the FRF of the firing barrel tip in the x direction provides a frequency spectrum of the response. The frequency spectrum can be used to interpret which retained modes are participating in the response.

Figure 5.11 is the displacement FRF of the firing barrel tip in the x direction. The fact that there is a large peak at 15 Hz, indicates that mode 3 at 15.46 Hz is present. A smaller peak at 14.4 Hz indicates that modes 2 and 3 are participating in the response. Mode 3 is the recoil mode of the gun and mode 2 is the pitching mode of the gun. Mode 3 with a large amplitude peak is contributing significantly

more than mode 2. The width of the two peaks indicates the differences in their respective damping values. Mode 2 has a damping ratio of 0.02 and mode 3 has a damping ratio of 0.35. These results confirm the observations from the time response.

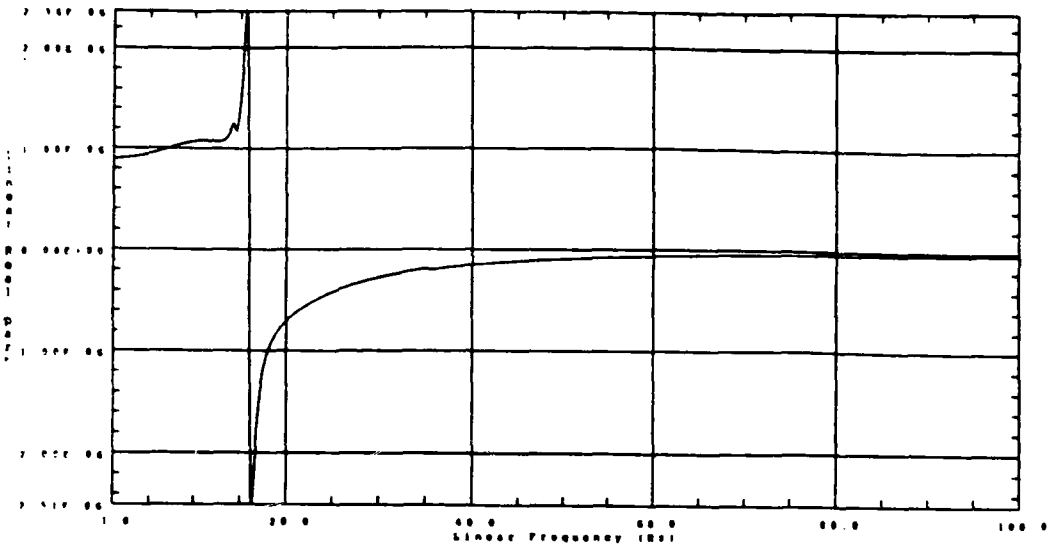

Figure 5.11. Frequency response of the firing barrel tip in the x direction.

In the previous chapter, a multi-degree-of-freedom system was analyzed. Systems with multi-degrees-of-freedom are likely to have coupling of vibrations. Modes are considered to be tightly coupled, if the coupling term is large. In general, the highest natural frequency is increased and the lowest is decreased (Ref. 44). The result is a pair of widely separated natural frequencies. For loosely coupled modes, the converse is true. The two modes do not effect each other. In a sense, they vibrate independently. Figure 5.12 shows two systems: one that is tightly coupled, the other loosely coupled (Ref. 46). Modes 2 and 3 are considered loosely coupled.

Figure 5.13 is the displacement FRF of the firing barrel tip in the z direction. There is a large peak at 14 Hz indicating that mode 2 at 14.4 Hz, is participating. A smaller peak at 15.4 Hz indicates that modes 2 and 3 are participating in this response. It is sensible that mode 2, the yawing mode, is the main contributor.

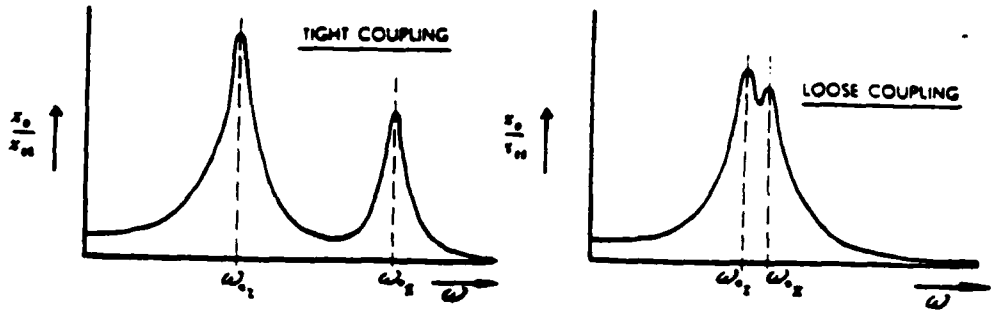

Figure 5.12. Systems with tightly coupled and loosely coupled modes.

The spacing of the peaks also indicates that the two modes are loosely coupled. The sharpness of the peaks are also significantly different, indicating their differing damping ratios. The z response is comprised of combinations of modes 2 and 3, the same as the x response. However, the relative contributions of the two modes are opposite.

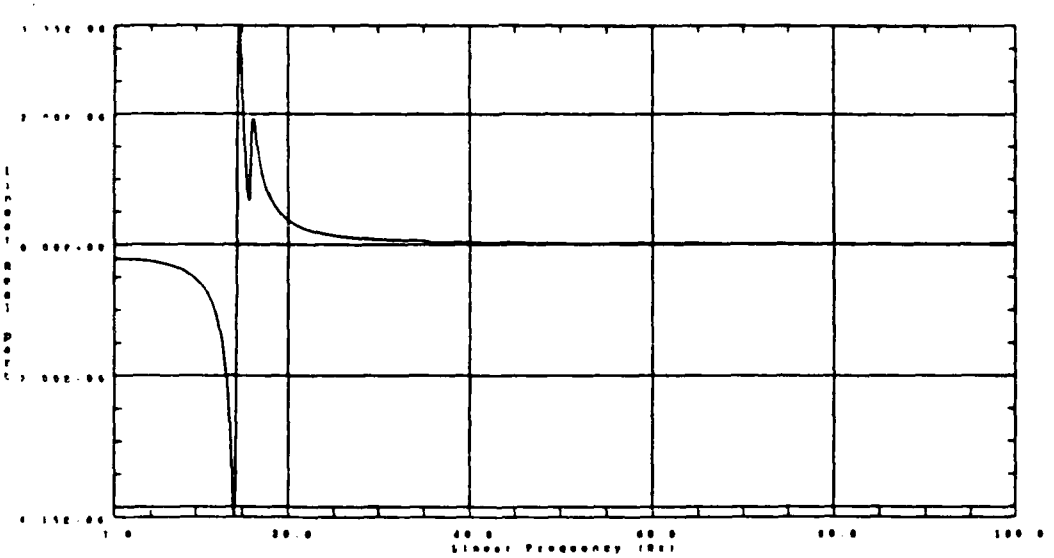

Figure 5.13. Frequency response of the firing barrel tip in the z direction.

Figure 5.14 is the displacement FRF of the firing barrel tip in the y direction. The fact that there is a peak at 16 Hz indicates that mode 4 at 16.0 Hz is participating in this response. Mode 4 is the pitching mode of the gun. The FRF does not reveal the participation of two modes. However, the time response indicates two mode participation. This will require further investigation. With more distinctive damping values, the participation of modes may become more distinct.

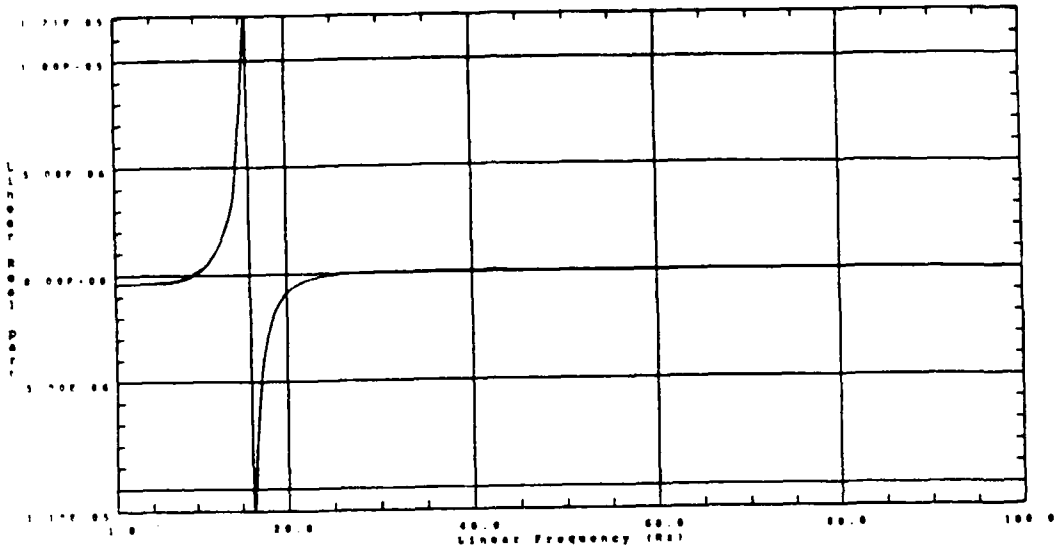

Figure 5.14. Frequency response of the firing barrel tip in the y direction.

The results of the FRF's provide an understanding of the modes of vibration involved in the dynamic response of the gun and the phasing of these modes with respect to the excitation force. Understanding these modes allows undesirable effects of the gun's dynamics to be controlled, eliminated, or reduced. There are certain characteristics of the gun's components that determine these mode shapes and natural frequencies. The damping of these modes determines the phasing of the response and excitation force. Damping is a function of the structure's material and the method used to assemble the components. Using this valuable information assists the FE engineer in making design decisions, to cancel or reduce

the participation of certain modes in a response. This will allow timely and efficient redesign or system modification.

VI. FUTURE WORK

A. MUZZLE RESTRAINT

A proposed solution for improving the excessive dispersion of PHALANX uses a muzzle restraint. Hughe's Missile has developed three different prototype muzzle restraints. The premise of the design is to restrict the motion of the end of the six-barrel system. One of the prototypes is shown in Figure 6.1 (Ref. 47). All designs incorporate a lightweight support structure and roller bearing. The differences between the three designs are primarily in the types and installations of roller bearings used. The restraint has a three point attachment to the PHALANX' mounting box or isogrid and a fourth to the end of the six-barrels by means of a roller bearing. The roller bearing allows normal rotation of the six-barrel system as well as the recoil translation in the longitudinal direction.

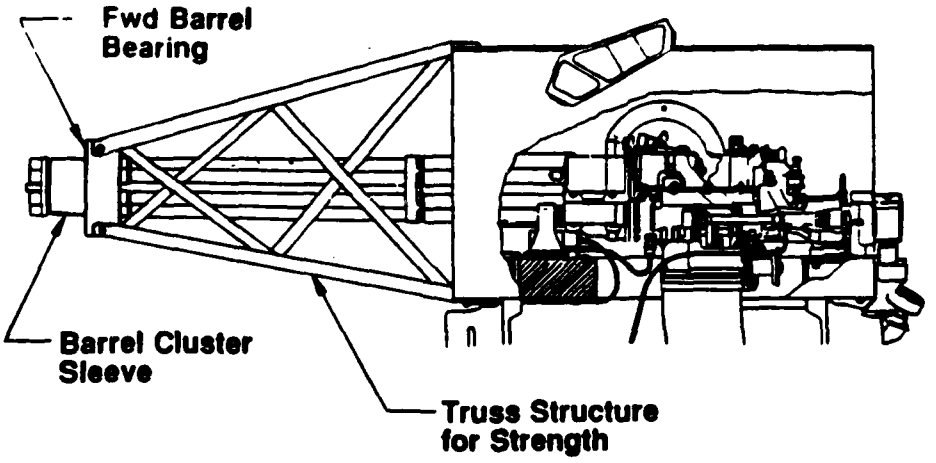

Figure 6.1. Muzzle restraint.

With a restraint, it is observed that the bursts with the largest dispersion values of 1.9 - 2.0 mradians do not occur, but the moderate dispersion values are still possible.

The restraint as well as the gun's isogrid should be included in the current model. It is also important to do a complete dynamic analysis of the restraint, including the development of FRF's. This will ensure that any possible resonance excitation between the gun and the restraint will be identified. The analysis should also include an investigation into the optimal placement of the muzzle restraint. Perhaps the restraint may do well at the mid-barrel point. Location of the restraint should be optimized with respect to limiting barrel tip displacement.

B. IMPROVEMENTS TO THE MODEL

The FEM process is itself a dynamic process. Successive analyses continually provide insight into future model improvements. The latest analysis has provided valuable insight into reducing the number of model DOF, and replacing particular elements with those that have better kinematic and elastic behavior. The following recommendations enhance the dynamic analysis of the current model, and also significantly reduce the number of DOF.

(1) Replace the muzzle clamp with a combination of a lumped mass element and rigid elements for support. A lumped mass element is created at a single node. It is used to represent the mass and inertia properties of a component that may not be an active participant in a model's dynamics; the component's mass, inertial and stiffness properties are its only contribution to the system response. The lumped mass element is simply created by choosing a node that is consistent with a specific component's CG. The component's mass and inertial properties are entered in the lumped mass physical property table.

The muzzle clamp can be replaced by a single lumped mass element located at its CG, and two rigid elements to provide a means to intra-connect the six-barrels as

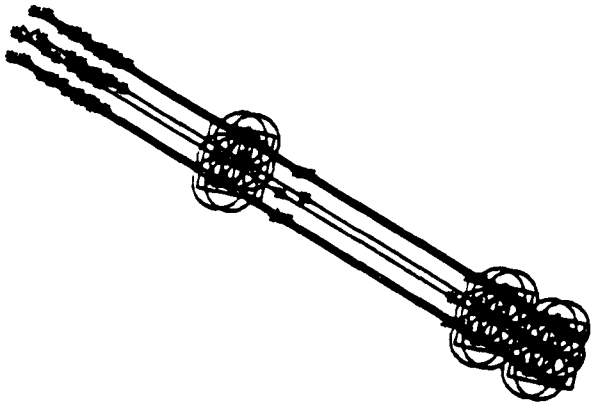

Figure 6.2. Schematic of proposed six-barrel assembly with modified muzzle and mid-barrel clamps.

shown in Figure 6.2. This modification will represent the boundary conditions imposed by the muzzle clamp and also contribute the same kinematic elastic behavior to the six-barrel system. The benefit is a significant reduction in the number of DOF.

(2) The same approach as discussed in (1) can be used for the mid-barrel clamp as shown in Figure 6.2. A lumped mass with the same mass and inertia properties as the mid-barrel clamp located at its CG, and a single rigid element to intra-connect all six barrels and the lumped mass. Again the benefit is a reduction in the number of DOF.

(3) Improve the interface of the double axial roller bearing and the housing. This interface is crucial in understanding the dynamics of the model. It is the critical load path of the firing rounds to the recoil adapters. In order to capture the dynamic effects of the bearing race / housing interface, it is recommended that the solid bricks in bearing races be replaced with beam elements. Using I-DEAS BEAM SECTION modeling, the exact profile of the bearing race can be modeled. It is understood that beam elements represent

bending behavior better than solid brick elements. In conjunction, the housing should be modeled as a continuum of shell elements, rather than a direct interface of shell elements with solid elements. The use of beam elements in the bearing races is conducive to achieving the latter modeling goal. Also, more detail of the housing should be incorporated. The housing is a support structure between the recoil adapters and the angular contact bearing. It is an important component in the load path. Rather than treat the housing as a simple cylinder, there should be an effort to capture the actual features of the housing.

(4) The rotor can also be simplified using a lumped mass and rigid elements. However, only a portion of the rotor should be modified. It is important to preserve the elastic and kinematic behavior between the axial roller bearing and the rotor, as well as the needle bearing and the rotor. Therefore, only a mid-section of the rotor should be replaced with an appropriately positioned lumped mass and two rigid elements. This will serve to eliminate elements that are not directly involved with the dynamics, but still allow enough of the rotor to remain intact to preserve the interface with the bearings. The benefit here is also a reduction in DOF.

(5) The recoil adapter's support structure should be eliminated and replaced with two rigid elements. The rigid elements will serve to model the attachment between the gun housing and the recoil adapter. It is important to emphasize that the lateral offset distance of the recoil adapters from the housing must be preserved. The recoil adapter's line-of-action is important in the dynamic analysis. Lumped mass could also be created at the node interconnecting the node-to-node translational springs and rigid elements.

(6) The node-to-node translational springs that are critical elements in the ball joint, double angular contact bearing, and recoil adapters should be reoriented. Currently these springs exist between two non-coincident nodes

that are spaced to reflect the actual geometry of these components. Depending on the load condition, a stiffness in any direction other than the line joining the two nodes may create a moment load on the springs. This is unrealistic for the actual components. This is a scenario unique to these components, because of the modeling method used. For example, in the bearings springs are used to represent the ball bearings. In the actual bearing, the ball bearings' dimensions are specified as is the spacing between the inner and outer races of the bearing. The decision was made to preserve the spacing between the races, but allow the springs, representing ball bearings, to span this space to connect the races. Currently, a dynamic analysis cannot be done in I-DEAS with gaps or spaces between components. In order to retain the appropriate geometry of these components and prevent moment loading of the springs, rigid elements can be used in conjunction with coincident nodes. Two coincident nodes should be created at a mid-point distance between the springs. Again using the contact bearing as an example, two coincident nodes should be created at a point mid-way between the inner and outer races. Each of these nodes will be connected to one of the former attachment points on the two bearing races using rigid elements. The spring element will be created between the two coincident nodes. This retains the correct component geometry and removes the possibility of undesirable moments about the spring.

C. MODEL VALIDATION

Upon completion of the above recommendations, the next essential step is model validation / correlation and determination of modal damping values. The correlation of analytical and experimental modal analysis provides a valuable method to uncover modeling errors. It can also detect inaccuracies in the connections between subcomponents or boundary conditions. An M61A1 Gatling

gun that has reached the end of its service life is currently on loan to the Naval Postgraduate School. Using this gun, extensive modal analysis should be performed. The testing should be conducted on the component level as well as various subassemblies, like the barrel cluster. This will provide insight into the vital characteristics of the components and their impact on gun dynamics. A thorough understanding of the various interactions is essential to a complete understanding of the system. It will aid in determining the coupled motion between components at different natural frequencies, and also potential phasing problems between components. The ultimate result of the correlation is to arrive at a validated model. A validated model can be used as a powerful analysis tool to make confident future design modifications.

D. ROTATIONAL EFFECTS

The modifications in Section B should be followed with the introduction of the gun rotational effects into the current model. I-DEAS SYSTEM DYNAMIC ANALYSIS provides the tools to include gyroscopic effects into the model.

I-DEAS offers a rotational matrix connector. The elements of the matrix connector define individual values for rotational DOF in the mass/inertia, damping and stiffness matrices. The terms used to represent the gyroscopic effects of the rotating assembly are entered in the viscous damping matrix. Connectors represent the dynamic properties of elements without geometry definition. The values of the matrix connector are dependent on a specific rotational speed. Therefore, a new matrix connector must be created for each rotational speed. Matrix connectors for a range of various rotational speeds should be developed. The speeds should represent the rotational speeds as the gun ramps up to operational speed, and through the theoretical maximum rotation rate of 1000 RPM.

E. ANALYTICAL MODEL

An analytical model is in development as part of a synergistic analysis effort. The use of the two analyses to determine the dynamic characteristics of the system will be more accurate than if they were studied separately. The analytical model will complement the computer analysis, specifically with respect to the rotational effects.

F. GYROSCOPIC WHIRL

Gyroscopic whirl is a mechanism of self-excited vibration that begins to vibrate on its own. The energy supplying the vibrations is provided by a mechanism in the system causing oscillating forces. This alternating force is created by the motion of the system itself; when the motion stops, the oscillating force disappears. This is in contrast to a forced vibration where the sustaining force exists independent of the motion. (Ref. 48)

Self-excited vibrations are characterized by the presence of a mechanism that will cause the system to vibrate at its own natural frequency, independent of an outside force. The motion is described by the homogeneous solution to the equation of motion. Self-excited vibration pervades rotating mechanical systems (Ref. 49).

Figure 6.3 (Ref. 50) shows the schematic of a typical system susceptible to gyroscopic effects. The springs to ground represent the gun's combined bearing stiffnesses, Ω is the rotational speed of the six-barrel system and I_2 is the rotational inertia of the gun's rotating assembly. In the drawing below, ω represents the angular velocity of whirl of the shaft centerline and T_k is the torque about O for $\phi = 1$ radian. When a shaft that spins about its longitudinal axis bends about that axis, the bent shaft will whirl about its original axis of rotation. In addition, the shaft will also continue to rotate about its bent longitudinal axis. This effect can be caused by loose or worn bearings, or an imbalance in the system. The disc attached to the end of an overhung beam will not whirl in its own plane.

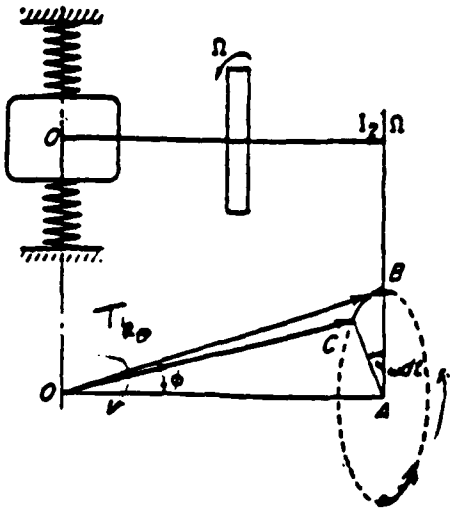

Figure 6.3. A system susceptible to whirl.

This is due to the fact that the centrifugal forces of the various particles of the disk do not lie in one plane. Consider the machine to be completely balanced and whirling at its critical speed in a slightly deflected position. The angular velocity of the whirl of the center of the shaft is assumed to be the same as the angular velocity of rotation of the shaft. This implies that a particular point on the disk which is outside will always be outside; the shaft fibers in tension remain in tension and those in compression remain in compression. Thus, any point on the disk moves in a circle in a plane perpendicular to the undistorted line of the shaft. Whirl can occur at frequencies greater than or less than the frequency of rotation. (Ref. 51)

Note the dispersion pattern shown in Figure 6.4 (Ref. 52). The geometric centers of the six individual barrels' aim point errors are denoted with a circle and the respective barrel number. The displacement of the six barrels is consistent with a whirl pattern. From the discussion of whirl, the gun has three distinct characteristics that could initiate or support whirl. First of all, the gun is a rotating system. Secondly, the bearings are not preloaded and may not have sufficient stiffness to support the high rotation rate and large forces of the firing

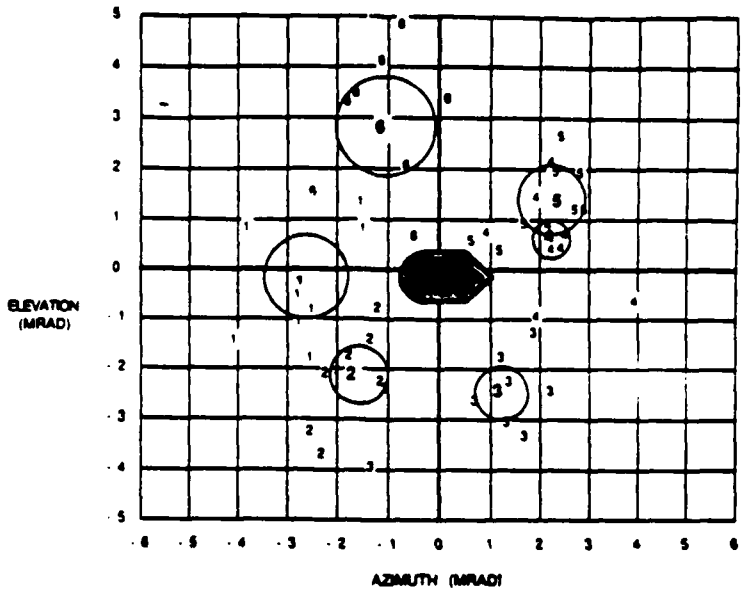

Figure 6.4. Two dimensional dispersion pattern.

cycle. Finally, imbalances pervade the gun system during operation. There is an imbalance created by the firing of the gun. The firing sequence starts 12.5 degrees prior to TDC. Since only one barrel fires at a time, there is an imbalance which may be the mechanism for the onset of whirl. Also, the force of a single shot is a following force. As the gun rotates from the point where the firing is initiated to the point where the bullet leaves the barrel, the magnitude and direction of the force is changing with both position and time. The manufacturing tolerances of the barrels allow for a variation between the masses of barrels of up to 0.3 kg out of 8 kg. Although the resulting imbalance is slight, it may be sufficient to initiate whirl. The gun's rotation rate is also a source of imbalance. The rotation rate of the gun can have up to a ± 50 RPM variation. This is only about ten percent of the gun's lowest firing rate, but it may provide the necessary instability to initiate whirl. The premise of this thesis has been to explore all sensitivities of the six-barrel system to displacements. Therefore, the concept of whirl and all possible contributions must be investigated and understood.

G. BEARINGS

During the model's development stage, a large amount of effort was spent on the gun's two bearings. There was not a lot of available information regarding design specifications and bearing design life. It was surprising to find that both bearings were catalogue bearings from both of their respective companies. While investigating stiffness parameters for the bearings, the manufacturers required that the bearing's operational load and geometry be defined. Both bearings were at the upper values for their respective operational loading. There was also a specific concern for the taper of the needle bearing's axle. It was too excessive. These parameters should be revisited. Perhaps alternate bearings could be substituted into the model and their behavior evaluated. The contribution of the bearings to the displacement of the six-barrel system must be explored further. Bearings are sensitive components with respect to whirl and provide the critical path for coupling gyroscopic effects. The addition of more massive barrels may prove to be futile in solving the dispersion problem.

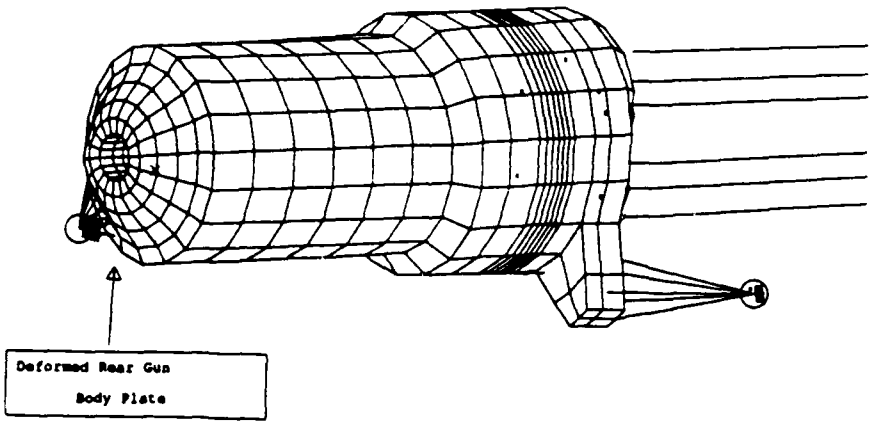

Figure 6.5 Cover plate deformation.

Review of the first nine mode shapes in Chapter IV shows significant deformation of the cover plate and needle bearing axle. This is shown in Figure

6.5. Possible design modifications or stiffening of theses components should be investigated.

H. DISPERSION PATTERN FREQUENCY SPECTRUM

Figure 6.6 is the FFT of the horizontal position as a function of time for a dispersion firing. Figure 6.7 is the same except for the vertical component (Ref. 53). It may be possible that the frequencies in this spectrum are correlated to natural frequencies in the gun's displacement response. It makes sense that a significant contribution would be at the gun's rotational rate of around 10 Hz, as seen in both figures. It is also interesting to note that in both figures there is a significant contribution of a low frequency component around 5 Hz. This is a possible contribution from a whirl frequency. No attempt will be made to draw conclusions from these plots since the initial conditions and raw data are not available. However, a similar analysis should be pursued. It may provide a valuable means of correlating analytical and empirical data as well as giving insight into gun dynamics.

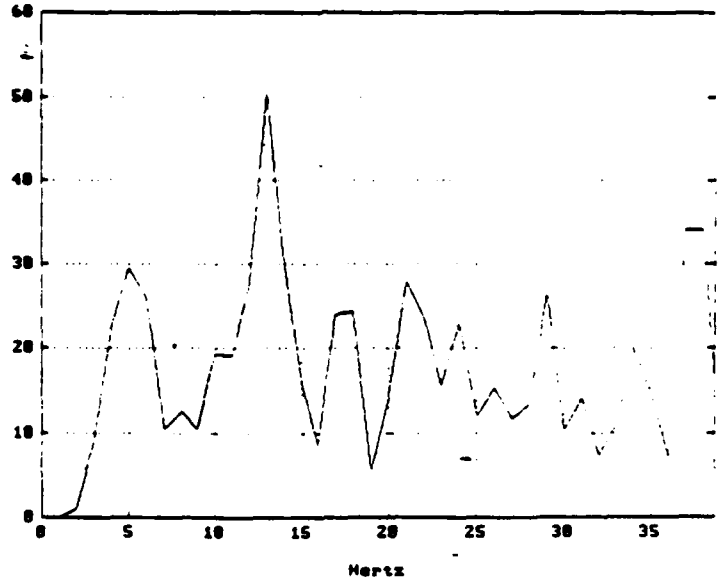

Figure 6.6 FFT of dispersion pattern in the horizontal direction.

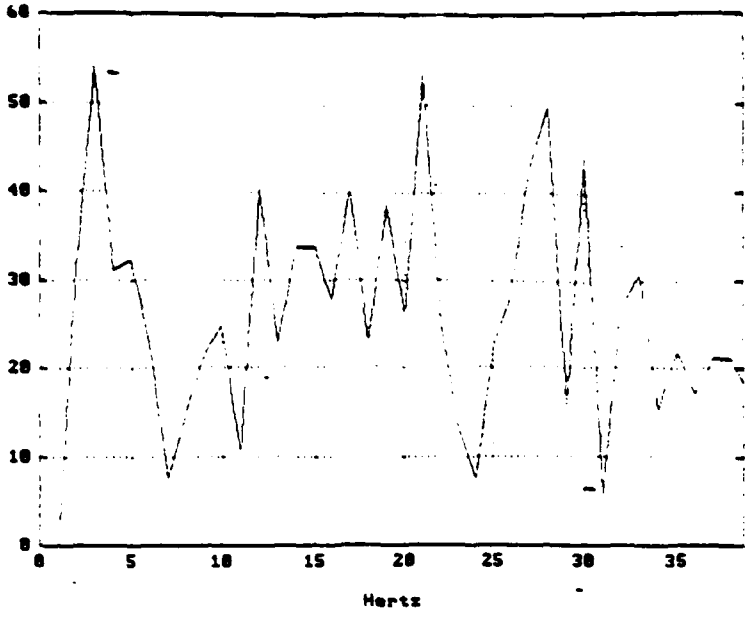

Figure 6.7 FFT of dispersion pattern in the vertical direction.

VII. CONCLUSIONS

In an effort to meet the increasing threat and improve the PHALANX dispersion, an optimized barrel design is underway with the possibility of a faster, enhanced-lethality round. The effort is focused on designing a significantly larger barrel that will accommodate the proposed round. These design modifications carry with them a host of system impact considerations. The finite element analysis is conducive to system impact studies. It provides engineers with timely and inexpensive evaluations. The use of finite element FE analysis is essential in the future design of all systems. The end costs of today's high tech projects are too great. Defense budgets no longer provide for projects with high financial risk. The FE method does not replace traditional engineering practices, nor does it preclude the building of prototypes. It does provide a timely analysis to assist in the early stages of design, and can highlight potential future shortcomings in the design.

The finite element analysis has provided valuable insight into aim point errors and their contribution to dispersion. Understanding the modes of vibration and the specific components that identify them can assist in eliminating undesirable responses.

This thesis has uncovered a potential significant contribution to dispersion: the double angular contact bearing. Also, the concept of gyroscopic whirl has been highlighted as a potential contributor to dispersion. The conclusions of the thesis have corroborated many years worth of observed data. The barrel tip response plots, in the y and z directions, shown in Figures 5.10 and 5.11, reveal that the displacements for the two directions are unequal. This leads to the conclusion that a two dimensional dispersion pattern is actually elliptical. This has always been the observed pattern. However, dispersion has always been defined in terms of the radius of a circle as shown in Figure 7.1 (Ref. 54).

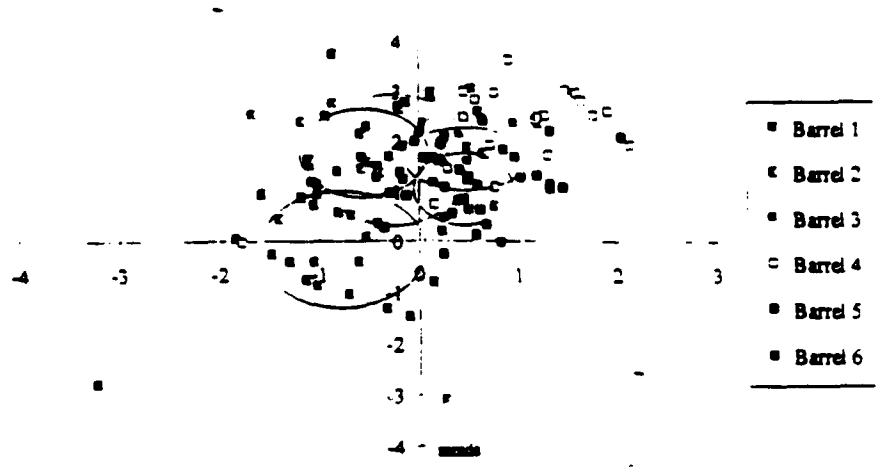

Figure 7.1 Dispersion ellipse.

High-speed, low radar cross-section, sea-skimming missiles are a huge threat to the U.S. Navy surface fleet. With the future emphasis of the navy's involvement in littoral warfare, a short range surprise launch from shore could devastate a ship. A close-in-weapon system may be called upon to serve as the outer layer as well as the inner layer of defense. With advancing technologies, anti-ship missiles are becoming smaller and faster and in a word, more lethal. Defensive weapons must be able to defend against this increased threat. The survivability of a one billion dollar cruiser and the lives of its crew are dependent upon the effectiveness of the PHALANX. The dispersion problem of the PHALANX must be understood and corrected.

APPENDIX A. MISSILE DEBRIS COMPUTER PROGRAM

A listing of the computer program in C follows.

```
/*************************************************
    ****  PHALANX Missile Debris Simulation ****
*************************************************/
#include  <stdio.h>
#include  <cmath.h>
#include  <greeks.c>
main() {
float x[20], vx[20], y[20], vy[20], z[20], vz[20], vt[20], v0, v[20], vf, t, dt,
 g, R, vtc, xsc, zsc, xmx, T, rho, cd, a, m, e, n, r1, r2, r3, max, pi, hit ;
int   ixo[20], iyo[20], izo[20], ix[20], iy[20], iz[20], sd, I, i, status[20], N
, h, nt, kill, miss, fn, pc;

/*------------------- read in parameters -------------------*/
printf("\n*** Debris Simulation ***\n"); g=9.8; h=10;
printf("  R(m) v0(m/s) dt(s) M(kg) Cd  A (m*m)  rho (kg/m3) num frag sd, fig no\
n");
scanf("%f%f%f%f%f%f%f%d%d%d",&R,&v0,&dt,&m,&cd,&a,&rho,&N,&sd,&fn);
vtc=sqrt(2*m*g/(cd*rho*a));
xmx=50.0; xsc=1000.0/xmx; zsc=1000.0/R;
ixo[1]=(int)(xsc*h); iyo[1]=0; izo[1]=0;
n=1;
pi=3.141592;
/*------------------------- heading -------------------------*/
init(); color_scale("bluescale"); grey_scale("greyscale1"); window0();
bgcol(7); erase(); color(0); mode("F1"); rect(187,80,791,195); color(2);
rect(180,75,784,190); mode("F0"); color(0); rect(180,75,784,190);
move(310,90); color(1); printf("*** Debris Simulation ***"); color(0);
move(240,150); printf("V"); sub ('t'); printf("=%-3.0fm/s",vtc);
move(440,150); printf("V"); sub ('0'); printf("=%-3.0fm/s",v0);
move(620,150); printf("R=%gm",R);
/*------------------- x-z graphics, side view --------------------*/
window(120,200,600,430); bgcol(3);  erase();
color(1); rect(120,200,600,430);    color(0); window0();
move(125,205); printf("side view"); move(82,205); printf("%g",xmx);
move(55,300); printf("x(m)");       move(97,410); printf("0");
/*------------------- y-z graphics, top view -------------------*/
window(120,435,600,665); bgcol(3);  erase();
color(1); rect(120,435,600,665);    color(0); window0();
move(125,440); printf("top view");  move(82,437); printf("%g",xmx);
move(55,530); printf("y(m)");       move(65,650); printf("%g",-xmx);
move(120,670); printf("0");         move(330,670); printf("z(m)");
move(535,670); printf("%g",R);
/*------------------- x-y graphics, end view --------------------*/
window(605,200,835,430); bgcol(3);  erase();
color(1); rect(605,200,835,430);    color(0); window0();
move(610,205); printf("end view");  move(700,435); printf("y(m)");
move(840,300); printf("x(m)");
/*------------------- initialize fragmnets --------------------*/
status[1]=0;
max=pow(2.0,31.0)-1.0;
srandom(sd); nt=0;
for (i=0;i<N;++i) { for (nt=0;nt<n;++nt) {
x[i]=h;
y[i]=0;
z[i]=0;
r1=random()/max;
r2=random()/max;
I=(int)(10*(sqrt(-2*log(r1))*cos(2*pi*r2)));
vx[i]=I;
r1=random()/max;
r2=random()/max;
I=(int)(10*(sqrt(-2*log(r1))*cos(2*pi*r2)));
vy[i]=I;

r1=random()/max;
r2=random()/max;
I=(int)(10*(sqrt(-2*log(r1))*cos(2*pi*r2)));
vz[i]=v0+I;

ixo[i]=(int)(xsc*x[i]);
iyo[i]=(int)(xsc*y[i]);
izo[i]=(int)(zsc*z[i]);

while (vt[i]<10) {
r3=random()/max; I=(int)(-vtc*(log(r3)));
vt[i]=I;  } }

/*------------------- calculate trajectories -------------------*/
kill=0; miss=0;
while (hit<N) {
for (i=0;i<N;++i) { if (status[i]<1) {
v[i]=sqrt(vx[i]*vx[i]+vy[i]*vy[i]+vz[i]*vz[i]);
  vx[i]=vx[i]-(g+(g/(vt[i]*vt[i])))*v[i]*vx[i])*dt; vy[i]=vy[i]-(g/(vt[i]*vt[i]))
*v[i]*vy[i]*dt;
                                vz[i]=vz[i]-(g/(vt[i]*vt[i]))*v[i]*vz[i]*dt;
  x[i]=x[i]+vx[i]*dt; y[i]=y[i]+vy[i]*dt; z[i]=z[i]+vz[i]*dt; t=t+dt;
  ix[i]=(int)(xsc*x[i]); iy[i]=(int)(xsc*y[i]); iz[i]=(int)(zsc*z[i]);


  /*------- x-z graphics, side view --------*/ color(4);
  window(120,200,600,430); scale(0,1000,1000,0);
  vector(izo[i],ixo[i],iz[i],ix[i]); window0();
  if (z[i]>R) { status[i]=1;++hit;++kill; }
  if (x[i]<0) { status[i]=1;++hit;++miss; }

 /*------- y-z graphics, top view --------*/
  window(120,435,600,665); scale(0,500,1000,-500);
  vector(izo[i],iyo[i],iz[i],iy[i]); window0();
  if (z[i]>R) { status[i]=1; }
  if (y[i]<-500/xmx && y[i]>500/xmx) { status[i]=1; }
 /*------- x-y graphics, end view --------*/
  window(605,200,835,430); scale(-500,1000,500,0);
  vector(iyo[i],ixo[i],iy[i],ix[i]); window0();
  if (x[i]<0) { status[i]=1;}
  if (y[i]<-500/xmx && y[i]>500/xmx) { status[i]=1; }
  ixo[i]=ix[i]; iyo[i]=iy[i]; izo[i]=iz[i];
   } } }

/*------------------- final -------------------*/ color(0);
move(640,500); printf("Ship hits -%d", kill);
move(640,540); printf("Misses-%d", miss);
move(640,580); printf("Fragments-%d",N);
move(640,620); greek(Sigma);printf("=%-3.0f m/s", vtc);
move(640,660); printf("seed=%d", sd);
move(820,990); printf("Figure %d", fn);    }
```

APPENDIX B. GUN MODEL MODE SHAPES

The following are line drawings of the deformed model mode shapes. All are side views, in ascending order by frequency.

SDRC I-DEAS V1.1(S): IF Modeling & Analysis 19-MAY-93 16:07:09

Database phalanxgun
View SIDE
Task Post Processing
Model: 8 MODEL8

Units CM
Display N, Stored Option
Model Bin 1 MAIN
Associated Workset: 9 WORKING SET9

phalanxgun

LOAD SET 3 MODE 3 FREQ 14.405972
DISPLACEMENT NORMAL MIN 0.00 MAX 10.00

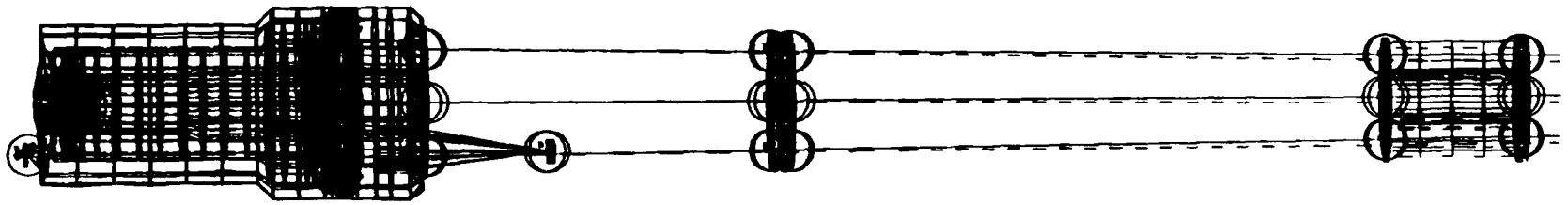

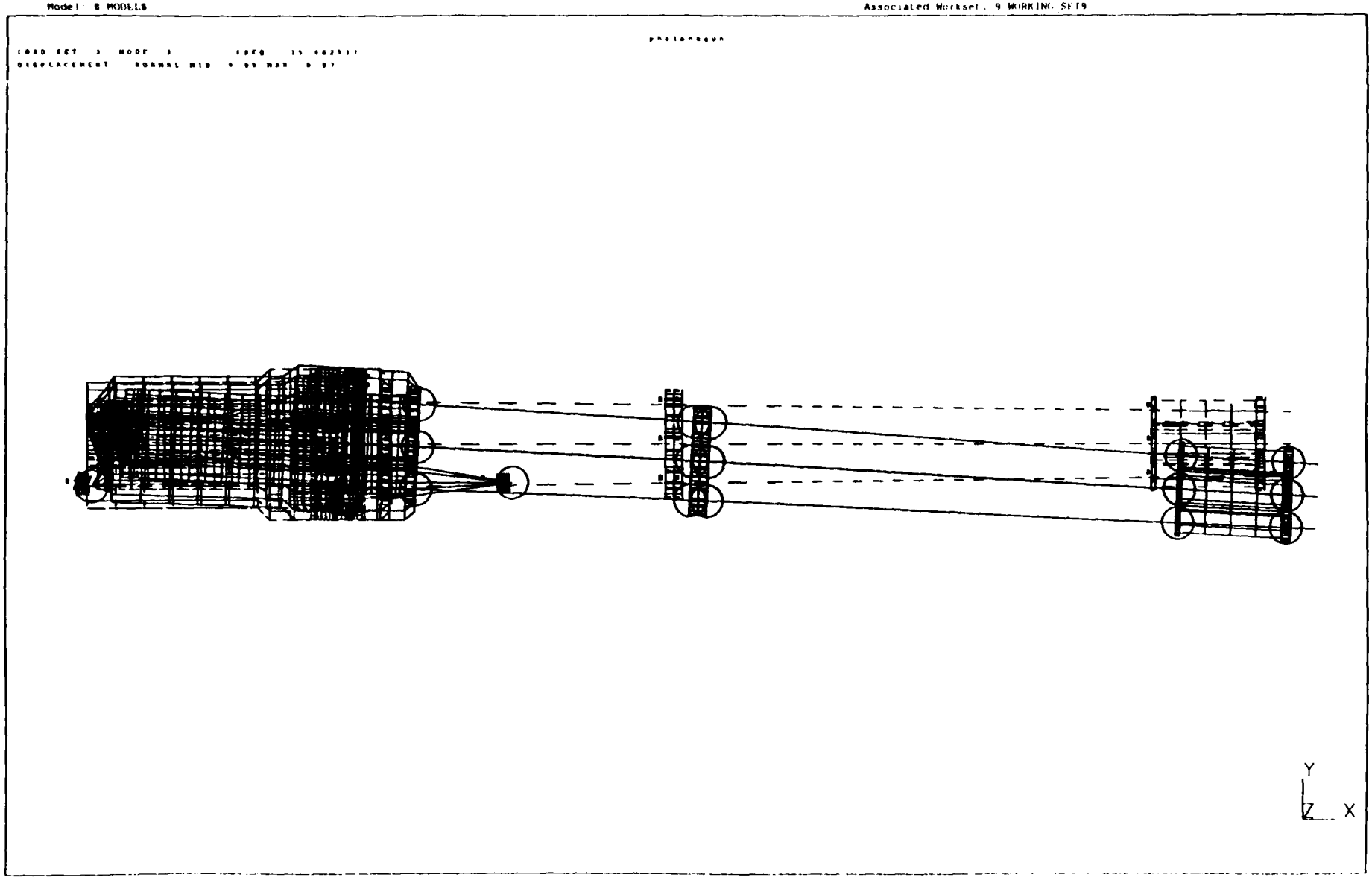
Database phalanxgun
View STDF
Task Post Processing
Model 0 MODELS
19 MAY-97
19:38:40
Units CM
Display
Model Rtn 1 MAIN
Associated Workset 9 WORKING SET9
phalanxgun
LOAD SET 3 MODE 3 FREQ 15.662517
DISPLACEMENT NORMAL MIN 0.00 MAX 0.97
Y
Z
X

phalanxgun

LOAD SET 4 MODE 4 FREQ 19.95252
DISPLACEMENT NORMAL MIN 0.00 MAX 0.12

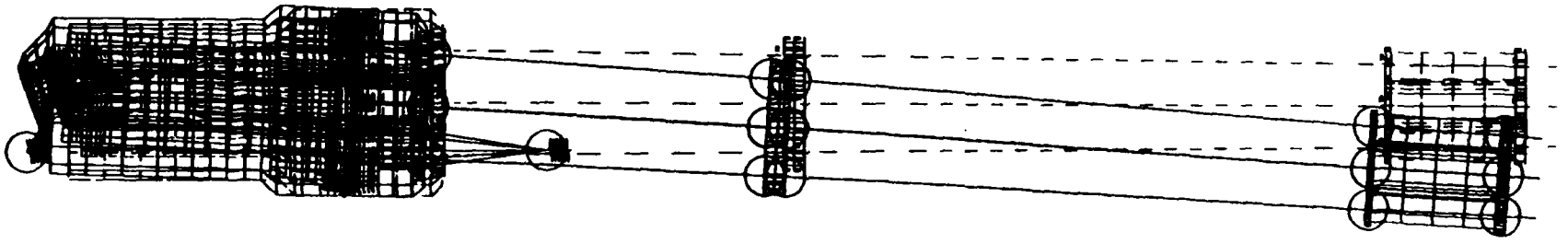

SDRC I-DEAS V[illegible](5): FE Modeling & Analysis 1--MAY-9[illegible] 20:51:22

Database: phalanxgun
View : No stored View
Task: Post Processing
Model: 6 MODEL6
Units CM
Display : No stored Option
Model Blk: 1 MAIN
Associated Workset 9 WORKING SET9

phalanxgun

LOAD SET 5 MODE 5 FRQ 35.33191
DISPLACEMENT NORMAL MIN 0.00 MAX 4.33

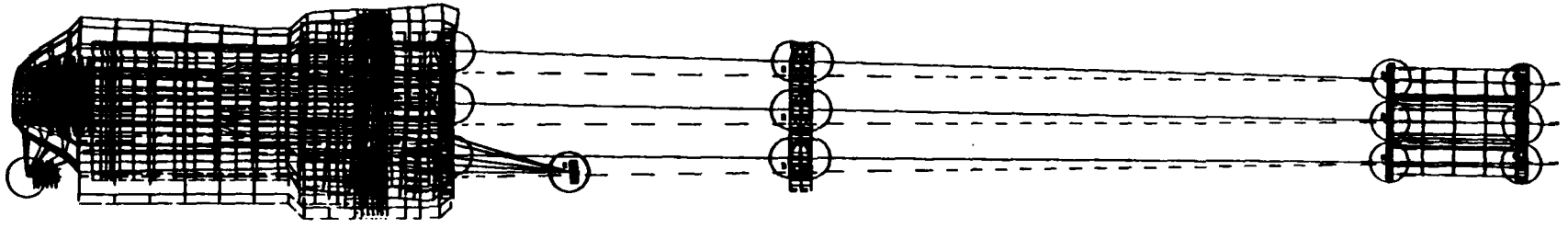

phalanxgun

LOAD SET 6 MODE 6 1 FREQ 55.5169
DISPLACEMENT NORMAL MIN 0 MAX 2.73

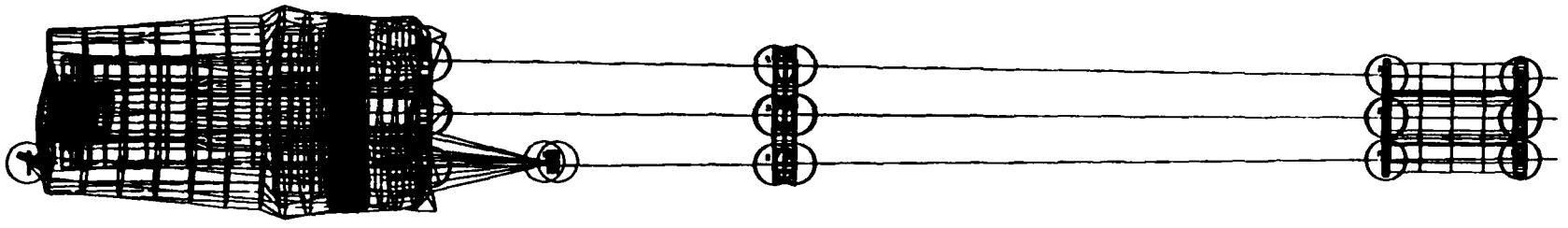

SDRC I-DEAS V[illegible](s): FE Modeling & Analysis 19-MAY-9[illegible] [19:58:11]

Database phalanxgun
View : SIDE
Task: Post Processing
Model: 0:MODEL0

Units : CM
Display : No Stored Option
Model B-n : 1 MAIN
Associated Workset : 9 WORKING SET9

phalanxgun

LOAD SET: 7 MODE: 7 * FREQ LIN SOLZY
DISPLACEMENT NORMAL MIN 0.00 MAX: 3.03

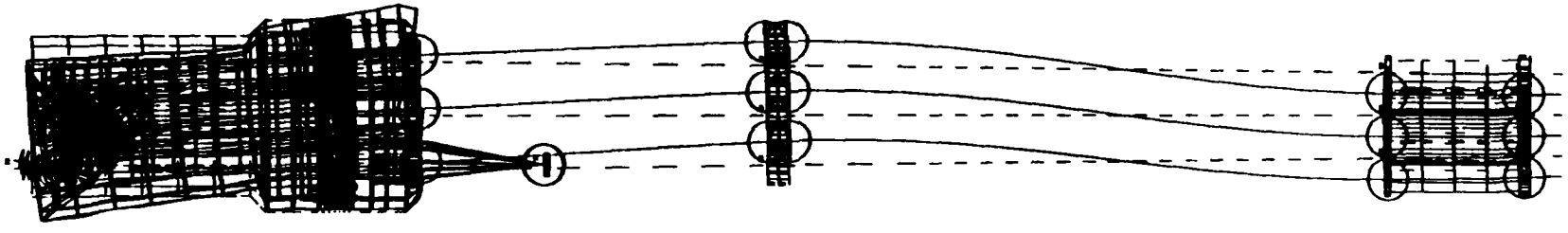

SDRC I-DEAS V1.1(s): FE Modeling & Analysis 17-MAY-91 2:;4:37

Database: phalanxgun Units : CM
View : No stored View Display : No stored Option
Task: Post Processing Model Bin: 1 MAIN
Model: 0 MODEL0 Associated Workset: 9 WORKING SET9

phalanxgun

LOAD SET 0 MODE 0 FREQ: 116.3018
DISPLACEMENT NORMAL MIN 0.00 MAX 4.93

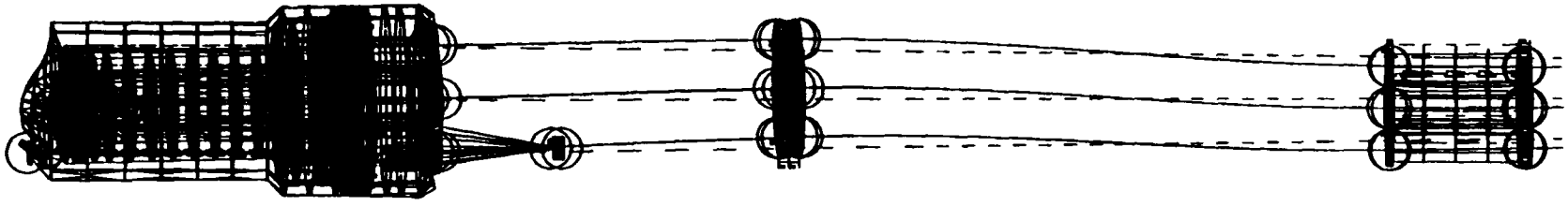

SDRC I-DEAS V1.1( ): FE Modeling & Analysis

17-MAY-93 21:29:28

Database: phalanxgun
View : No stored View
Task: Post Processing
Model: 8 MODEL8

Display N stored Options
Model Bin 1 MAIN
Associated Workset: 9 WORKING SET9

phalanxgun

LOAD SET 9 MODE 9 FREQ 129.3528
DISPLACEMENT NORMAL MIN .5 CC MAX 3.06

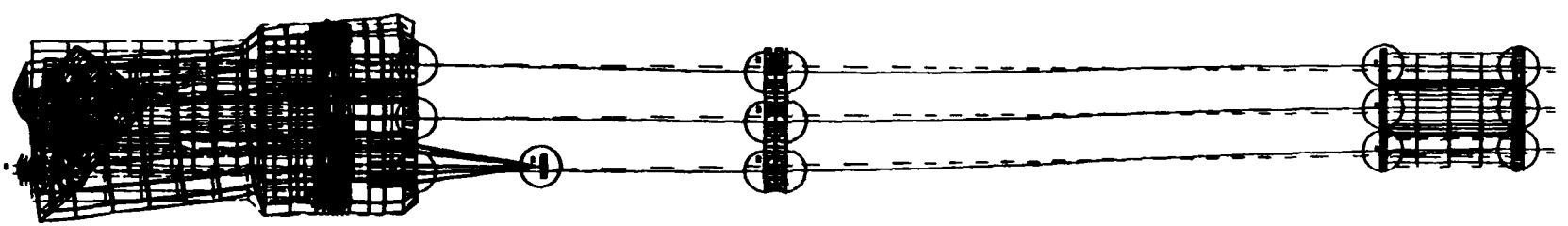

Y
X

SDRC I-DEAS V1..(S): II Modeling & Analysis

Database phalanxgun
View No stored View
Task Post Processing
Model 0 MODEL0

! MAY 9.

Units CM

Display No stored Display
Model Bin 1 MAIN
Associated Workset 9 WORKING SET 9

phalanxgun

LOAD SET 10 MODE 10 FREQ 165.03622
DISPLACEMENT NORMAL MIN 0.00 MAX 1.53

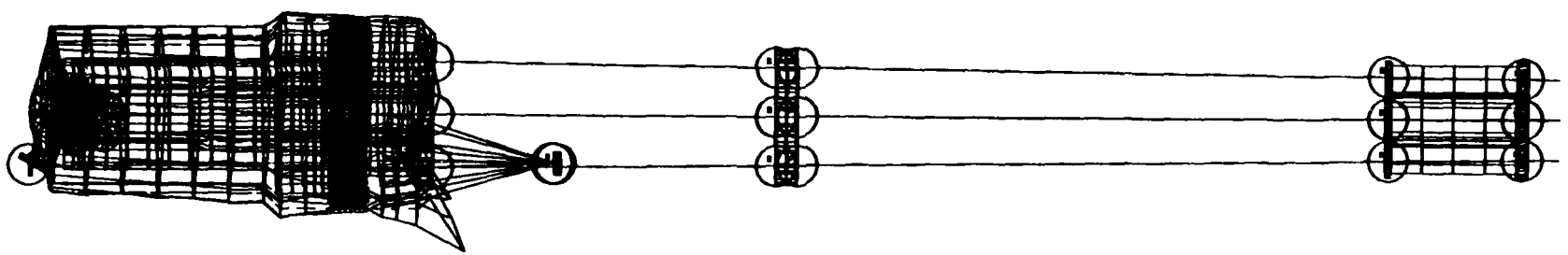

Y
Z X

Database phalanxgui
View SIDE
Task Post Processing
Model 8 MODEL8

Display No stored option
Model Base I MAIN
Associated Workset 9 WORKING SET9

phalanxgui

LOAD SET 11 MODE 11 EDCG ITG ANGLE
DISPLACEMENT NORMAL MIN 0.00 MAX 5.50

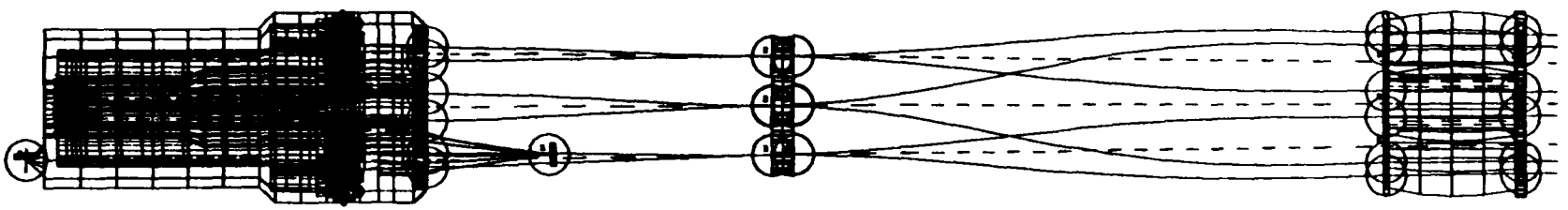

Y
Z X

SDRC I-DEAS V1.1(s): IE Modeling & Analysis 19-MAY 9x 20:24:59

Database phalanxgun
View : SIDE
Task: Post Processing
Model: 8 MODEL8

Units CM
Display No Stored Option
Model Bin : MAIN
Associated Workset : 9 WORKING SET9

phalanxgun

LOAD SET 12 MODE 12 FREQ 231.1257
DISPLACEMENT NORMAL MIN 0.00 MAX 2.23

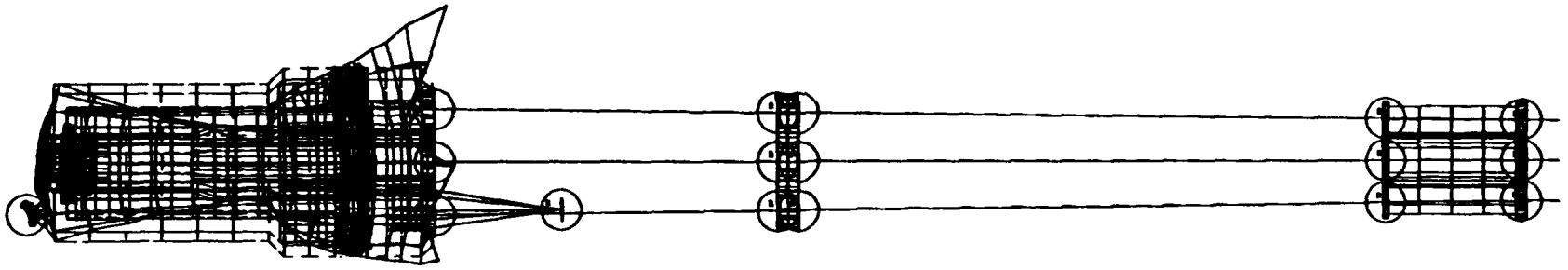

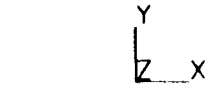

SDRC I-DEAS V[illegible] (s): [illegible] Modeling & Analysis 19-MAY-9[illegible] [illegible]:[illegible]:19

Database phalanxgun
View : SIDE
Task: Post Processing
Model: 8 MODEL8

Units CM
Display No stored Option
Model Run 1 MAIN
Associated Workset: 9 WORKING SET9

phalanxgun

LOAD SET 13 MODE 13 FREQ 242.45662
DISPLACEMENT NORMAL MIN 0.00 MAX 1.91

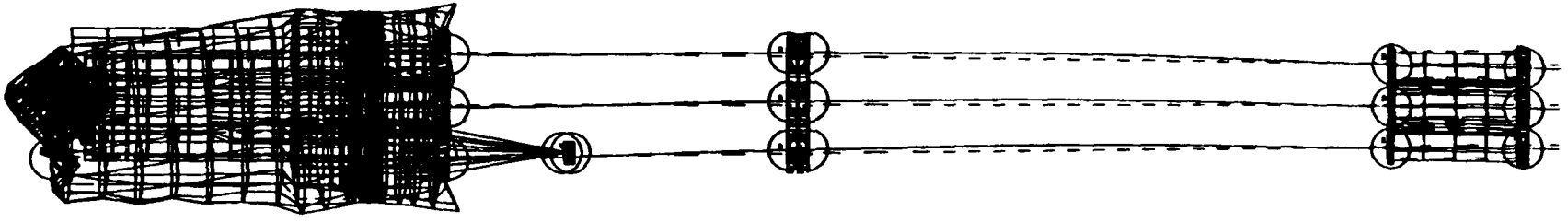

SDRC I-DEAS V1.1(s): FE Modeling & Analys..

Database phalanxgun
View SIDE
Task: Post Processing
Model: 8 MODEL.8

19-MAY-9x 20:38:25
Units = CM
Display No stored option
Model Rule 1 MAIN
Associated Workset: 9 WORKING SET 9

LOAD SET 14 MODE 14 FREQ 246.7870
DISPLACEMENT NORMAL MIN 0.00 MAX 1.65

phalanxgun

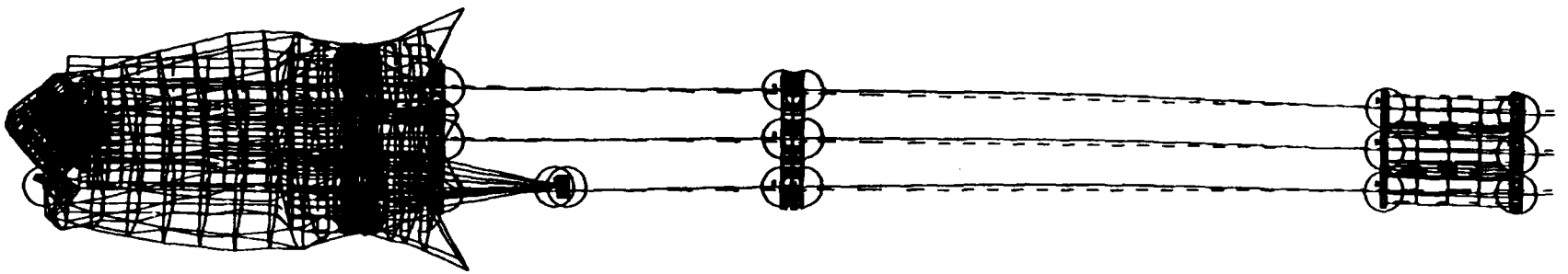

SDRC I-DEAS VI.1(s): FE_Modeling_&_Analysis 16-JUN-93 09:08:44

Database: phaiangun
View : SIDE (modified)
Task: Post Processing
Model: 2-MODEL2

Units : CM
Display : No stored Option
Model Bin: 1-MAIN
Associated Workset: 26-WORKING_SET26

LOAD SET: 15 MODE: 15 FREQ: 354.34020
DISPLACEMENT - NORMAL MIN: 0.000430 MAX: 2.16

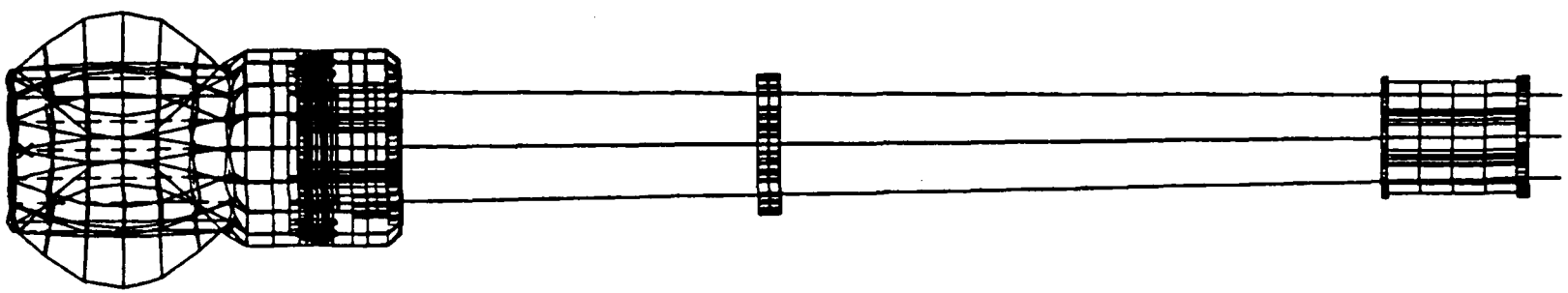

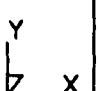

SDRC I-DEAS VI.1(s): FE_Modeling_&_Analy_is 16-JUN-93 09:11:17

Database: phalanxgun Units : CM

View : SIDE (modified) Display : No stored Option

Task: Post Processing Model Bin: 1-MAIN

Model: 2-MODEL2 Associated Workset: 26-WORKING_SET26

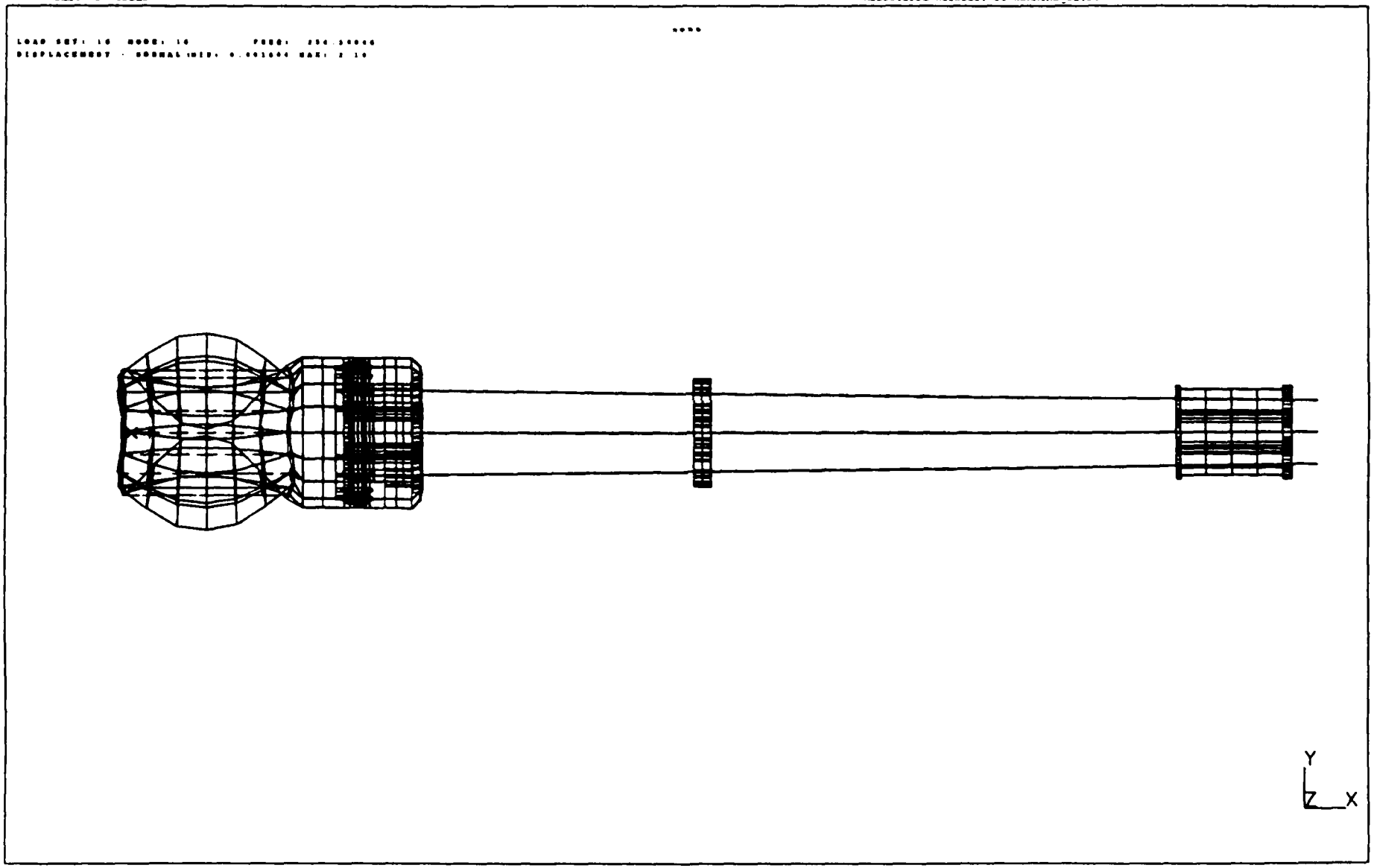

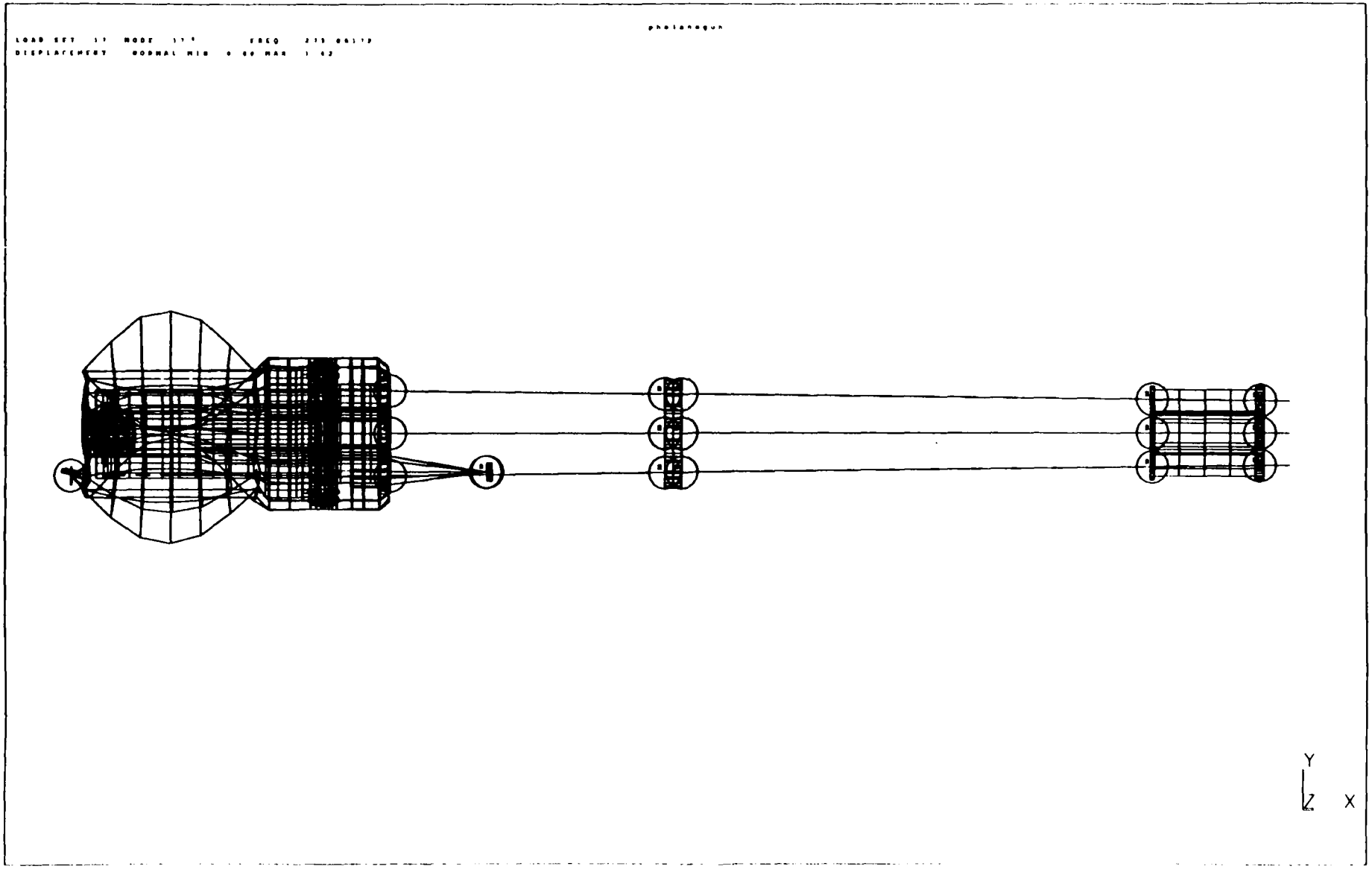
Database phalangjn
View STDE
Task Post Processing
Model 0 MODEL0
phalangjn
Y
X

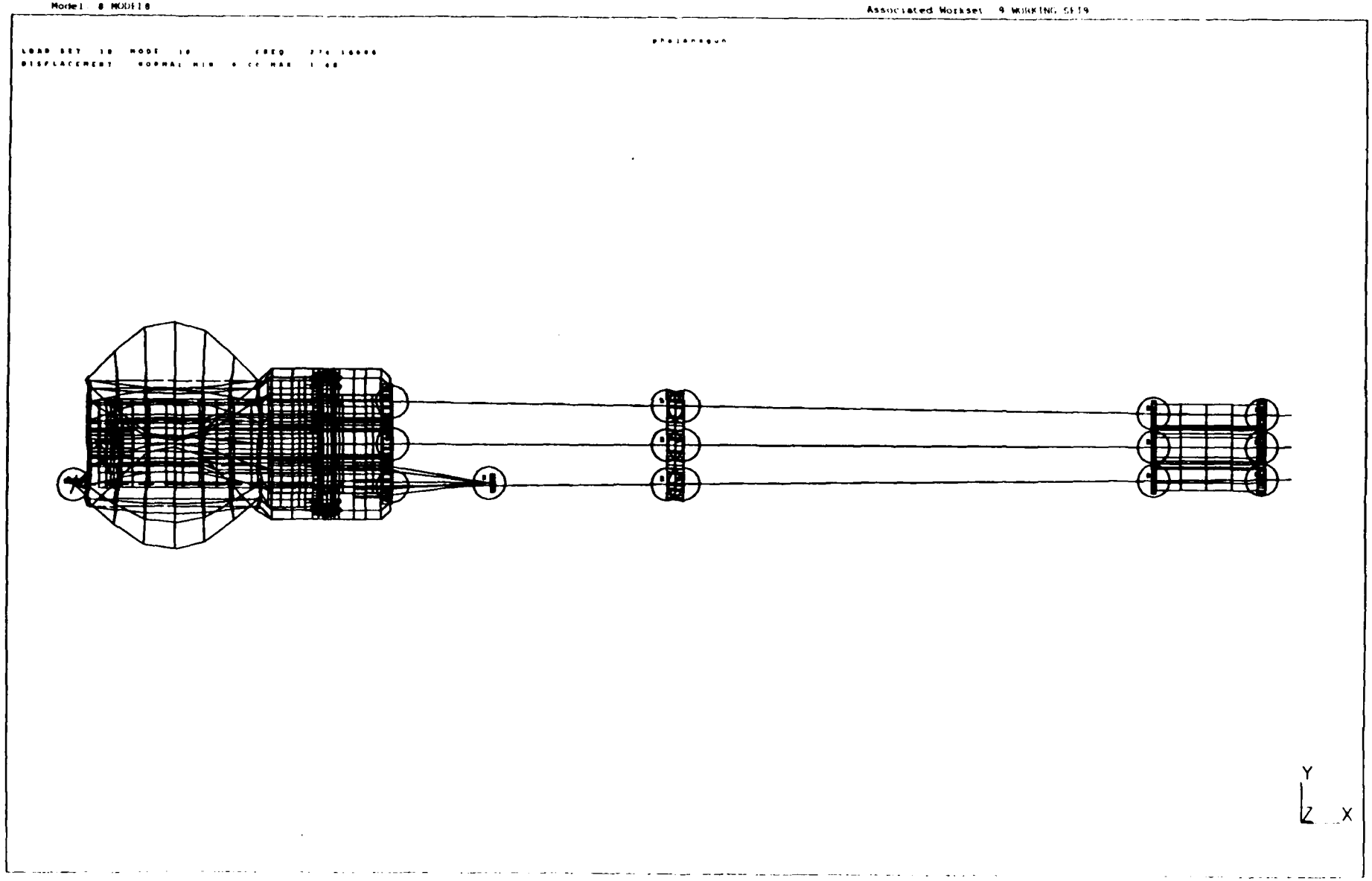
phalanagun
LOAD SET 10 MODE 10 FREQ 2?s 10000
DISPLACEMENT NORMAL MIN 0.00 MAX 1.00
Y
Z
X

SDRC I-DEAS V1.1(s): FE Modeling & Analysis 19-MAY-94 21:18:05

Database phalanxgun
View SIDE
Task Post Processing
Model 8 MODEL8

Units CM
Display No stored Option
Model Bin 1 MAIN
Associated Workset 9 WORKING SET9

phalanxgun

LOAD SET 10 MODE 19 FREQ 288.8867
DISPLACEMENT NORMAL MIN 0.00 MAX 1.00

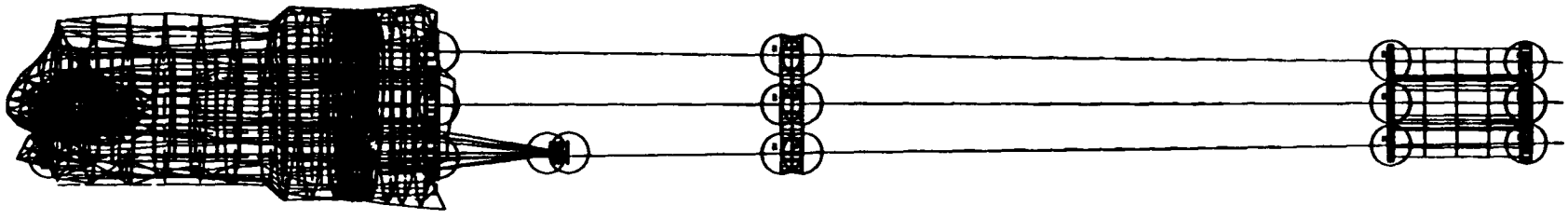

phalanxgun

LOAD SET 20 MODE 20 FREQ 300.39679
DISPLACEMENT NORMAL MIN 0.00 MAX 2.71

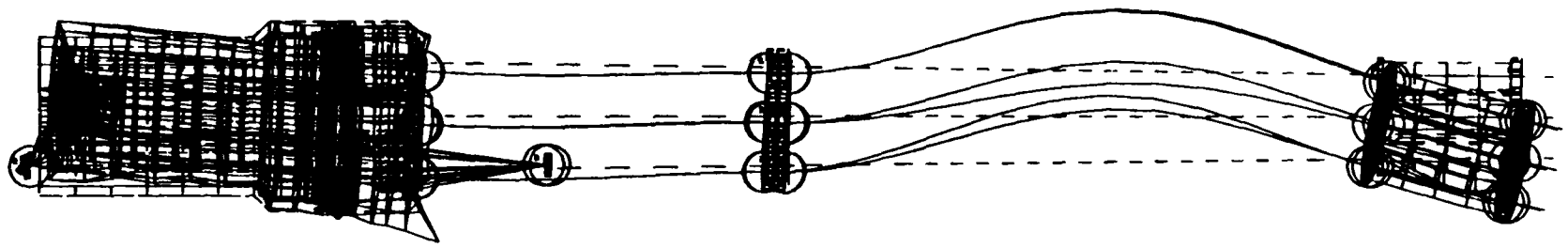

LIST OF REFERENCES

1. *Close-In Weapon System MK 15 Mods 1 Thru 4 and 6 (PHALANX): Introduction to CIWS* , pp. 1-0, Naval Sea Sytems Command, 1987.
2. *Close-In Weapon System MK 15 Mods 1 Thru 4 and 6 (PHALANX): Introduction to CIWS* , pp. 1-0, Naval Sea Sytems Command, 1987.
3. *Close-In Weapon System Mk 15 MODS 1 Thru 4 and 6 (PHALANX): Functional Description* , pp. 2-9.1 - 2-9.8, Naval Sea Systems Command, 1987.
4. Notes from Hughes Missile Systems Company, Pomona, California, 23 October 1992.
5. Notes from Hughes Missile Systems Company, Pomona, California, 23 October 1992.
6. Notes from Hughes Missile Systems Company, Pomona, California, 23 October 1992.
7. Garner, F. G., *Hit Probability for Small and Medium Calibre Belt-Fed Cannon* , International Defense Review, November 1991.
8. Notes from Hughes Missile Systems Company, Pomona, California, 23 October 1992.
9. Notes from Hughes Missile Systems Company, Pomona, California, 23 October 1992.
10. Notes from Hughes Missile Systems Company, Pomona, California, 23 October 1992.
11. Wolff, P. C., *Load/Deflection Test and Analysis of M61 Gun* , test report presented to Dick Sirola, Burlington, Vermont, 9 August, 1989.
12. Knight, C. E., *The Finite Element Method in Mechanical Design* , pp. 20-36, PWS-KENT Publishing Co., 1993.

13. Lawry, M. H., *I-DEAS Student Guide* , pp. 201-208, Structural Dynamics Research Corp., 1991.

14. *I-DEAS Model Solution and I-DEAS Optimization User's Guide* , pp. (18-69)-(18-75), Structural Dynamics Research Corp., 1990.

15. Lecture by Joshua H. Gordis, Assistant Professor, Naval Postgraduate School, Monterey, California, 15 January 93.

16. *Close-In Weapon System Mk 15 MODS 1 Thru 4 and 6 (PHALANX): Functional Description* , pp. 2-9.1 - 2-9.8, Naval Sea Systems Command, 1987.

17. Notes from Hughes Missile Systems Company, Pomona, California, 23 October 1992.

18. Data Provided by Dick Sirola, Martin Marietta Armament Systems, Burlington, Vermont, 25 February 1993.

19. Telephone conversation between Tim Murphy, Torrington Bearing Co., and LT Don MacNeil, Naval Postgraduate School, April 1993.

20. Computer simulation results by Michael Hatch, Mechanical Engineer, Palo Alto, California, April 1993.

21. Lawry, M. H., *I-DEAS Student Guide* , pp. 201-208, Structural Dynamics Research Corp., 1991.

22. Lawry, M. H., *I-DEAS Student Guide* , pp. 201-208, Structural Dynamics Research Corp., 1991.

23. Knight, C. E., *The Finite Element Method in Mechanical Design* , pp. 20-36, PWS-KENT Publishing Co., 1993.

24. Knight, C. E., *The Finite Element Method in Mechanical Design* , pp. 20-36, PWS-KENT Publishing Co., 1993.

25. *I-DEAS Model Solution and I-DEAS Optimization User's Guide* , pp. (18-69)-(18-75), Structural Dynamics Research Corp., 1990.

26. Knight, C. E., *The Finite Element Method in Mechanical Design*, pp. 20-36, PWS-KENT Publishing Co., 1993.

27. James, W. L. / Smith, G. M. / Wolford J. C. / Whaley P. W., *Vibration of Mechanical and Structural Systems* , pp. 43-112, Harper and Row Publishers, 1989.

28. Lawry, M. H., *I-DEAS Student Guide*, pp. 201-208, Structural Dynamics Research Corp., 1991.

29. *I-DEAS Model Solution and I-DEAS Optimization User's Guide* , pp. (18-69)-(18-75), Structural Dynamics Research Corp., 1990.

30. Knight, C. E., *The Finite Element Method in Mechanical Design* , pp. 20-36, PWS-KENT Publishing Co., 1993.

31. Experimental testing of the normal modes of vibration of a single PHALANX barrel assisted by Professor J. H. Gordis, Department of Mechanical Engineering, Naval Postgraduate School, Monterey, California, March 1993.

32. James, W. L. / Smith, G. M. / Wolford J. C. / Whaley P. W., *Vibration of Mechanical and Structural Systems* , pp. 43-112, Harper and Row Publishers, 1989.

33. James, W. L. / Smith, G. M. / Wolford J. C. / Whaley P. W., *Vibration of Mechanical and Structural Systems* , pp. 43-112, Harper and Row Publishers, 1989.

34. James, W. L. / Smith, G. M. / Wolford J. C. / Whaley P. W., *Vibration of Mechanical and Structural Systems* , pp. 43-112, Harper and Row Publishers, 1989.

35. Boyce, W. E. and DiPrima, R. C., *Elementary Differential Equations and Boundary Value Problems* , pp. 301 - 310, John Wiley and Sons, 1986.

36. James, W. L. / Smith, G. M. / Wolford J. C. / Whaley P. W., *Vibration of Mechanical and Structural Systems* , pp. 408-450, Harper and Row Publishers, 1989.

37. Fowles, G. R., *Analytic Mechanics* , pp. 64-68, Holt, Rhinehart and Winston, Inc., 1986.

38. Fowles, G. R., *Analytic Mechanics* , pp. 64-68, Holt, Rhinehart and Winston, Inc., 1986.

39. Fowles, G. R., *Analytic Mechanics* , pp. 64-68, Holt, Rhinehart and Winston, Inc., 1986.

40. Crede, C. E., and Harris, C. M., *Shock and Vibration Handbook* , pp. 5-1 - 5-14, McGraw-Hill Book Company, 1976.

41. Data Provided by Dick Sirola, Martin Marietta Armament Systems, Burlington, Vermont, 25 February 1993.

42. Van Santen, G. W., *Introduction to a Study of Mechanical Vibration* , pp. 30 - 40, Philips' Techanical Library, 1958.

43. James, W. L. / Smith, G. M. / Wolford J. C. / Whaley P. W., *Vibration of Mechanical and Structural Systems* , pp. 134-170, Harper and Row Publishers, 1989.

44. Van Santen, G. W., *Introduction to a Study of Mechanical Vibration* , pp. 30 - 40, Philips' Techanical Library, 1958.

45. Data Provided by Dick Sirola, Martin Marietta Armament Systems, Burlington, Vermont, 25 February 1993.

46. Van Santen, G. W., *Introduction to a Study of Mechanical Vibration* , pp. 30 - 40, Philips' Techanical Library, 1958.

47. Blueprints of the PHALANX muzzle restraint provided by Scott Martin, Hughes Missile Systems Company, Pomona Division, 6 May 1993.

48. Crede, C. E., and Harris, C. M., *Shock and Vibration Handbook* , pp. 5-1 - 5-14, McGraw-Hill Book Company, 1976.

49. Crede, C. E., and Harris, C. M., *Shock and Vibration Handbook* , pp. 5-1 - 5-14, McGraw-Hill Book Company, 1976.

50. Crede, C. E., and Harris, C. M., *Shock and Vibration Handbook* , pp. 5-1 - 5-14, McGraw-Hill Book Company, 1976.

51. Crede, C. E., and Harris, C. M., *Shock and Vibration Handbook* , pp. 5-1 - 5-14, McGraw-Hill Book Company, 1976.

52. Data provided by LCDR P.J. White, RN, PHALANX Program Office, Naval Surface Warefare Center, Dahlgren Division, 21 October 1992.

53. Naval Surface Warfare Center, Dahlgren Division, PHALANX Dispersion Study, by P. J. White, 27 May 1993.

INITIAL DISTRIBUTION LIST

1.	Defense Technical Information Center Cameron Station Alexandria, Virginia 22304-6145	2
2.	Library, Code 52 Naval Postgraduate School Monterey, California 93943-5002	2
3.	Professor William B. Colson, Code PH/Cw Department of Physics Naval Postgraduate School Monterey, California 93943-5000	2
4.	Professor Joshua H. Gordis, Code ME/Gj Department of Mechanical Engineering Naval Postgraduate School Monterey, California 93943-5000	2
5.	Professor Steven F. Baker, Code PH/Bs Department of Physics Naval Postgraduate School Monterey, California 93943-5000	1
6.	Mike Hatch 2163 Woodleaf Way Mountain View, California, 94040	1

7. LCDR Paul J. White, RN — 2
Dahlgren Division
Naval Surface Warfare Center
PHALANX Program Office
Code G30
Dahlgren, Viginia 22448-5000

8. Yuji Wilson — 1
Port Hueneme Division
Naval Surface Warfare Center
Code 4l21
Port Hueneme, California, 93043

9. Scott Martin — 1
Building 50, Mail Station 50-38
Hughes Missile Systems Company
PO Box 2507
Pomona, California 91769-2507

10. Dick Sirola — 1
Martin Marietta Company
Armament Systems Department
Lakeside Avenue
Burlington, Vermont 05401-4985